# Of ice crystals, clouds and climate

Measuring and modeling cold clouds in the Arctic

Britta Schäfer

Supervisors:
Trude Storelvmo
Michael Gausa
Øivind Hodnebrog

*Series of dissertations submitted to the*
*Faculty of Mathematics and Natural Sciences, University of Oslo*
*No. 2774*

ISSN 1501-7710



Cover: UiO.
Print production: Graphic center, University of Oslo.

**Abstract**

Clouds are important elements in the atmosphere and the whole climate system as they transport water and impact incoming and outgoing radiation. They may consist of liquid water, ice or a mixture of both. Among other factors the relation between liquid water and ice is governing how much longwave radiation and thereby heat a cloud traps between itself and the surface. These effects are not only relevant in the Arctic, but especially important there, as shortwave radiation is absent from the Arctic during large parts of the year.
The first part of this thesis uses both long-term lidar measurements and shorter-term intensive in-situ observations to characterize cold clouds in the Norwegian Arctic. In the second part it aims to better represent Arctic mixed-phase clouds in a regional weather model. This is achieved by using observationally-constrained aerosol concentrations and adding processes for so-called secondary ice production, i.e. mechanisms that create new ice particles based on existing ice. Finally, the optimized model is used to study how Arctic mixed-phase clouds may change in a warmer climate.

**Sammendrag**

Skyer er en viktig brikke i jordsystemet og atmosfæren. De kan bestå av flytende vann, ispartikler eller en blanding av begge deler. Hvordan denne blandingen ser ut i en sky, har mye å si for hvordan den absorberer og reflekterer stråling og dermed også dens effekt på klimaet. Spesielt effekten på langbølget stråling er viktig i arktiske områder i vinterhalvåret. Denne avhandlingen karakteriserer i første del arktiske skyer som inneholder kun is eller både flytende vann og is ved bruk av flere år med lidarobservasjoner fra Andøya og in-situ målinger fra Svalbard i årene 2019-2020. Deretter fokuserer avhandlingen på simuleringer av skyer med både flytende vann og is i Arktis i en værmodell. Simuleringene forbedres ved å tilpasse aerosolkonsentrasjoner til målte verdier og ved å ta med flere prosesser for isdannelse i skyer enn i en standardmodell. I siste del brukes den forbedrede modellen til å undersøke hvordan arktiske skyer bestående av både flytende vann og is endrer seg i et varmere klima.

# Preface

This thesis is submitted for the degree of philosophiae doctor (PhD) at the Section for Meteorology and Oceanography (MetOs), Department of Geosciences, University of Oslo. The work has been conducted in the period from October 2019 until February 2024. The thesis consists of four papers of which the first and second are published after peer review, the third is included in the revised version that is at the time of the printing and disputation of the thesis accepted for publication after peer review and the fourth paper is still a draft and not submitted yet. The third paper was included in the first submitted version when the thesis was submitted for evaluation as the peer review process was not completed yet, but it had already received positive reviews and the revisions in between the two versions were of a minor character. The papers are preceded by an introduction and a summary of findings and conclusions.

**Paper I** **Britta Schäfer**, Tim Carlsen, Ingrid Hanssen, Michael Gausa, and Trude Storelvmo, (2022), Observations of cold-cloud properties in the Norwegian Arctic using ground-based and spaceborne lidar, Atmospheric Chemistry and Physics (ACP), doi:10.5194/acp-22-9537-2022

**Paper II** Julie Pasquier, Robert Oscar David, Gabriel Freitas, Rosa Gierens, Yvette Gramlich, Sophie Haslett, Guangyu Li, **Britta Schäfer**, Karolina Siegel, Jörg Wieder, Kouji Adachi, Franco Belosi, Tim Carlsen, Stefano Decesari, Kerstin Ebell, Stefania Gilardoni, Martin Gysel-Beer, Jan Henneberger, Jun Inoue, Zamin A. Kanji, Makoto Koike, Yutaka Kondo, Radovan Krejci, Ulrike Lohmann, Marion Maturilli, Mauro Mazzolla, Robin Lewis Modini, Claudia Mohr, Ghislain Motos, Athanasios Nenes, Alessia Nicosia, Sho Ohata, Marco Paglione, Sangjong Park, Rosaria Erika Pileci, Fabiola Ramelli, Matteo Rinaldi, Christoph Ritter, Kazutoshi Sato, Trude Storelvmo, Yutaka Tobo, Rita Traversi, Angelo Viola and Paul Zieger, (2022), The Ny-Ålesund Aerosol Cloud Experiment (NASCENT) Overview and First Results, Bulletin of The American Meteorological Society (BAMS), doi:10.1175/BAMS-D-21-0034.1

**Paper III** **Britta Schäfer**, Robert Oscar David, Paraskevi Georgakaki, Julie Pasquier, Georgia Sotiropoulou, and Trude Storelvmo, (2023), Simulations of primary and secondary ice production during an Arctic mixed-phase cloud case from the NASCENT campaign, EGUsphere, doi:10.5194/egusphere-2023-2907

**Paper IV** **Britta Schäfer**, Robert Oscar David, Øivind Hodnebrog and Trude Storelvmo, Simulations of the response of an Arctic mixed-phase cloud to aerosol perturbations and warming, planned submitted to Geophysical Research Letters, spring 2024

Other articles published during the PhD period, but not included in the thesis:

**I** **Britta Schäfer**, Gerd Baumgarten and Jens Fiedler, (2020), Small-scale structures in noctilucent clouds observed by lidar, Journal of Atmospheric and Solar-Terrestrial Physics (JASTP), doi:10.1016/j.jastp.2020.105384
(based on results from master thesis)

# Acknowledgements

After my more than four years as a PhD student at the University of Oslo, the number of people who I met during this period illustrates the most to me, what a rich time that has been. It is impossible to thank everyone individually who had an impact on the progress of my research or made the time enjoyable in various other ways. The following attempt is by no means exclusive.

First of all, I thank my main supervisor Trude for the opportunity to work with her and in such an inspiring research group, for the possibility to participate in field campaigns and for many interesting research discussions. Moreover, I would like to thank you for the trust expressed in letting me combine being a researcher with being a professional musician. Your willingness to make that possible is highly appreciated. Thanks also to my co-supervisors Michael and Øivind for your support during the first and last period of the PhD, respectively.

From my research group I want to especially thank Rob and Tim for sharing their knowledge and experience and for numerous good discussions about topics inside and outside science. Thanks also to Astrid and Stian for enjoyable fellow train and bus travels to Andenes and to Rob and Jenny for taking a critical look at my thesis manuscript.

Thanks to fantastic office mates (Marius deserves a special mention here) and to everyone else at MetOs for section events, lunch breaks and non-work activities spent together. Thanks as well to colleagues and students that I worked together with during teaching and supervising activities, I really enjoyed that part of the PhD, too.

In the broader research community, a huge thanks goes to the NASCENT campaign team who let me use their dataset. This thesis would not have been possible without. I would also like to thank the research school CHESS for connecting PhD students in Norway, the possibility to both participate in and organize courses and everyone I met there. The experience from CHESS was for sure an underlying cause why I spontaneously volunteered to join the board of Norsk Geofysisk Forening in November 2022.

Outside of the science community, a special thanks goes to my colleagues in Strømsø bykirke and my musician friends for their genuine interest in what I'm spending my time with at university, but also offering great distraction from research.

Finally, I want to thank my family and a few more close friends that I always found listening ears when I needed it.

# Contents

# Part I

# Thesis

# Chapter 1

# Motivation and objectives

Being a physicist, it is not implicit that the topic of my PhD thesis would be something everybody can relate to. Therefore, in conversations with friends having different professions, I consider myself lucky that the main study object of my PhD thesis - clouds - is familiar to everyone, at least in the macroscopic view. At the same time, I wish that human-induced climate change in the Arctic was not occurring as rapidly as it is, making research on cloud changes as relevant and urgent as it currently is, but this is a different topic.

Clouds are powerful players in the climate system and they are expected to change considerably in the Arctic, the currently fastest warming region on Earth. Depending on the character of the cloud changes they may either accelerate or counteract warming. To improve our knowledge about Arctic clouds and their future changes, both experimental and theoretical/computational modeling methods need to be applied. Even though clouds are widespread and usually not difficult to spot with the naked eye, measuring and computationally simulating their microphysical properties is more challenging. Long-term observations of clouds in the Arctic are especially valuable since the region is, on average, embossed by a harsh and remote environment and has a lower density of permanently operated measurement stations than lower latitudes and more densely populated areas. One method suitable for long-term monitoring of clouds is to observe them by lidar, both with ground-based and spaceborne instruments.

Similarly, the wide range of scales on which cloud processes occur, from the nanometer-size aerosol particles that they form on to the tens-of-kilometer-size cloud fields, represents a challenge for computational models. Cloud formation processes are examples of processes that need to be described using parametrizations. Designing parametrizations requires weighing accuracy against computational cost, and the results are generally far from perfect representations of the actual atmospheric processes. To constantly improve model performance and agreement with nature, direct comparisons between observations and model simulations are essential. So far, the number of cloud modeling studies who have applied observationally-constrained aerosol/ice-nucleating particle concentrations to case studies in pristine Arctic regions is limited (Fu et al. 2019; Knopf et al. 2023; Gjelsvik 2022; Young, Connolly, et al. 2017). Another shortcoming of standard models is that they do not necessarily include all known cloud processes. Regarding ice production in clouds, this applies to secondary ice production, i.e. new ice

formation from existing ice particles. Only one process is commonly included in models while up to six are known. This thesis includes two more processes that are, depending on background conditions, capable of increasing ice crystal concentrations by up to orders of magnitude.

## Objectives

The objectives and scope of this thesis are to better understand the physics of Arctic cold clouds, including present-day occurrence, processes and composition, as well as how these may change in a warmer climate. The main objectives are:

1. Characterize the occurrence and properties of cold clouds (mixed-phase and ice clouds) in the Norwegian Arctic
2. Understand the interplay of different ice production processes in Arctic mixed-phase clouds
3. Explore how Arctic mixed-phase clouds may change in a warmer future climate

Characteristic for this thesis is a combination of observational and modeling approaches to achieve the objectives above. The first objective, addressed in the first two papers, is purely exploiting observational research tools, the second relies on both observations and modeling, while the last part addressing the third objective on future climate is purely model-based.

For characterizing the occurrence and properties of cold clouds in the Norwegian Arctic, I used lidar data from the Northern Norwegian island of Andøya and in-situ observations from Ny-Ålesund, Svalbard. This first study based on lidar measurements adds a site to the generally sparse network of long-term cloud datasets from the Arctic. By comparison with satellite measurements from the same region and time period, we are able to assess whether there are important differences between the monitoring from space and using ground-based sites that provide a higher temporal resolution, but smaller horizontal coverage. While the lidar measurements mostly cover ice clouds, the in-situ observations are used to characterize lower level mixed-phase clouds and the relative importance of different ice formation mechanisms.

The second objective aims specifically at quantifying the processes leading to a given number and mass of ice and liquid water particles inside Arctic mixed-phase clouds. The availability of high-resolution in-situ measurements of both aerosols and cloud particles from Ny-Ålesund makes it possible to constrain aerosol concentrations in a weather model, motivates the implementation of more secondary ice production processes than traditionally used and allows verification of the model's results with the observations. The study concentrates on observations from one selected day in November 2019 and analyzes this cloud case in detail.

Finally, the last part dealing with objective 3 and future changes in mixed-phase cloud properties requires a model that represents cloud processes at present-day correctly. Therefore it makes use of the cloud case and improved model from the

previous part, when applying the so-called Pseudo Global Warming method to simulate a warmer climate. Additionally, the study relies on information about the future warming in the Arctic taken from a climate model experiment.
Further background and descriptions of the research tools used are given in Chapters 2 and 3.

## A short note on changes in the Ph.D. project due to the pandemic

One of the first things every Ph.D. candidate has to do when starting at the University of Oslo, is to deliver a project description. Around the same time, the candidate is typically told by more senior Ph.D. candidates, PostDocs or professors that it is completely normal that plans change along the way. In that light, it would not be necessary to mention that also some parts of my project description looked different than the final thesis. I do so anyway, because the Covid19-pandemic had major unforeseen impacts on the realization of my outlined research plan beyond more common issues such as research results turning out differently than expected. The pandemic did not only affect course work, teaching and the general working environment, but also led to restrictions on measurement campaigns. In short, the following paragraph explains why I participated in three measurement campaigns on Andøya during my Ph.D. period (early spring 2021, 2022 and 2023), but none of these ended up playing a major role in this thesis.

While the topic and main objectives of the Ph.D. project stayed the same, other details had to be adapted. Originally, data for addressing objective 2 and 3 was supposed to be collected through a campaign with base on Andøya in March 2020. Data was going to be collected during research flights northwards and the research questions of my project would have been answered in the same region as covered in the first part. The measurement campaign in 2020 had to be canceled completely at the last minute due to the pandemic. The following two years, restrictions on international travel still made conducting a full campaign including aircraft in-situ measurements impossible, and in full-scale, this campaign could first be conducted in 2023. As this was too late for the sake of my Ph.D., instead data from an earlier measurement campaign that took place on Svalbard from autumn 2019 until spring 2020 was used. The campaign was called the Ny-Ålesund Aerosol Cloud Experiment (NASCENT) and turned out to be a very suitable replacement for the campaign data that was originally intended to be analysed in this thesis. Although I was not part of the campaign team on Svalbard, I was given the opportunity to use their data and become involved in the interpretation of results through model simulations. The locations of Andøya and Ny-Ålesund are given in Fig. 1 for reference.

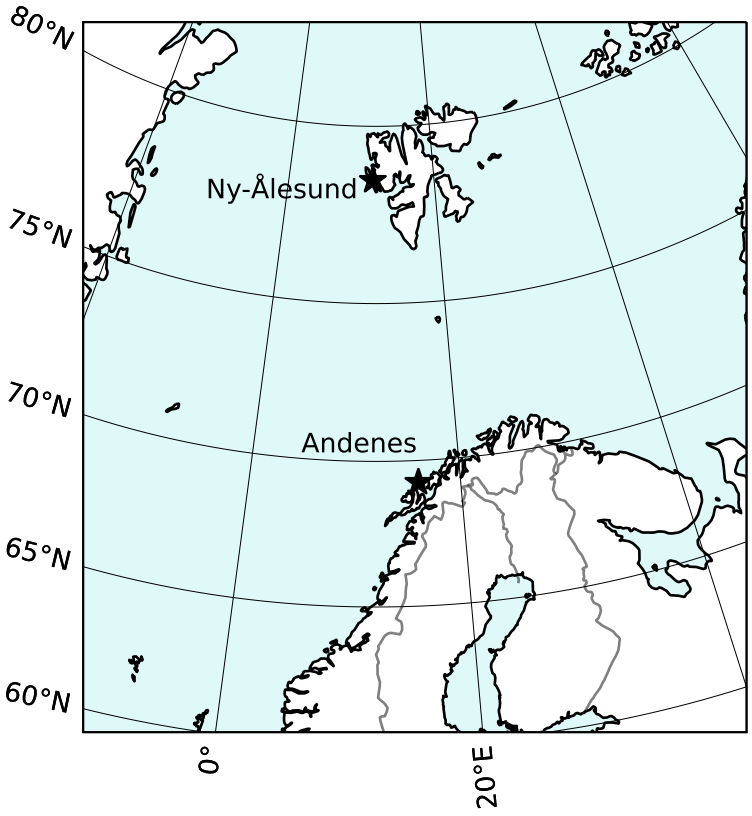


Figure 1: Measurement locations of observations used in the first paper (Andenes) and in the second and third paper (Ny-Ålesund): Both locations are marked by black stars.

# Chapter 2

# Background

## 2.1 Cloud droplet and ice crystal nucleation

Cloud droplet formation requires that the air is supersaturated with water vapor, i.e. that the relative humidity is higher than 100%. Typical in-cloud values of supersaturation are a few percent, but exact values are highly dependent on the development stage of the cloud. Classical nucleation theory shows that much larger supersaturation would be required if droplets were to form from pure water without the help of any aerosol particles. Therefore, droplet nucleation in the atmosphere always happens heterogeneously with the help of so-called cloud condensation nuclei (CCN). Consequently, the number of droplets formed in a cloud is directly dependent on the number of available CCN (e.g. Moore et al. 2013; Reutter et al. 2009; Motos et al. 2023).

Similarly, in the ice phase, energy barriers limit homogeneous ice nucleation, i.e. the formation of ice without the help of aerosol particles, to temperatures below -38 °C (Vali et al. 2015). Thus, unlike our daily-life experience with water, water in clouds does not freeze immediately when the temperature drops below 0 °C. Cloud droplets will stay supercooled and liquid down to 38 °C below the freezing point temperature, unless freezing is triggered by a special type of aerosol particles referred to as ice-nucleating particles (INPs; e.g. Kanji et al. 2017).

Exactly how INPs help to form ice crystals in clouds is still a topic of ongoing research, and a number of processes is proposed, illustrated in Fig. 2b-d. Deposition freezing (Fig. 2b) describes the only heterogeneous nucleation mechanism where water directly goes from the gas phase (vapor) to the solid phase, as ice deposits onto an aerosol particle (Vali et al. 2015). However, recent studies suggest that even in this mechanism bulk liquid water may be involved, condensed in nano-scale cracks or pores, initiating freezing (David, Marcolli, et al. 2019; David, Fahrni, et al. 2020; Marcolli 2014; Campbell and Christenson 2018). Deposition freezing is especially relevant in cirrus clouds (e.g. Gierens, Monier, and Gayet 2003; Kärcher et al. 2022).

In clouds at higher temperatures than the cirrus regime (>-30 °C; Heymsfield et al. 2017; DeMott et al. 2010), heterogeneous ice formation typically happens via two different processes, namely immersion and contact freezing. Immersion freezing (Fig. 2c) describes the process when a droplet freezes due to an immersed

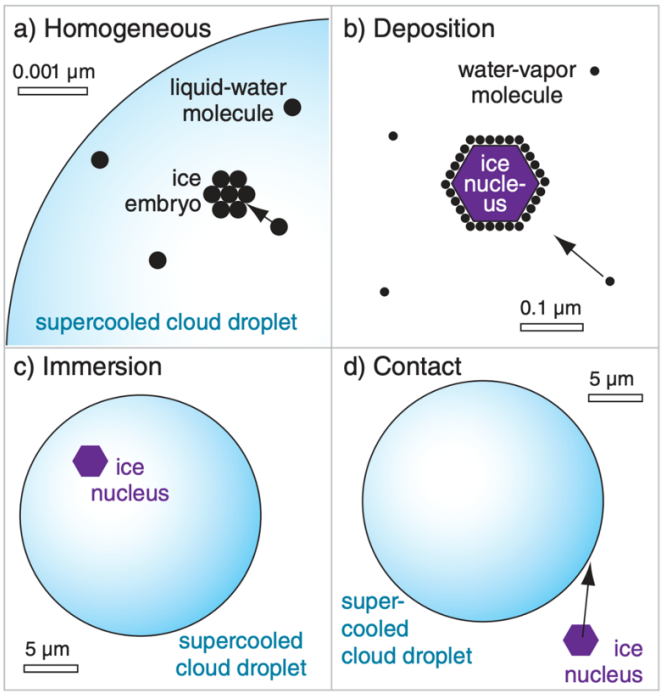


Figure 2: Primary ice nucleation mechanisms: a) homogeneous nucleation, b) deposition freezing, c) immersion freezing, d) contact freezing. The term "ice nucleus" in the illustration is synonymous to the term "ice-nucleating particle" used in this thesis. The illustration is taken from Stull 2015.

INP and is especially relevant in Arctic mixed-phase clouds (e.g. de Boer, Hashino, and Tripoli 2010; de Boer, Morrison, et al. 2011; Solomon et al. 2018). Contact freezing (Fig. 2d) describes freezing of a droplet when colliding with an INP from ambient air. Both are stochastic processes, but the number of aerosols acting as INPs increases at colder temperatures. Therefore, INP concentrations are, for modeling purposes, often described mathematically as a function of temperature only (in the contact mode additionally accounting for collision likelihood) (e.g. Cooper 1986; Meyers, DeMott, and Cotton 1992; Li et al. 2022). However, some studies also convey the stochastic aspect of the freezing mechanism by using classical nucleation theory (Hoose et al. 2010; Ickes, Welti, and Lohmann 2017; Knopf et al. 2023) or including a distribution to pick from per temperature rather than a single INP concentration value (Frostenberg et al. 2023). This way, small-scale fluctuations in INP concentrations inside a cloud may be represented.

Experimentally, the concentration of immersion INPs may be measured through droplet-freezing experiments such as the DRoplet Ice Nuclei Counter Zurich (DRINCZ; David, Cascajo-Castresana, et al. 2019; Wieder et al. 2022) used during the NASCENT campaign described in paper II. A tray with 96 wells is cooled down starting from 0 °C until all droplets are frozen, while the number of frozen droplets per temperature step is recorded (David, Cascajo-Castresana, et al. 2019; Li et al. 2022). For INP measurements from snow, melted snow water is used, while for measurements of INPs in air, the aerosols are caught in pure water using a liquid impinger. From a number of such measurements,

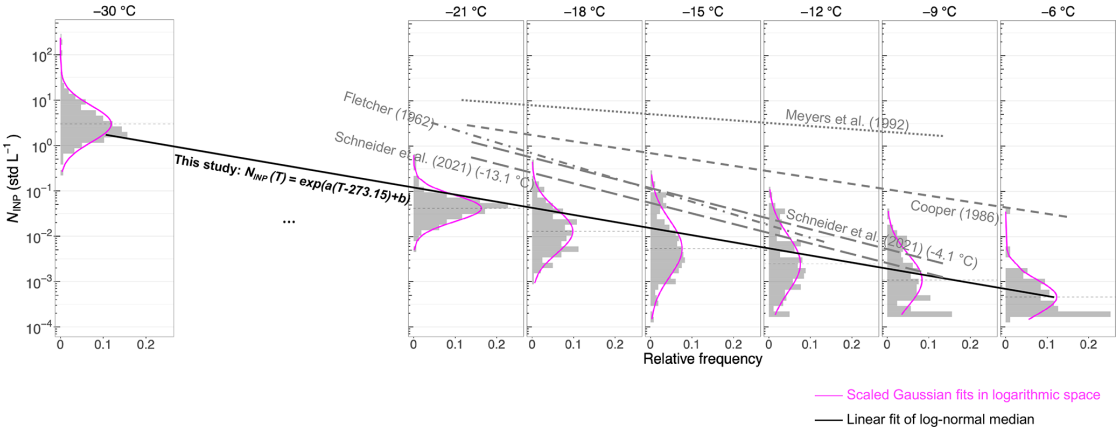


Figure 3: INP parametrizations based on temperature: The gray histograms and the black line show measurements from Ny-Ålesund, Svalbard, (Li et al. 2022), the gray lines show older parametrizations for comparison (Cooper 1986; Meyers, DeMott, and Cotton 1992; Fletcher 1962; Schneider et al. 2021). The figure is taken from Li et al. 2022.

distributions of INP concentrations at different temperatures can be computed. Finally, an exponential fit for the INP concentration as a function of temperature can be calculated. Both the distributions at different temperatures and the final fit are illustrated in Fig. 3 (Li et al. 2022). The figure indicates also that the concentration found by Li et al. 2022 on Svalbard 2019-2020 (black line) is much lower than other existing parametrizations, shown as grey lines e.g. Cooper 1986; Meyers, DeMott, and Cotton 1992. This is not surprising as it is known that the Arctic is a more pristine environment than the mid-latitude regions where common parametrizations have been tested the most. In remote regions such as the Arctic and the Southern Ocean, an important source of INPs is the sea surface microlayer emitting biological particles into the air through sea spray aerosol (e.g. Carlsen and David 2022; McCluskey et al. 2018; Ickes, Porter, et al. 2020; Abbatt et al. 2019; Wilson et al. 2015). In the Arctic, mineral dust particles from long-range transport or local sources play a role as well (Abbatt et al. 2019; Shi et al. 2022; Irish et al. 2019).

## 2.2 Secondary ice production

Apart from homogeneous ice nucleation at temperatures below -38 °C and heterogeneous ice nucleation involving INPs, both representing primary ice production processes, ice crystals may also be formed through secondary ice production (SIP) processes, also called ice multiplication (e.g. Field et al. 2017; Korolev and Leisner 2020). In contrast to primary ice production, these processes depend on preexisting ice crystals. They have been suggested in part because of decades of observational evidence that ice crystal number concentrations regularly exceed INP concentrations by orders of magnitude (e.g. Auer, Veal, and Marwitz 1969; Beard 1992). In recent years, the number of studies addressing the importance of secondary ice production is increasing, especially for clouds in polar

regions (e.g. Sinclair, Moisseev, and Lerber 2016; Young, Lachlan-Cope, et al. 2019; Sotiropoulou, Sullivan, et al. 2020; Sotiropoulou, Vignon, et al. 2021; Zhao et al. 2021; Järvinen et al. 2022; Georgakaki et al. 2022; Karalis et al. 2022).

An overview of the six currently suggested mechanisms is for example given by Korolev and Leisner 2020 (see Fig. 4). The earliest discovered SIP mechanism is rime splintering (Fig. 4b), first described by Hallett and Mossop 1974. The process is assumed to occur at temperatures between -8 and -3 °C and is still the only SIP process that is commonly included in weather and climate models (e.g. Field et al. 2017; Zhao et al. 2021; Atlas et al. 2022). Further processes that are beginning to be implemented in models are droplet shattering that happens during freezing of droplets (Fig. 4a) and fragmentation during ice-ice collisions (Fig. 4c), following the parametrizations by e.g. Phillips, Yano, et al. 2017; Phillips, Patade, et al. 2018. Three more processes are so far rarely implemented in models, namely ice fragmentation during thermal shock (Fig. 4d), fragmentation during sublimation (Fig. 4e) and the activation of INPs in transient supersaturation (Fig. 4f).

From observations, an assessment of how many ice crystals were produced through SIP is often based on size (Korolev, Heckman, et al. 2020). For an assessment of the contributions of the individual ice formation processes, ice crystals shapes (e.g. classified after Kikuchi et al. 2013) may be used in combination with the ambient temperature to identify certain mechanisms (Pasquier et al. 2022). However, an exact attribution of the observed ice crystal number in a cloud to the different ice formation processes remains challenging (e.g. Järvinen et al. 2022). For Arctic mixed-phase clouds, Pasquier et al. 2022 found that SIP occurred during 40% of the in-cloud measurements performed in Ny-Ålesund over six days and that droplet shattering likely played an important role in events with high SIP. These findings highlight the importance of appropriately representing SIP in models.

## 2.3 Clouds and radiation

To again reference our daily-life experience, it is common knowledge that the sun feels stronger on sunny days than on cloudy days, and that clear nights tend to be colder than cloudy nights. Thus, it is no surprise that clouds have a large impact on radiative transfer through the atmosphere and consequently, surface temperature and climate in general. In the aforementioned example, the former is through a cloud's effect on shortwave, the latter through its effect on longwave radiation.

Individual clouds may have a net warming or cooling effect, but on a global average, clouds collectively cool the climate by a net cloud radiative effect of -20 $\mathrm{Wm}^{-2}$ at present-day conditions as estimated by the IPCC (Forster et al. 2021). This number is a composite of the difference in longwave (LW) and shortwave (SW) radiative fluxes at the top of the atmosphere between the real cloudy atmosphere and a hypothetical atmosphere without clouds. Net SW radiative effects always refer to the difference in incoming solar radiation and reflected outgoing radiation, while net LW effects refer to outgoing radiation only, as there is no appreciable incoming LW radiation at the top of atmosphere (e.g. Zhang et al. 2004). Due to

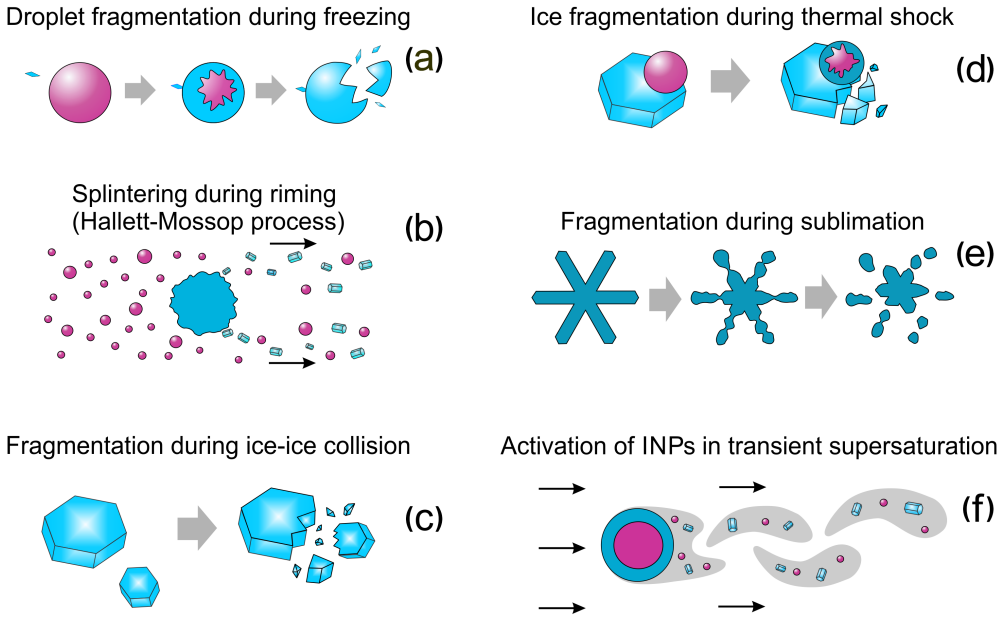


Figure 4: Illustration of six different secondary ice production mechanisms (the figure and the following description are taken from Korolev and Leisner 2020): (a) fragmentation droplets during freezing, (b) rime splintering (Hallett–Mossop process), (c) fragmentation of ice particles during ice–ice collision, (d) fragmentation of ice particles during thermal shock caused by a freezing drop attached to their surfaces, (e) fragmentation of ice particles during their sublimation, and (f) activation of supersaturation-sensitive INPs in the transient supersaturation formed around freezing drops or wet graupel/hailstones. Blue color refers to ice phase and red color to liquid phase.

this inherent difference, SW radiation is sometimes also just referred to as solar radiation and LW radiation as terrestrial radiation.

In the following, I focus on radiative impacts of cold clouds since they are the topic of this thesis. The radiative effect of cirrus clouds, present at high altitudes and low temperatures, tends to be dominated by the LW (warming) influence, as emitted longwave radiation from a cloud is directly related to its temperature via Planck's law. Cold bodies emit less energy, therefore the LW cloud radiative effect increases with the temperature difference between the cloud and the surface. The SW radiative effect typically dominates for lower clouds which receive (and reflect) large amounts of sunlight and depends on the surface albedo below the cloud in addition to the cloud albedo itself.

Back to the individual cloud level, apart from cloud height, thickness and lifetime, the microphysical composition of a cloud including cloud phase determines its radiative effect. Thus, it is important to know to which degree clouds are composed of liquid, ice or a mixture of both when modeling future climate. As the number of INPs decreases with rising temperature, cloud phase is generally seen as being a strong function of temperature (e.g. DeMott et al. 2010; Tan, Storelvmo, and Choi 2014). A typical mixed-phase cloud consists of mainly supercooled liquid water droplets and begins to form ice, when a small number of INPs enables the first ice formation (e.g. Hoose et al. 2010). Once ice crystals are present,

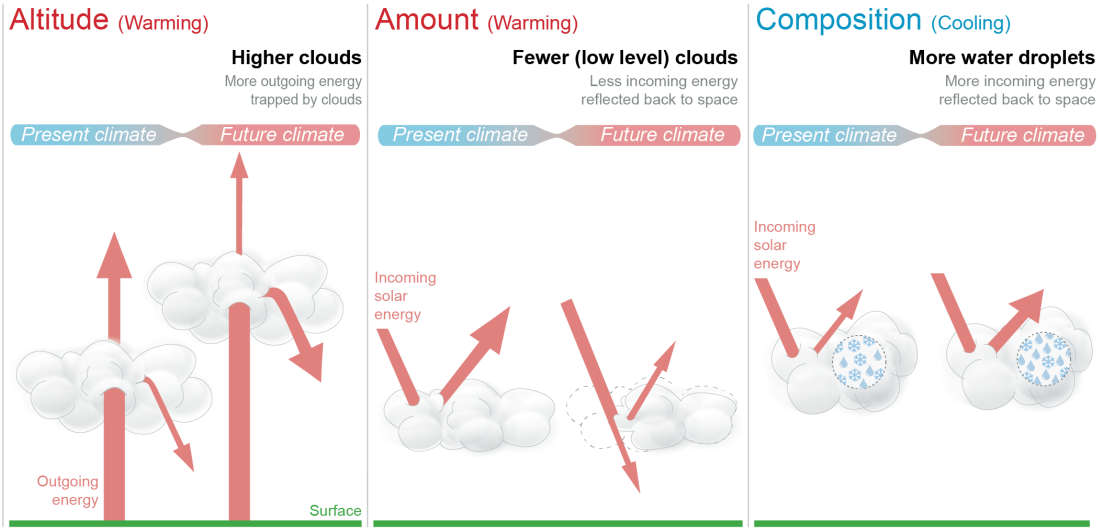


Figure 5: "What is the role of clouds in a warming climate?": The Figure is taken from chapter 7 of the $6^{th}$ assessment report of the IPCC, Working Group 1 (Forster et al. 2021, FAQ 7.2) and illustrates the expected interactions of cloud changes and global warming in the future in the global average.

they continue to grow via water vapor deposition. The transfer of water from supercooled liquid cloud droplets to ice through the gas phase happens since the saturation water vapor pressure is higher over water than over ice and is generally referred to as the Wegener-Bergeron-Findeisen mechanism (WBF; Wegener 1911; Bergeron 1928; Findeisen 1938; Storelvmo and Tan 2015). The change in phase composition towards more ice through the WBF mechanism decreases the optical thickness of the cloud and leads to higher precipitation rates. Global climate models have been found to underestimate the fraction of supercooled liquid water in mixed-phase clouds (Komurcu et al. 2014) and the study by Tan, Storelvmo, and Zelinka 2016 implies that forcing them to run with the observed liquid water content from satellite (CALIPSO; Winker et al. 2009) leads to a higher climate sensitivity, i.e. a larger global mean surface warming as a response to a doubling in atmospheric $CO_2$ concentration. This highlights the importance of a correct representation of cloud phase in models. In a global view, Matus and L'Ecuyer 2017 found from satellite observations that the global cloud radiative effect from mixed-phase clouds was -3.4 $Wm^2$ during the analyzed period from 2006 to 2011. In the future, the increase in liquid and decrease in ice water content in clouds with warming is expected to have a cooling impact on climate (negative cloud phase feedback; Choi et al. 2014; Ceppi et al. 2017). This will counteract some of the expected warming due to cloud changes in altitude (higher clouds) and amount (less low-level clouds) as illustrated in Fig. 5.

In contrast to the global average, clouds in the Arctic have a warming effect on the surface. This is due to the absence of shortwave radiation during large parts of the year, a high surface albedo due to ice and snow cover and strong temperature inversions, among others (Curry et al. 1996). Depending on the site, clouds have been found to exert a warming effect during the whole year or most of the year

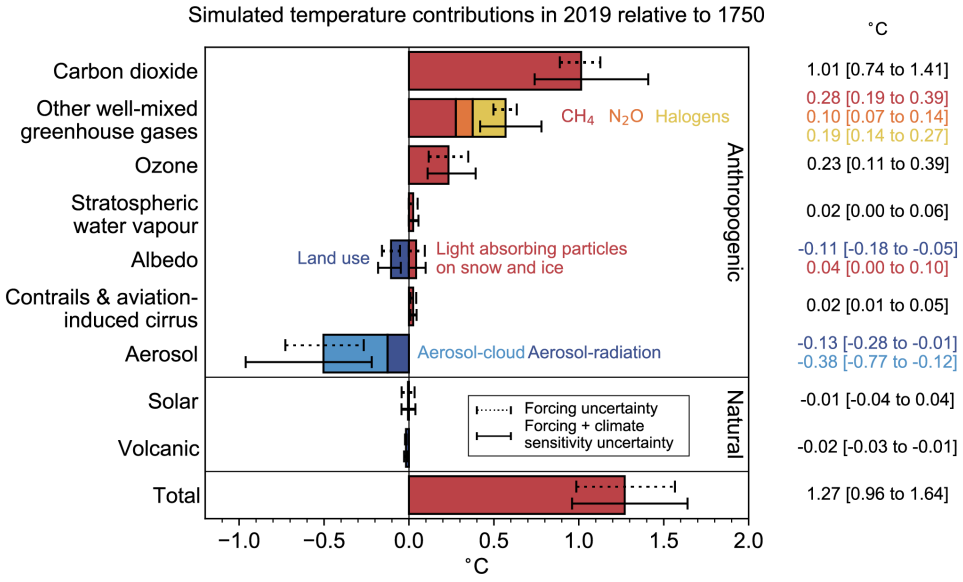


Figure 6: Simulated contributions to the temperature increase in 2019 relative to 1750 from different anthropogenic and natural elements: The light-blue bar and its corresponding uncertainty indicate the role of aerosol-cloud interactions. The figure is taken from chapter 7 of the $6^{th}$ assessment report of the IPCC, Working Group 1 (Forster et al. 2021, Fig. 7.7).

with the exception of a short period in summer (e.g. Intrieri et al. 2002; Shupe and Intrieri 2004; Miller et al. 2015).

## Aerosol effects on cloud radiative properties

As introduced in Chapter 2.1, the number of droplets in a cloud is strongly coupled to the number of CCN. At equal water content in mass, a cloud with more numerous and smaller droplets will appear brighter (have a larger cloud optical depth) and reflect more incoming solar radiation back to space. This effect is called the first aerosol indirect effect or Twomey-effect (Twomey 1977). As a further consequence of smaller cloud particles, precipitation efficiency may be reduced and the lifetime of the cloud increased. This is called the second aerosol indirect effect and leads, similar to the first aerosol indirect effect, to a cooling for clouds where the shortwave impact dominates the radiation balance in total. While the mentioned mechanisms are in general well understood for liquid clouds, aerosol impacts on the radiative properties of ice-containing clouds are far more uncertain, yet potentially powerful as well (Storelvmo 2017). In mixed-phase clouds, ice crystals are typically fewer and larger than liquid water droplets, as INP concentrations are small compared to CCN concentrations and ice particles grow rapidly via the WBF process. An increase in the number of available INPs is therefore expected to lead to optically thinner clouds in the mixed-phase temperature regime (between -38 °C and 0 °C; the so-called cloud glaciation effect).

Aerosol emissions have increased along with greenhouse gas emissions and have

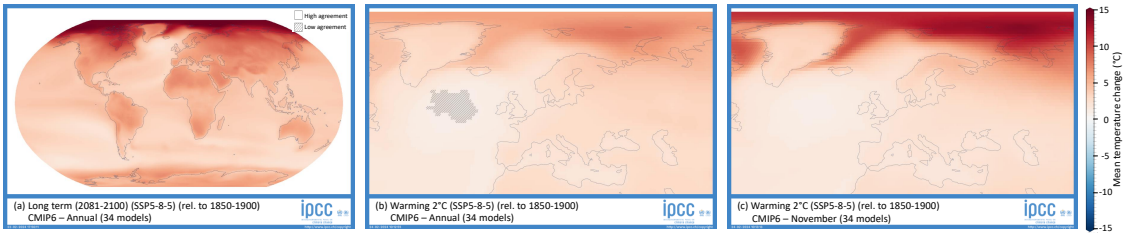


Figure 7: Maps generated inside the IPCC Interactive Atlas (Gutiérrez et al. 2021; Iturbide et al. 2021), all based on scenario SSP5-8.5: Panel (a) shows the global annual mean surface temperature change relative to the preindustrial period (1850-1900) in the long-term (2081-2100) perspective, panel (b) shows the annual mean temperature change in Europe for the time when a global mean surface warming of 2 K is reached, and finally, (c) is similar to (b), but showing the temperature change in November only instead of the annual mean.

so far counteracted some of the warming induced by greenhouse gases through their cooling effect (Fig. 6). The majority of the aerosol radiative forcing is caused by interactions with clouds and likewise, a large proportion of the uncertainty in the total simulated temperature increase originates from aerosol-cloud interactions (Forster et al. 2021). This serves as a great motivation to extend our knowledge on aerosol-cloud interactions in general and to contribute to improving these processes in models. This aim may, among other strategies, be achieved by constraining CCN and INP concentrations in models by aerosol observations for cases where measurements are available - in order to avoid compensating model errors and simulations that get the right answers for the wrong reasons.

## 2.4 Climate change in the Arctic

The global increase in temperature from anthropogenic climate change is not evenly distributed geographically. Warming is larger over continents than over oceans, larger in polar regions than at lower latitudes and larger in the Arctic than in the Antarctic (see Fig. 7a). Surface warming in the Arctic is especially pronounced during wintertime when no sunlight is present. For illustration, I show the temperature increase over Europe and the European Arctic at a global warming level of 2 °C in the annual mean (Fig. 7b) and in November (Fig. 7c). November was chosen because the case study used in paper III and IV is from this month. The maps in Fig. 7 are based on the output from 34 global climate models and created by the WG1 Interactive Atlas by the Intergovernmental Panel on Climate Change (IPCC). For a short summary on the IPCC and climate change scenarios, see the box with blue background.

The fact that climate change in the Arctic, and around Svalbard in particular, is happening at faster rates than in any other region on Earth has various impacts not only on the climate system, but also on ecosystems and wildlife (e.g. Descamps et al. 2017), permafrost (e.g. Etzelmüller et al. 2011; Humlum, Instanes, and Sollid

2003) and potential human activities in the Northern polar regions. Among the latter, Arctic shipping might increase, leading to increased emissions that directly or indirectly affect local radiation balances (Peters et al. 2011; Gilgen et al. 2018; Marelle et al. 2016). Gilgen et al. 2018 found that the indirect effect of future shipping emissions through increasing cloud optical depth and lifetime (cooling effect) is larger than the direct effect from the particles themselves.

Ultimately, global modelling studies have shown that mixed-phase clouds play an important role in Arctic climate change (Tan and Storelvmo 2019). The strength of the cloud phase feedback is strongly dependent on the simulated ratio of liquid water and ice in mixed-phase clouds as well as ice crystal sizes due to their link to precipitation (Tan, Storelvmo, and Zelinka 2016; Tan and Storelvmo 2019; Bjordal et al. 2020; Zelinka et al. 2020). This clearly shows the necessity of improving the representation of Arctic mixed-phase clouds in models in order to accurately predict future climate change.

### Intergovernmental Panel on Climate Change and climate change scenarios

The Intergovernmental Panel on Climate Change (IPCC) was established in 1988 by the World Meteorological Organization and the United Nations Environment Programme and has the task of providing governments all scientific information relevant to climate policies (IPCC 1988). The latest series of assessment reports from the sixth assessment cycle of the IPCC came out in 2021-2023: the report from Working Group (WG) 1: The Physical Science Basis in September 2021, the report from WG2: Impacts, Adaptation and Vulnerability in February 2022, the report from WG3: Mitigation of Climate Change in April 2022 and finally the synthesis report in March 2023. All working groups take part in the framing of different future scenarios of societal and economic development and emissions with resulting radiative forcing. In the sixth assessment cycle, five different development paths are assessed, so-called Shared Socio-Economic Pathways (SSPs). Combined with a level of radiative forcing, they make up different future scenarios with names like SSP1-2.6, where SSP1 stands for Shared Socio-Economic Pathway no. 1 and 2.6 characterizes the approximate radiative forcing in $Wm^{-2}$ resulting from the scenario in year 2100. Out of the five scenarios mainly used by WG1 (SSP1-1.9, SSP1-2.6, SSP2-4.5, SSP3-7.0 and SSP5-8.5), SSP5-8.5 has the highest radiative forcing and largest resulting warming by the end of the century (see Figure below, taken from IPCC 2021: Summary for Policymakers, Fig. SPM.8).

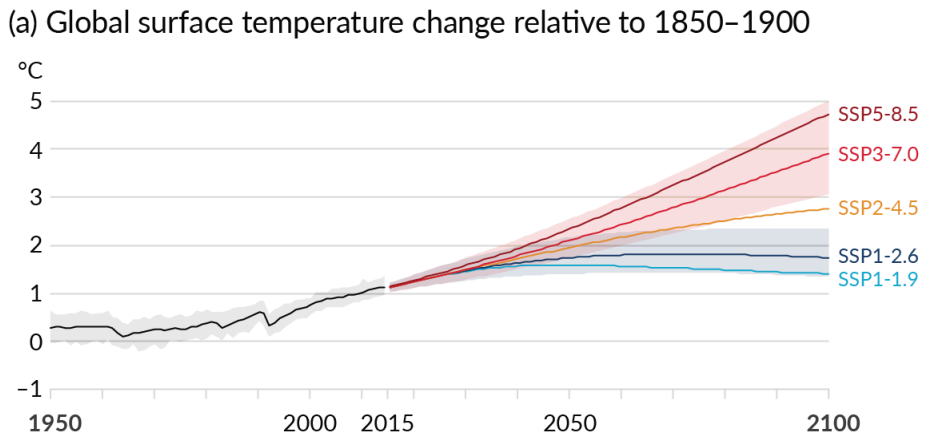

# Chapter 3

# Research tools

As indicated earlier, this thesis combines experimental methods and computational modeling. Regarding experimental methods, I here focus on the methods I have used myself, and not methods that have mainly been used by my collaborators and in this way contributed data to parts of Papers II, III and IV.

## 3.1 Lidar observations

Clouds can be observed by many means and with many different instruments. One active remote sensing method commonly used for long-term ground-based measurements at single sites is a lidar. This word is actually an acronym standing for LIght Detection And Ranging. Lidars used for atmospheric remote sensing applications consist of a transmitter, i.e. a laser, and a receiver, i.e. a telescope, followed by detectors and data acquisition that record how much of the light emitted is scattered back to the telescope and at which wavelength and polarization (Fig. 8) (Wandinger 2005a). If the transmitted laser light is linearly polarized, one can from the depolarization ratio of the backscattered light conduct whether the light was scattered by spherical particles like liquid droplets (no change in polarization angle) or by aspherical shapes like ice crystals (causing a rotation in the polarization angle). Thereby, splitting the received light using polarizing beam splitters can be used to discriminate liquid and phase in clouds and also distinguish between ice crystal shapes (e.g. Sassen 1991; Sassen and Benson 2001; Noel et al. 2002; Freudenthaler 2016).

Lidar applications are especially powerful in monitoring high and middle clouds. In low clouds that often have a high liquid water content, a large portion of the light is attenuated soon after entering the cloud which results in a short penetration depth (typically 100-200 m in optically dense water clouds; Wandinger 2005b) from which photons are returned and can be analyzed. Additionally, the reflection from low clouds can lead to too strong signals for the detection system that needs to cover a large range of signal powers already as the signal strength decreases with the square of the distance from the receiver (surface). The optical detection in the lidar used in this thesis is better suitable for middle and high clouds as well as aerosols. Reliable results on cloud thickness are restricted to single-layer clouds as the beam might not penetrate a second or third layer completely. This

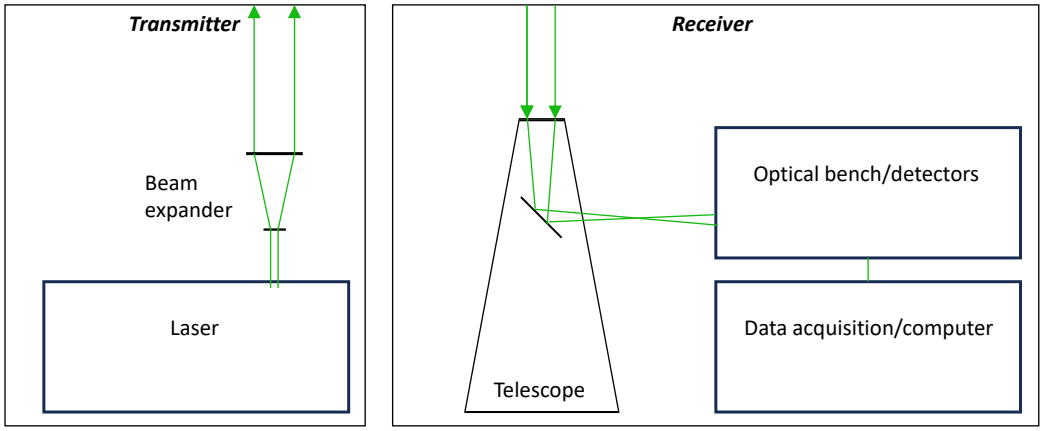


Figure 8: Basic lidar principle: The transmitter branch consists of a laser whose beam is transmitted into the atmosphere via a beam expander to limit dispersion. The receiver branch consists of a telescope, detectors and finally data acquisition. Figure adapted from Wandinger 2005a.

is especially important when aiming to compare observations from ground-based and spaceborne lidars. Both types of lidars typically have high vertical resolutions of a few meters, but differ in their temporal resolution. While spaceborne lidars from satellite must average over several kilometers and only visit the same place on Earth with long breaks in between, ground-based lidars are able to record changes on second-scale resolution, giving insight into the horizontal structures of clouds as well, if horizontal wind speeds are known.

The ground-based lidar used in this thesis is part of the research observatory ALOMAR (Arctic Lidar Observatory for Middle Atmosphere Research) and is located on the Northern Norwegian island Andøya, on top of the mountain Ramnan a few kilometers from the town of Andenes (Frioud et al. 2006). As the name of the observatory suggests, it is co-located with instruments observing the stratosphere and mesosphere, and is therefore referred to as the ALOMAR tropospheric lidar. It transmits and detects pulsed laser light at the three wavelengths 1064 nm, 532 nm and 355 nm. In principle, also inelastic scattering could be detected and analyzed (Raman scattering from nitrogen at 387 nm and 608 nm), but in many applications including long-term cloud studies only the elastic Rayleigh and Mie scattering channels are used and the detection branch for 608 nm is not a part of the system anymore. This is due to the low signal quality at daytime which again is due to low Raman scattering signals compared to background sunlight. For elastic scattering with larger absolute signals, narrow optical wavelength filters in the receiver branch enable the detection at daytime. Without inelastic scattering signals, the aerosol or cloud extinction and backscatter coefficients cannot be obtained independently, but when assuming a relation between them (lidar ratio), backscattering coefficients can be calculated using the Klett-algorithm (Klett 1981). As the ALOMAR lidar is part of the European Aerosol Research Lidar Network to Establish an Aerosol Climatology (EARLINET), their standardized Single Calculus Chain software can be used for calculating the lidar constant which is specific to each individual lidar

system and depends on parameters like laser power, pulse length and the aperture of the receiver (D'Amico et al. 2015).

## 3.2 Regional modeling

It seems unnecessary to state that computational modeling in the form of numerical weather prediction is a powerful tool in everyday-life. Similar to when speaking of clouds, everybody knows what a weather forecast is and probably uses it daily. Thus, everybody has seen the results of a weather model simulation, delivered to the public in a customized way. Besides being used in operational forecasting, numerical weather prediction (NWP) models are important research tools as well. One possible research application used in this thesis is to run the model for a time period in the past rather than near future, and to compare these model results with observations. While observations show the state of the atmosphere, precipitation amounts etc., a model based on physical laws can tell how this state was reached and connect observations from different places.

NWP models are generally physics- and not data-driven, i.e. after being initialized with meteorological data at a specific time, the model may run "free". However, for research applications where a specific case shall be studied, the model may in certain intervals be "nudged" towards the observed weather. For this, as well as for setting the boundary and initial conditions, data from a larger-scale model or so-called reanalysis data can be used. For simulations in this thesis, the widely used ERA5 reanalysis dataset produced by the European Centre for Medium-Range Weather Forecasts (ECMWF) is applied for grid nudging (Hersbach et al. 2020).

Starting from basic dynamic equations like the Navier-Stokes equations and the hydrostatic balance, numerical weather prediction models have grown to very complex systems containing separate schemes for the treatment of different processes. The cloud microphysics scheme is of most interest from a cloud physics perspective, and deals with everything from the formation of a droplet or ice crystal, via its growth from vapor, possible interactions with other cloud particles until its ultimate fate as it either sublimates/evaporates or leaves the atmosphere in the form of precipitation. It is inside this scheme that the changes improving cloud representation in this thesis are made.

Various microphysics schemes differ from each other in the number of different hydrometeor species used (cloud droplets, rain, ice crystals, snow, graupel, hail) and if the number and mass of the hydrometeors are prognostic variables that are treated individually (two-moment-schemes) or in a coupled way (one-moment-schemes).

The simulations in this thesis were performed with the Weather Research and Forecasting (WRF) model (Skamarock et al. 2019). This is a widely-used model offering a large number of different schemes, both for microphysics and other processes like radiation, convection and boundary layer processes. Apart from the parametrizations, the model resolution is important for the detail level of simulated aspects such as clouds. For cloud-resolving simulations, the horizontal resolution

should be no larger than a few kilometers (Guichard and Couvreux 2017) - in this thesis a resolution of 1 km is used.

## 3.3 Pseudo global warming approach

Few endeavours are as tempting to humankind as to learn about its own future, and it is not only the weather forecast that makes your daily life easier to plan. It is obvious that we humans have more than enough knowledge by now to state that we need to reduce greenhouse gas emissions drastically and fast. Still, improvements in modeling of future climate can contribute to reduced uncertainties in how the impacts of global warming will turn out regionally and help societies to prepare, not only for tomorrow's weather, but also the next generations' climate.

That being stated as an overall motivation, there are many ways to attempt to improve climate forecasts, and one of the larger uncertainties is connected to the radiative effect of clouds and the forcing due to aerosol-cloud interactions (Forster et al. 2021). These processes are getting represented in greater detail in state-of-the-art Earth System Models with proceeding development, but are still highly parametrized, simply because of the large difference between the scales resolved by global models and the scales at which cloud microphysics occur. On smaller model scales, besides downscaling of the results of global models, another approach exists to analyze how specific weather situations would have been different if they had appeared in a warmer future climate. This approach is called pseudo global warming (PGW), and while it comes with its own set of limitations, it is a very convenient way to make use of detailed information from observed clouds in the present by applying a model that has proven useful and correct today to tell us about the future.

In the PGW approach one adds a climate change signal $\Delta A$ to the present-day values of variable $A$ in initial and boundary conditions and then lets the model do the calculations of how this changes this and other variables over the duration of the simulation. In the simplest form, only the variables for air temperature, land-surface temperature and sea-surface temperature are perturbed. In this case the relative humidity must at the same time be kept constant to account for the fact that a warmer atmosphere is able to hold more water vapor (Schär et al. 1996).

# Chapter 4

# Findings/Paper summaries

The research accomplished in this thesis is presented in the following sections. Main findings and conclusions are summarized per paper. Also my individual contributions to the publications are specified per paper as the papers are all co-authored by several people. Paper I and II answer objective 1 from chapter 1 (characterizing occurrence and properties of Arctic cold clouds), paper II and III answer objective 2 (understanding in-cloud processes) and paper IV answers objective 3 (exploring cloud changes with climate change/warming).

## 4.1 Paper I: Observations of cold-cloud properties in the Norwegian Arctic using ground-based and spaceborne lidar

This paper exploits an existing dataset of ground-based lidar measurements from the Norwegian Arctic for the purpose of characterizing middle and high clouds. Given the limited number of observatories in the Arctic providing long-term datasets, the study is a valuable contribution to monitoring cold clouds in that region. It also compares the ground-based results with satellite observations from the same area and observations from different Arctic stations.

### Objectives

- ➔ Use the long-term observational lidar dataset from Andøya to create a cold-cloud climatology for this region and compare with satellite data from the Norwegian Arctic.
- ➔ Explore and demonstrate the capabilities of the tropospheric lidar on Andøya in determining cloud optical properties and phase composition through case studies of ice and mixed-phase clouds.

### Summary

"Cloud properties are important for the surface radiation budget. This study presents cold-cloud observations based on lidar measurements from the Norwegian

Arctic between 2011 and 2017. Using statistical assessments and case studies, we give an overview of the macro- and microphysical properties of these clouds and demonstrate the capabilities of long-term cloud observations in the Norwegian Arctic from the ground-based lidar at Andenes."

Short summary given on the journal's webpage at https://acp.copernicus.org

## Main findings

- The groundbased and the spaceborne lidar agree well on mean cloud top and base heights and thickness in a multiyear comparison as well as in a case study where the same cirrus cloud was observed from above and below as the satellite passed over the ground-based site.
- The depolarization ratio from the ground-based lidar together with multiple-scattering considerations helps to identify ice in a mainly liquid altocumulus cloud and also the vertical distribution of cloud phase.
- Our statistical assessment of cold clouds includes single-layer clouds with cloud base heights between 4000 m and 12000 m and cloud top temperatures below -20 °C. We find that these clouds are on average 2 km thick in the Norwegian Arctic.
- Cold cloud heights are 1-2 km higher in autumn (season with highest clouds) than in spring (lowest clouds).
- Cloud top temperatures are warmest in summer.

## Conclusions and recommendations

Cloud properties and their seasonal cycle in the Norwegian Arctic generally agree well with results from different Arctic stations. For single-layer middle and high clouds, the cloud height statistics from the Norwegian Arctic is very similar observed from the groundbased and spaceborne lidar with slightly lower average cloud top and base heights observed from the satellite. The groundbased lidar at Andøya is capable of in-depth studies of the optical properties and phase composition of cold clouds. A continuation of the dataset from Andøya will be valuable to identify trends in the future.

## Own contributions

I designed the study together with Tim Carlsen and Trude Storelvmo and led the interpretation of the presented case studies. I performed the processing of the lidar data from the ground-based lidar and the statistical analysis of the ground-based lidar data, while Tim Carlsen performed the processing and analysis of the spaceborne lidar data. I wrote the major part of the manuscript including figures.

## 4.2 Paper II: The Ny-Ålesund Aerosol Cloud Experiment (NASCENT): Overview and First Results

This paper gives an overview over the Ny-Ålesund Aerosol Cloud Experiment (NASCENT) which addressed the interplay between aerosols and cloud formation at an Arctic site throughout one year. The paper presents the scope of the campaign including first results. The given objectives will be answered in further detail by follow-up studies based on the collected dataset.

### Objectives

- ➔ Investigate interactions between aerosols, clouds and radiative fluxes at an Arctic site throughout one year.
- ➔ Identify factors that determine whether aerosol particles act as CCN and INPs in the Arctic, in particular chemical properties.
- ➔ Identify the relative importance of INPs and SIP in Arctic mixed-phase clouds under different conditions.

### Summary

The NASCENT campaign was conducted in Ny-Ålesund, Svalbard, between September 2019 and August 2020 and comprised both in-situ and remote sensing measurements. The main findings on the seasonality of meteorological and aerosol properties are presented in this overview article. In addition, one case study is used to highlight the potential of the dataset and supplemented with cloud-resolving simulations with the Weather Research and Forecasting model.

### Main findings

- Low clouds were most frequently of mixed phase, underlining their importance for local climate.
- The observations show clear differences in the molecular composition between the ambient aerosols in total and aerosol particles that were involved in cloud formation.
- Biological particles were active as INPs at warm temperatures.
- During the case study, cloud droplet formation was limited by the availability of CCN.
- During the same case study, SIP contributed significantly to the total ice crystal number concentration.

### Conclusions and recommendations

The NASCENT campaign created a unique and comprehensive dataset. Among the findings most relevant to this thesis are the evidence for periodically very high amounts of secondary ice production in clouds and the characterization of ambient INPs (both in terms of amount and chemical composition). The acquired data will continue to improve the understanding of aerosol-cloud interactions in the Arctic through further analysis and modeling studies. Paper III and IV in this thesis are only two examples of this.

### Own contributions

Both the performance of the NASCENT campaign itself and the writing of the overview paper were a large collaborative effort. My own contribution, i.e. also the contribution of this thesis to the paper, is the modeling section (apart from commenting on the rest of the manuscript). The objective of this part was to assess the agreement between the new observations and a standard weather model as well as a modified model version including the observed CCN and INP concentrations. Although the meteorological situation of the case study as well as the general cloud shape are well represented by the standard model, the microphysical composition is not captured correctly by default. Reducing the number of available INPs leads to excessive graupel production with the chosen microphysics scheme, which is also not in agreement with observations. These issues hint towards the limitations of standard model settings in such pristine environments. Paper III develops this case study further.

## 4.3 Paper III: Simulations of primary and secondary ice production during an Arctic mixed-phase cloud case from the NASCENT campaign

This paper builds on results from paper II and falls within the ongoing trend of growing interest for secondary ice production (see section 2.2). The impacts of secondary ice production are especially visible in regions with low INP concentrations such as Svalbard, making studies in the Arctic interesting for testing new SIP parametrizations in models.

### Objectives

- ➔ Overall: Understanding ice production in Arctic mixed-phase clouds.
- ➔ More specific: Modify the microphysics scheme of a regional weather model such that it represents cloud liquid and ice concentrations inside an Arctic mixed-phase cloud correctly and for the right reasons.

### Summary

"Mixed-phase clouds, i.e. clouds consisting of both ice and supercooled water, are very common in the Arctic. However, how these clouds form is often not correctly represented in standard weather models. We show that both ice crystals concentrations in the cloud and precipitation from the cloud can be improved in the model, when aerosol concentrations are prescribed from observations and more processes for ice multiplication, i.e. the production of new ice particles from existing ice, are added."

Short summary given on the journal's webpage at https://acp.copernicus.org

### Main findings

- Default microphysics schemes get the cloud's water content reasonably right, but for the wrong reasons, i.e. they overestimate cloud nucleation and underestimate SIP.
- The simulated liquid and ice water content as well as ice crystal number concentrations match the observations very well when aerosol concentrations are constrained with observed values and the representations of multiple SIP processes are modified and/or added in the model.
- The improvements in aerosol and SIP representation also improve the precipitation amount simulated by the model.

### Conclusions and recommendations

Secondary ice production is from observations known to be very efficient in pristine environments with few available ice-nucleating particles. Based on our results and earlier studies, we recommend to include collisional breakup and droplet shattering in standard microphysics schemes and, in the case of the Morrison microphysics scheme, lower the mixing ratio thresholds required for rime splintering to occur.

### Own contributions

This study was led by myself and I performed all model simulations, wrote the manuscript and made all figures. The design of the study and the interpretation of the results evolved during frequent exchanges with Trude Storelvmo and Robert Oscar David.

## 4.4 Paper IV: Simulations of the response of an Arctic mixed-phase cloud to aerosol perturbations and warming

Using models that represent cloud processes correctly in present climate is important when assessing cloud responses to a changing climate in the future. The results from paper III are therefore very valuable for this next study. Simulations

of a present-day Arctic mixed-phase cloud in different climate stages are performed applying the improved model from paper III and a climate change scenario taken from the most recent IPCC report. The paper uses the Pseudo Global Warming approach described in section 3.3.
That this paper is included as a draft means that the presentation quality will be further improved before submission to the scientific journal. However, the main scientific content and message are already conveyed in the version in this thesis.

## Objectives

➔ Assess how historical and future warming and aerosol changes influence Arctic mixed-phase clouds.

## Summary

The same cloud case as in paper III is simulated, but now under perturbed environmental conditions. In different simulations, the number of available INPs or/and the ambient temperature is reduced or increased. The near-surface warming levels -4 K, -2 K, +2 K, +4 K and +6 K are simulated and analyzed.

## Main findings

- When INP concentrations are increased by a factor of 10000, the cloud gets optically thinner and emits less longwave radiation to the surface while the outgoing longwave radiation at the top of atmosphere increases.
- The complete removal of INPs results, as expected, in an entirely liquid cloud, but its radiative properties differ little from the control simulation.
- When temperatures are perturbed to a surface warming level of 6 K warmer than today, we find more ice in the cloud. This intriguing finding can be explained by enhanced SIP.
- If the ice content of the cloud increases with warming, the phase change offsets some of the increase in longwave radiation at the surface due to the temperature increase itself.

## Conclusions and recommendations

The direction of cloud phase and radiation changes in response to aerosol perturbations are according to expectations. Regarding temperature perturbations, the results are more complex due to the temperature dependence of secondary ice production. Warming may lead to more ice in a mixed-phase cloud, if the temperature increase leads to a higher liquid water content inside the temperature range in which rime splintering is active. The importance of this effect should in future studies be investigated on larger temporal and spatial scales.

## Own contributions

This study is led by myself, again including that I performed all model simulations, wrote the manuscript and designed the figures. I received guidance from Trude Storelvmo and Øivind Hodnebrog in designing the Pseudo Global Warming simulations and discussed results in addition to with these two also with Robert Oscar David.

# Chapter 5

# Summary, conclusions and outlook

## 5.1 Summary

This thesis connects observations and regional modeling to improve the understanding of Arctic cold clouds. The motivating factor for all parts is to determine these clouds' role in current and future climate. This unifies both the statistical analysis of lidar observations of mid- and high-level clouds in paper I and the pseudo global warming case study in paper IV despite different research tools and methods.

Paper I presents a climatology of cold clouds based on seven years of observations from the present-day climate (years 2011-2017). The presented seasonal variability in cloud height and cloud top temperature may be used to validate global models' representation of Arctic cirrus clouds and has implications for the cloud radiative effect of cirrus clouds throughout the year. However, the observed day-to-day variability is larger than seasonal trends. The groundbased measurements are suitable for detailed studies of the phase composition and optical properties of individual clouds. Regarding studies of Arctic mixed-phase clouds, mainly two limitations exist in the applicability of lidar measurements: First, results are limited to single-layer clouds, and second, low clouds with high liquid water content can often not be analyzed or even measured due to the large attenuation even at short distances from the cloud base and the need to protect the instrument from too large reflected signals.

Low clouds and their properties are therefore measured using different methods during the NASCENT campaign conducted in 2019 and 2020 and described in paper II. Here, different kinds of in-situ measurements play a major role in characterizing cloud phase as well the chemical properties and concentrations of CCN and INPs. My personal contribution to paper II are the simulations performed with the WRF model. In particular for the third objective stated in 4.2, the simulations are an important tool to identify relevant processes for ice formation via both INPs (heterogeneous nucleation) and SIP and their relative importance.

The simulations of the case study from paper II are continued and greatly extended in paper III. One main outcome of this paper is a set of recommendations on the modeling of mixed-phase clouds. We find that in regions with few

available aerosols and in particular particles suitable for cloud droplet or ice crystal nucleation, ice formation in clouds is not necessarily highly underrepresented in total, but dominated by primary ice production where observations suggest that SIP played a dominant role. This misrepresentation might also lead to a misrepresentation of precipitation, in our case an underestimation. To represent SIP in the model in a sufficient amount to match observations of ice crystal numbers, we find that rime splintering must be enhanced and additional processes have to be included (collisional breakup, droplet shattering). Both retrieving an observational constraint on INP concentrations and ice formation via SIP are frequently visited topics in ongoing research, but the combination of both is a new aspect of this study. In paper III, we find that the combined approach is very successful and leads to an improved representation of the cloud including its radiative effect and precipitation from it. The updated scheme now remains to be applied to different cases and larger-scale studies covering different geographical regions and meteorological situations. Even though the modifications were tested for a specific day and place, they are of a general nature in terms of physical principles, suggesting that they are applicable in a more universal manner.

Finally, paper IV analyses how the well-described mixed-phase cloud from paper II and III could change in a different climate. While cloud changes in response to higher and lower INP concentration are more or less as expected (more INPs - more ice; more ice - higher OLR and less GLW), the cloud changes in response to a higher temperature are more intriguing. We find more ice than today at a warming level of +6 K, caused by more efficient rime splintering and subsequent SIP processes. The increased rime splintering is caused by the upward shift in altitude of the temperature region in which rime splintering is active towards the cloud region where the most liquid water is present and thereby the potential for riming is highest.

The following two sections are a synthesis of conclusions from this thesis in a broader research context and an outlook to one ongoing and one upcoming study, respectively, that build on the results achieved in this thesis.

## 5.2 Synthesis of conclusions

Overall, this thesis comprises findings about Arctic cold clouds at different altitude levels. The seasonal cycle of middle and high cold clouds is generally similar between Northern Norway and other Arctic stations. Single-layer clouds are on average 2 km thick and cloud heights are highest in autumn and lowest in spring. The thesis also demonstrates the lidar's ability to discriminate cloud phase inside an altocumulus cloud. Regarding low level clouds, the case studied during the second part of the thesis highlights the importance of secondary ice production. Standard weather models perform reasonably well in representing cloud shape, but are not able to reproduce observed ice particle number concentrations, especially not if INP concentrations are constrained by the low values common in the Arctic. SIP must be enhanced in the model both in terms of the number of included processes and their efficiency. SIP also plays an important role in the phase

composition change of the analyzed mixed-phase cloud in a future warmer climate due to the temperature dependence of rime splintering and the vertical distribution of liquid inside the cloud. As the relation between cloud nucleation and SIP is addressed by more ongoing projects in the broader research community, it will be very interesting to see how the results from this case compare to other studies in the future.

## 5.3 Outlook

### Mixed-phase cloud spatial heterogeneity

Apart from the absolute mass and numbers of liquid water and ice inside a cloud, it is important to know more about how well-mixed mixed-phase clouds actually are in a spatial sense. In-situ observations from aircraft suggest that mixed-phase clouds can be genuinely mixed (with liquid droplets and ice crystals uniformly distributed in a cloud volume) or conditionally mixed (with solid and liquid phase spatially separated into "pockets") (Korolev and Milbrandt 2022). The scales of such pockets vary from 100 km to the lower resolution limit of the measurements which is 100 m (Korolev and Milbrandt 2022). The spatial structure of the cloud phase is very relevant to the microphysical processes, as the WBF process is most efficient under genuinely mixed conditions, indicating that the conversion of liquid to ice would be less influential if the cloud was conditionally mixed. The simulations performed for paper III have already been used to analyze the heterogeneity of this mixed-phase cloud case during the master thesis of Stian Dammann where I was one of the supervisors (Dammann 2023). The results indicate that the changes made in the microphysics scheme's ice formation processes have an impact on the scale on which such pockets occur. While the spatial homogeneity cannot be compared with observations directly as observations are taken in only one place, a comparison of the variability in time is possible, i.e. how often the cloud volume switches between being ice only, liquid only or genuinely mixed. Preliminary results show that this temporal variability agrees much better between observations and simulations when the improved Morrison scheme is used compared to the default version. Stian Dammann is now a PhD student, still at the University of Oslo, and is continuing the research on this topic.

### Secondary ice production in mixed-phase clouds in a larger Arctic region

One of the biggest uncertainties in the implications of the results of the modeling part of this thesis is that it is based on only one case study that is very limited in both space and time. In order to assess both the general performance of the modified scheme and the relationship between SIP and future warming on larger scales in the Arctic, further studies covering a greater domain area and time period are planned. For this, besides the observational data from Svalbard during the NASCENT campaign, also measurement data from our campaigns in Andøya in

2021, 2022 and 2023 will be used to constrain the model, especially regarding CCN and INP concentrations.

# Abbreviations

The following list includes the most important abbreviations and acronyms used both in part I (thesis) and part II (papers I, III and IV). Paper II includes a table listing all abbreviations used there.

| | |
|---|---|
| **ALOMAR** | Arctic lidar observatory for middle atmosphere research |
| **BR** | Breakup during ice-ice collisions |
| **CALIOP** | Cloud-Aerosol Lidar with Orthogonal Polarization |
| **CALIPSO** | Cloud-Aerosol Lidar and Infrared Pathfinder Satellite Observation |
| **CCN** | Cloud condensation nucleus/nuclei |
| **CPR** | Cloud profiling radar |
| **CTH** | Cloud top height |
| **CTT** | Cloud top temperature |
| **DS** | Droplet shattering during freezing |
| **EARLINET** | European Aerosol Research Lidar Network |
| **ERA5** | Reanalysis product created by the European Centre for Medium-Range Weather Forecasts |
| **GLW** | Downward longwave radiation at the surface |
| **ICNC** | Ice crystal number concentration |
| **INP** | Ice-nucleating particle |
| **INPC** | INP concentration |
| **IPCC** | Intergovernmental Panel on Climate Change |
| **IWC** | Ice water content |
| **Lidar** | Active remote sensing optical instrument, actually an acronym for Light Detection and Ranging |
| **LW** | Longwave |
| **LWC** | Liquid water content |
| **MPC** | Mixed-phase cloud |
| **NASCENT** | Ny-Ålesund Aerosol Cloud Experiment |
| **OLR** | Outgoing longwave radiation at the top of atmosphere |
| **RS** | Rime splintering |
| **SIP** | Secondary ice production |
| **SW** | Shortwave |
| **UTC** | Coordinated Universal Time |
| **WRF** | Weather Research and Forecasting model |
| **WBF** | Wegener-Bergeron-Findeisen process |

# Bibliography


Abbatt, J. P. D. et al. (2019). "Overview paper: New insights into aerosol and climate in the Arctic." In: *Atmospheric Chemistry and Physics* 19.4, pp. 2527–2560. DOI: 10.5194/acp-19-2527-2019. URL: https://acp.copernicus.org/articles/19/2527/2019/.

Atlas, R. L., C. S. Bretherton, M. F. Khairoutdinov, and P. N. Blossey (2022). "Hallett-Mossop Rime Splintering Dims Cumulus Clouds Over the Southern Ocean: New Insight From Nudged Global Storm-Resolving Simulations." In: *AGU Advances* 3.2, e2021AV000454. DOI: https://doi.org/10.1029/2021AV000454. URL: https://agupubs.onlinelibrary.wiley.com/doi/abs/10.1029/2021AV000454.

Auer, A H, D L Veal, and J D Marwitz (1969). "Observations of Ice Crystal and Ice Nuclei Concentrations in Stable Cap Clouds." In: *Journal of the Atmospheric Sciences* 26.6, pp. 1342–1343. ISSN: 0022-4928.

Beard, Kenneth V. (1992). "Ice initiation in warm-base convective clouds: An assessment of microphysical mechanisms." In: *Atmospheric Research* 28.2, pp. 125–152. ISSN: 0169-8095. DOI: https://doi.org/10.1016/0169-8095(92)90024-5. URL: https://www.sciencedirect.com/science/article/pii/0169809592900245.

Bergeron, T. (1928). "Über die dreidimensional verknüpfende Wetteranalyse. Erster Teil. Prinzipielle Einführung in das Problem der Luftmassen- und Frontenbildung." In: *Geofys. Publ.* 5.6, pp. 1–118.

Bjordal, Jenny, Trude Storelvmo, Kari Alterskjær, and Tim Carlsen (2020). "Equilibrium climate sensitivity above 5 C plausible due to state-dependent cloud feedback." In: *Nature Geoscience* 13.11, pp. 718–721. DOI: 10.1038/s41561-020-00649-1.

Campbell, James M. and Hugo K. Christenson (2018). "Nucleation- and Emergence-Limited Growth of Ice from Pores." In: *Phys. Rev. Lett.* 120 (16), p. 165701. DOI: 10.1103/PhysRevLett.120.165701. URL: https://link.aps.org/doi/10.1103/PhysRevLett.120.165701.

Carlsen, T. and R. O. David (2022). "Spaceborne Evidence That Ice-Nucleating Particles Influence High-Latitude Cloud Phase." In: *Geophysical Research Letters* 49.14, e2022GL098041. DOI: https://doi.org/10.1029/2022GL098041. URL: https://agupubs.onlinelibrary.wiley.com/doi/abs/10.1029/2022GL098041.

Ceppi, Paulo, Florent Brient, Mark D. Zelinka, and Dennis L. Hartmann (2017). "Cloud feedback mechanisms and their representation in global climate models." In: *WIREs Climate Change* 8.4, e465. DOI: https://doi.org/10.1002/wcc.465. URL: https://wires.onlinelibrary.wiley.com/doi/abs/10.1002/wcc.465.

Choi, Yong-Sang, Chang-Hoi Ho, Chang-Eui Park, Trude Storelvmo, and Ivy Tan (2014). "Influence of cloud phase composition on climate feedbacks." In: *Journal of Geophysical Research: Atmospheres* 119.7, pp. 3687–3700. DOI: https://doi.org/10.1002/2013JD020582. URL: https://agupubs.onlinelibrary.wiley.com/doi/abs/10.1002/2013JD020582.

Cooper, William A. (1986). "Ice Initiation in Natural Clouds." In: *Precipitation Enhancement—A Scientific Challenge*. Boston, MA: American Meteorological Society, pp. 29–32. ISBN: 978-1-935704-17-1. DOI: 10.1007/978-1-935704-17-1_4. URL: https://doi.org/10.1007/978-1-935704-17-1_4.

Curry, Judith A., Julie L. Schramm, William B. Rossow, and David Randall (1996). "Overview of Arctic Cloud and Radiation Characteristics." In: *Journal of Climate* 9.8, pp. 1731–1764. DOI: 10.1175/1520-0442(1996)009<1731:OOACAR>2.0.CO;2. URL: https://journals.ametsoc.org/view/journals/clim/9/8/1520-0442_1996_009_1731_ooacar_2_0_co_2.xml.

D'Amico, Giuseppe, Aldo Amodeo, H Baars, I Binietoglou, Volker Freudenthaler, I Mattis, Ulla Wandinger, and Gelsomina Pappalardo (2015). "EARLINET Single Calculus Chain–overview on methodology and strategy." In: *Atmospheric Measurement Techniques* 8.11, pp. 4891–4916. DOI: 10.5194/amt-8-4891-2015. URL: https://amt.copernicus.org/articles/8/4891/2015/.

Dammann, Stian Leer-Salvesen (2023). *On the Homogeneity of Arctic Mixed-Phase Clouds*. URL: https://www.duo.uio.no/handle/10852/103726.

David, R. O., M. Cascajo-Castresana, K. P. Brennan, M. Rösch, N. Els, J. Werz, V. Weichlinger, L. S. Boynton, S. Bogler, N. Borduas-Dedekind, C. Marcolli, and Z. A. Kanji (2019). "Development of the DRoplet Ice Nuclei Counter Zurich (DRINCZ): validation and application to field-collected snow samples." In: *Atmospheric Measurement Techniques* 12.12, pp. 6865–6888. DOI: 10.5194/amt-12-6865-2019. URL: https://amt.copernicus.org/articles/12/6865/2019/.

David, R. O., J. Fahrni, C. Marcolli, F. Mahrt, D. Brühwiler, and Z. A. Kanji (2020). "The role of contact angle and pore width on pore condensation and freezing." In: *Atmospheric Chemistry and Physics* 20.15, pp. 9419–9440. DOI: 10.5194/acp-20-9419-2020. URL: https://acp.copernicus.org/articles/20/9419/2020/.

David, R. O., C. Marcolli, J. Fahrni, Y. Qiu, Y. A. Perez Sirkin, V. Molinero, F. Mahrt, D. Brühwiler, U. Lohmann, and Z. A. Kanji (2019). "Pore condensation and freezing is responsible for ice formation below water saturation for porous particles." In: *Proceedings of the National Academy of Sciences* 116.17, pp. 8184–8189. DOI: 10.1073/pnas.1813647116. URL: https://www.pnas.org/doi/abs/10.1073/pnas.1813647116.

de Boer, Gijs, Tempei Hashino, and Gregory J. Tripoli (2010). "Ice nucleation through immersion freezing in mixed-phase stratiform clouds: Theory and numerical simulations." In: *Atmospheric Research* 96.2. 15th International Conference on Clouds and Precipitation, pp. 315–324. ISSN: 0169-8095. DOI: https://doi.org/10.1016/j.atmosres.2009.09.012. URL: https://www.sciencedirect.com/science/article/pii/S0169809509002695.

de Boer, Gijs, Hugh Morrison, Matthew D. Shupe, and Richard Hildner (2011). "Evidence of liquid dependent ice nucleation in high-latitude stratiform clouds

from surface remote sensors." In: *Geophysical Research Letters* 38.1. DOI: https://doi.org/10.1029/2010GL046016. URL: https://agupubs.onlinelibrary.wiley.com/doi/abs/10.1029/2010GL046016.

DeMott, P. J., A. J. Prenni, X. Liu, S. M. Kreidenweis, M. D. Petters, C. H. Twohy, M. S. Richardson, T. Eidhammer, and D. C. Rogers (2010). "Predicting global atmospheric ice nuclei distributions and their impacts on climate." In: *Proceedings of the National Academy of Sciences* 107.25, pp. 11217–11222. DOI: 10.1073/pnas.0910818107. URL: https://www.pnas.org/doi/abs/10.1073/pnas.0910818107.

Descamps, Sébastien, Jon Aars, Eva Fuglei, Kit M. Kovacs, Christian Lydersen, Olga Pavlova, Åshild Ø. Pedersen, Virve Ravolainen, and Hallvard Strøm (2017). "Climate change impacts on wildlife in a High Arctic archipelago – Svalbard, Norway." In: *Global Change Biology* 23.2, pp. 490–502. DOI: https://doi.org/10.1111/gcb.13381. URL: https://onlinelibrary.wiley.com/doi/abs/10.1111/gcb.13381.

Etzelmüller, B., T. V. Schuler, K. Isaksen, H. H. Christiansen, H. Farbrot, and R. Benestad (2011). "Modeling the temperature evolution of Svalbard permafrost during the 20th and 21st century." In: *The Cryosphere* 5.1, pp. 67–79. DOI: 10.5194/tc-5-67-2011. URL: https://tc.copernicus.org/articles/5/67/2011/.

Field, P. R., R. P. Lawson, P. R. A. Brown, G. Lloyd, C. Westbrook, D. Moisseev, A. Miltenberger, A. Nenes, A. Blyth, T. Choularton, P. Connolly, J. Buehl, J. Crosier, Z. Cui, C. Dearden, P. J. DeMott, A. Flossmann, A. Heymsfield, Y. Huang, H. Kalesse, Z. A. Kanji, A. Korolev, A. Kirchgaessner, S. Lasher-Trapp, T. Leisner, G. McFarquhar, V. Phillips, J. Stith, and S. Sullivan (2017). "Secondary Ice Production: Current State of the Science and Recommendations for the Future." In: *Meteorological Monographs* 58, pp. 7.1–7.20. DOI: https://doi.org/10.1175/AMSMONOGRAPHS-D-16-0014.1. URL: https://journals.ametsoc.org/view/journals/amsm/58/1/amsmonographs-d-16-0014.1.xml.

Findeisen, W. (1938). "Die kolloidmeteorologischen Vorgänge bei der Niederschlagsbildung 121–133." In: *Meteorologische Zeitschrift* 55, pp. 121–133.

Fletcher, N.H. (1962). *The physics of rainclouds*. Cambridge University Press.

Forster, Piers, Trude Storelvmo, Kyle Armour, William Collins, Jean-Luis Dufresne, David Frame, Daniel J. Lunt, Thorsten Mauritsen, Matthew D. Palmer, Masahiro Watanabe, Martin Wild, and Xuebin Zhang (2021). "The Earth's Energy Budget, Climate Feedbacks, and Climate Sensitivity." In: *Climate Change 2021: The Physical Science Basis. Contribution of Working Group I to the Sixth Assessment Report of the Intergovernmental Panel on Climate Change*. Ed. by Valérie Masson-Delmotte, Panmao Zhai, Anna Pirani, Sarah L. Connors, C. Péan, Sophie Berger, Nada Caud, Y. Chen, Leah Goldfarb, Melissa I. Gomis, Mengtian Huang, Katherine Leitzell, Elisabeth Lonnoy, J. B. Robin Matthews, Thomas K. Maycock, Tim Waterfield, Özge Yelekçi, R. Yu, and Botao Zhou. Cambridge University Press.

Freudenthaler, V. (2016). "About the effects of polarising optics on lidar signals and the Δ90 calibration." In: *Atmospheric Measurement Techniques* 9.9, pp. 4181–4255. DOI: 10.5194/amt-9-4181-2016. URL: https://amt.copernicus.org/articles/9/4181/2016/.

Frioud, Max, Michael Gausa, Gerd Baumgarten, Jon Egill Kristjansson, and Ivan Føre (2006). "New tropospheric lidar system in operation at ALOMAR (69 ◦ N, 16 ◦ E)." In: *Reviewed and Revised Papers of the 23rd International Laser Radar Conference (ILRC)*, pp. 24–28.

Frostenberg, H. C., A. Welti, M. Luhr, J. Savre, E. S. Thomson, and L. Ickes (2023). "The chance of freezing – a conceptional study to parameterize temperature-dependent freezing by including randomness of ice-nucleating particle concentrations." In: *Atmospheric Chemistry and Physics* 23.19, pp. 10883–10900. DOI: 10.5194/acp-23-10883-2023. URL: https://acp.copernicus.org/articles/23/10883/2023/.

Fu, Shizuo, Xin Deng, Matthew D. Shupe, and Huiwen Xue (2019). "A modelling study of the continuous ice formation in an autumnal Arctic mixed-phase cloud case." In: *Atmospheric Research* 228, pp. 77–85. ISSN: 0169-8095. DOI: https://doi.org/10.1016/j.atmosres.2019.05.021. URL: https://www.sciencedirect.com/science/article/pii/S0169809518313905.

Georgakaki, P., G. Sotiropoulou, É. Vignon, A.-C. Billault-Roux, A. Berne, and A. Nenes (2022). "Secondary ice production processes in wintertime alpine mixed-phase clouds." In: *Atmospheric Chemistry and Physics* 22.3, pp. 1965–1988. DOI: 10.5194/acp-22-1965-2022. URL: https://acp.copernicus.org/articles/22/1965/2022/.

Gierens, Klaus M., Marie Monier, and Jean-Francois Gayet (2003). "The deposition coefficient and its role for cirrus clouds." In: *Journal of Geophysical Research: Atmospheres* 108.D2. DOI: https://doi.org/10.1029/2001JD001558. URL: https://agupubs.onlinelibrary.wiley.com/doi/abs/10.1029/2001JD001558.

Gilgen, A., W. T. K. Huang, L. Ickes, D. Neubauer, and U. Lohmann (2018). "How important are future marine and shipping aerosol emissions in a warming Arctic summer and autumn?" In: *Atmospheric Chemistry and Physics* 18.14, pp. 10521–10555. DOI: 10.5194/acp-18-10521-2018. URL: https://acp.copernicus.org/articles/18/10521/2018/.

Gjelsvik, Astrid Bragstad (2022). "Ice Nucleating Particles in Arctic Clouds and Their Impact on Climate." MA thesis. URL: http://urn.nb.no/URN:NBN:no-98231.

Guichard, Françoise and Fleur Couvreux (2017). "A short review of numerical cloud-resolving models." In: *Tellus A: Dynamic Meteorology and Oceanography* 69.1, p. 1373578. DOI: 10.1080/16000870.2017.1373578. URL: https://doi.org/10.1080/16000870.2017.1373578.

Gutiérrez, J.M., R.G. Jones, G.T. Narisma, L.M. Alves, M. Amjad, I.V. Gorodetskaya, M. Grose, N.A.B. Klutse, S. Krakovska, J. Li, D. Martínez-Castro, L.O. Mearns, S.H. Mernild, T. Ngo-Duc, B. van den Hurk, and J.-H. Yoon (2021). "Atlas." In: *Climate Change 2021: The Physical Science Basis. Contribution of Working Group I to the Sixth Assessment Report of the Intergovernmental Panel on Climate Change*. Ed. by V. Masson-Delmotte, P. Zhai, A. Pirani, S.L. Connors, C. Péan, S. Berger, N. Caud, Y. Chen, L. Goldfarb, M.I. Gomis, M. Huang, K. Leitzell, E. Lonnoy, J.B.R. Matthews, T.K. Maycock, T. Waterfield, O. Yelekçi, R. Yu, and B. Zhou. Interactive Atlas available from https://interactive-atlas.ipcc.ch. Cambridge University Press.

Hallett, J and SC Mossop (1974). "Production of secondary ice particles during the riming process." In: *Nature* 249.5452, pp. 26–28.

Hersbach, Hans, Bill Bell, Paul Berrisford, Shoji Hirahara, András Horányi, Joaquín Muñoz-Sabater, Julien Nicolas, Carole Peubey, Raluca Radu, Dinand Schepers, Adrian Simmons, Cornel Soci, Saleh Abdalla, Xavier Abellan, Gianpaolo Balsamo, Peter Bechtold, Gionata Biavati, Jean Bidlot, Massimo Bonavita, Giovanna De Chiara, Per Dahlgren, Dick Dee, Michail Diamantakis, Rossana Dragani, Johannes Flemming, Richard Forbes, Manuel Fuentes, Alan Geer, Leo Haimberger, Sean Healy, Robin J. Hogan, Elías Hólm, Marta Janisková, Sarah Keeley, Patrick Laloyaux, Philippe Lopez, Cristina Lupu, Gabor Radnoti, Patricia de Rosnay, Iryna Rozum, Freja Vamborg, Sebastien Villaume, and Jean-Noël Thépaut (2020). "The ERA5 global reanalysis." In: *Quarterly Journal of the Royal Meteorological Society* 146.730, pp. 1999–2049. DOI: https://doi.org/10.1002/qj.3803. URL: https://rmets.onlinelibrary.wiley.com/doi/abs/10.1002/qj.3803.

Heymsfield, Andrew J., Martina Krämer, Anna Luebke, Phil Brown, Daniel J. Cziczo, Charmaine Franklin, Paul Lawson, Ulrike Lohmann, Greg McFarquhar, Zbigniew Ulanowski, and Kristof Van Tricht (2017). "Cirrus Clouds." In: *Meteorological Monographs* 58, pp. 2.1–2.26. DOI: 10.1175/AMSMONOGRAPHS-D-16-0010.1. URL: https://journals.ametsoc.org/view/journals/amsm/58/1/amsmonographs-d-16-0010.1.xml.

Hoose, Corinna, Jón Egill Kristjánsson, Jen-Ping Chen, and Anupam Hazra (2010). "A Classical-Theory-Based Parameterization of Heterogeneous Ice Nucleation by Mineral Dust, Soot, and Biological Particles in a Global Climate Model." In: *Journal of the Atmospheric Sciences* 67.8, pp. 2483–2503. DOI: 10.1175/2010JAS3425.1. URL: https://journals.ametsoc.org/view/journals/atsc/67/8/2010jas3425.1.xml.

Humlum, Ole, Arne Instanes, and Johan Ludvig Sollid (2003). "Permafrost in Svalbard: a review of research history, climatic background and engineering challenges." In: *Polar Research* 22.2, pp. 191–215. DOI: https://doi.org/10.1111/j.1751-8369.2003.tb00107.x. URL: https://onlinelibrary.wiley.com/doi/abs/10.1111/j.1751-8369.2003.tb00107.x.

Ickes, L., G. C. E. Porter, R. Wagner, M. P. Adams, S. Bierbauer, A. K. Bertram, M. Bilde, S. Christiansen, A. M. L. Ekman, E. Gorokhova, K. Höhler, A. A. Kiselev, C. Leck, O. Möhler, B. J. Murray, T. Schiebel, R. Ullrich, and M. E. Salter (2020). "The ice-nucleating activity of Arctic sea surface microlayer samples and marine algal cultures." In: *Atmospheric Chemistry and Physics* 20.18, pp. 11089–11117. DOI: 10.5194/acp-20-11089-2020. URL: https://acp.copernicus.org/articles/20/11089/2020/.

Ickes, L., A. Welti, and U. Lohmann (2017). "Classical nucleation theory of immersion freezing: sensitivity of contact angle schemes to thermodynamic and kinetic parameters." In: *Atmospheric Chemistry and Physics* 17.3, pp. 1713–1739. DOI: 10.5194/acp-17-1713-2017. URL: https://acp.copernicus.org/articles/17/1713/2017/.

Intrieri, Janet M., C. W. Fairall, M. D. Shupe, P. O. G. Persson, E. L. Andreas, P. S. Guest, and R. E. Moritz (2002). "An annual cycle of Arctic surface cloud forcing

at SHEBA." In: *Journal of Geophysical Research: Oceans* 107.C10, SHE–13. DOI: https://doi.org/10.1029/2000JC000439. URL: https://agupubs.onlinelibrary.wiley.com/doi/abs/10.1029/2000JC000439.

IPCC (2021). "Figure SPM.8 in IPCC, 2021: Summary for Policymakers." In: *Climate Change 2021: The Physical Science Basis. Contribution of Working Group I to the Sixth Assessment Report of the Intergovernmental Panel on Climate Change*. Cambridge University Press, Cambridge, UK and New York, NY, USA, 332. DOI: 10.1017/9781009157896.001.

IPCC, Intergovernmental Panel on Climate Change (1988). Accessed on 24.02.2024. URL: https://www.ipcc.ch/.

Irish, Victoria E., Sarah J. Hanna, Megan D. Willis, Swarup China, Jennie L. Thomas, Jeremy J. B. Wentzell, Ana Cirisan, Meng Si, W. Richard Leaitch, Jennifer G. Murphy, Jonathan P. D. Abbatt, Alexander Laskin, Eric Girard, and Allan K. Bertram (2019). "Ice nucleating particles in the marine boundary layer in the Canadian Arctic during summer 2014." In: *Atmospheric Chemistry and Physics* 19.2, pp. 1027–1039. DOI: 10.5194/acp-19-1027-2019. URL: https://acp.copernicus.org/articles/19/1027/2019/.

Iturbide, Maialen, Jesús Fernández, José Manuel Gutiérrez, Joaquín Bedia, Ezequiel Cimadevilla, Javier Díez-Sierra, Rodrigo Manzanas, Ana Casanueva, Jorge Baño-Medina, Josipa Milovac, Sixto Herrera, Antonio S. Cofiño, Daniel San Martín, Markel García-Díez, Mathias Hauser, David Huard, and Özge Yelekci (2021). *Repository supporting the implementation of FAIR principles in the IPCC-WGI Atlas*. Version v2.0-final. DOI: 10.5281/zenodo.5171760. URL: https://doi.org/10.5281/zenodo.5171760.

Järvinen, Emma, Christina S. McCluskey, Fritz Waitz, Martin Schnaiter, Aaron Bansemer, Charles G. Bardeen, Andrew Gettelman, Andrew Heymsfield, Jeffrey L. Stith, Wei Wu, John J. D'Alessandro, Greg M. McFarquhar, Minghui Diao, Joseph A. Finlon, Thomas C. J. Hill, Ezra J. T. Levin, Kathryn A. Moore, and P. J. DeMott (2022). "Evidence for Secondary Ice Production in Southern Ocean Maritime Boundary Layer Clouds." In: *Journal of Geophysical Research: Atmospheres* 127.16, e2021JD036411. DOI: https://doi.org/10.1029/2021JD036411. URL: https://agupubs.onlinelibrary.wiley.com/doi/abs/10.1029/2021JD036411.

Kanji, Zamin A., Luis A. Ladino, Heike Wex, Yvonne Boose, Monika Burkert-Kohn, Daniel J. Cziczo, and Martina Krämer (2017). "Overview of Ice Nucleating Particles." In: *Meteorological Monographs* 58, pp. 1.1–1.33. DOI: https://doi.org/10.1175/AMSMONOGRAPHS-D-16-0006.1. URL: https://journals.ametsoc.org/view/journals/amsm/58/1/amsmonographs-d-16-0006.1.xml.

Karalis, Michail, Georgia Sotiropoulou, Steven J Abel, Elissavet Bossioli, Paraskevi Georgakaki, Georgia Methymaki, Athanasios Nenes, and Maria Tombrou (2022). "Effects of secondary ice processes on a stratocumulus to cumulus transition during a cold-air outbreak." In: *Atmospheric Research* 277, p. 106302. DOI: https://doi.org/10.1016/j.atmosres.2022.106302. URL: https://www.sciencedirect.com/science/article/pii/S0169809522002885.

Kärcher, B., P. J. DeMott, E. J. Jensen, and J. Y. Harrington (2022). "Studies on the Competition Between Homogeneous and Heterogeneous Ice Nucleation in Cirrus Formation." In: *Journal of Geophysical Research: Atmospheres* 127.3, e2021JD035805. DOI: https://doi.org/10.1029/2021JD035805. URL: https://agupubs.onlinelibrary.wiley.com/doi/abs/10.1029/2021JD035805.

Kikuchi, Katsuhiro, Takao Kameda, Keiji Higuchi, and Akira Yamashita (2013). "A global classification of snow crystals, ice crystals, and solid precipitation based on observations from middle latitudes to polar regions." In: *Atmospheric Research* 132-133, pp. 460–472. ISSN: 0169-8095. DOI: https://doi.org/10.1016/j.atmosres.2013.06.006. URL: https://www.sciencedirect.com/science/article/pii/S0169809513001841.

Klett, James D (1981). "Stable analytical inversion solution for processing lidar returns." In: *Applied optics* 20.2, pp. 211–220.

Knopf, Daniel A., Israel Silber, Nicole Riemer, Ann M. Fridlind, and Andrew S. Ackerman (2023). "A 1D Model for Nucleation of Ice From Aerosol Particles: An Application to a Mixed-Phase Arctic Stratus Cloud Layer." In: *Journal of Advances in Modeling Earth Systems* 15.10, e2023MS003663. DOI: https://doi.org/10.1029/2023MS003663. URL: https://agupubs.onlinelibrary.wiley.com/doi/abs/10.1029/2023MS003663.

Komurcu, Muge, Trude Storelvmo, Ivy Tan, Ulrike Lohmann, Yuxing Yun, Joyce E Penner, Yong Wang, Xiaohong Liu, and Toshihiko Takemura (2014). "Intercomparison of the cloud water phase among global climate models." In: *Journal of Geophysical Research: Atmospheres* 119.6, pp. 3372–3400. DOI: https://doi.org/10.1002/2013JD021119. URL: https://agupubs.onlinelibrary.wiley.com/doi/abs/10.1002/2013JD021119.

Korolev, Alexei, I. Heckman, M. Wolde, A. S. Ackerman, A. M. Fridlind, L. A. Ladino, R. P. Lawson, J. Milbrandt, and E. Williams (2020). "A new look at the environmental conditions favorable to secondary ice production." In: *Atmospheric Chemistry and Physics* 20.3, pp. 1391–1429. DOI: 10.5194/acp-20-1391-2020. URL: https://acp.copernicus.org/articles/20/1391/2020/.

Korolev, Alexei and Thomas Leisner (2020). "Review of experimental studies of secondary ice production." In: *Atmospheric Chemistry and Physics* 20.20, pp. 11767–11797. DOI: 10.5194/acp-20-11767-2020. URL: https://acp.copernicus.org/articles/20/11767/2020/.

Korolev, Alexei and Jason Milbrandt (2022). "How Are Mixed-Phase Clouds Mixed?" In: *Geophysical Research Letters* 49.18, e2022GL099578. DOI: https://doi.org/10.1029/2022GL099578. URL: https://agupubs.onlinelibrary.wiley.com/doi/abs/10.1029/2022GL099578.

Li, Guangyu, Jörg Wieder, Julie T. Pasquier, Jan Henneberger, and Zamin A. Kanji (2022). "Predicting atmospheric background number concentration of ice-nucleating particles in the Arctic." In: *Atmospheric Chemistry and Physics* 22.21, pp. 14441–14454. DOI: 10.5194/acp-22-14441-2022. URL: https://acp.copernicus.org/articles/22/14441/2022/.

Marcolli, C. (2014). "Deposition nucleation viewed as homogeneous or immersion freezing in pores and cavities." In: *Atmospheric Chemistry and Physics* 14.4,

pp. 2071–2104. DOI: 10.5194/acp-14-2071-2014. URL: https://acp.copernicus.org/articles/14/2071/2014/.

Marelle, L., J. L. Thomas, J.-C. Raut, K. S. Law, J.-P. Jalkanen, L. Johansson, A. Roiger, H. Schlager, J. Kim, A. Reiter, and B. Weinzierl (2016). "Air quality and radiative impacts of Arctic shipping emissions in the summertime in northern Norway: from the local to the regional scale." In: *Atmospheric Chemistry and Physics* 16.4, pp. 2359–2379. DOI: 10.5194/acp-16-2359-2016. URL: https://acp.copernicus.org/articles/16/2359/2016/.

Matus, Alexander V. and Tristan S. L'Ecuyer (2017). "The role of cloud phase in Earth's radiation budget." In: *Journal of Geophysical Research: Atmospheres* 122.5, pp. 2559–2578. DOI: https://doi.org/10.1002/2016JD025951. URL: https://agupubs.onlinelibrary.wiley.com/doi/abs/10.1002/2016JD025951.

McCluskey, C. S., T. C. J. Hill, R. S. Humphries, A. M. Rauker, S. Moreau, P. G. Strutton, S. D. Chambers, A. G. Williams, I. McRobert, J. Ward, M. D. Keywood, J. Harnwell, W. Ponsonby, Z. M. Loh, P. B. Krummel, A. Protat, S. M. Kreidenweis, and P. J. DeMott (2018). "Observations of Ice Nucleating Particles Over Southern Ocean Waters." In: *Geophysical Research Letters* 45.21, pp. 11, 989–11, 997. DOI: https://doi.org/10.1029/2018GL079981. URL: https://agupubs.onlinelibrary.wiley.com/doi/abs/10.1029/2018GL079981.

Meyers, M. P., P. J. DeMott, and W. R Cotton (1992). "New primary ice-nucleation parameterizations in an explicit cloud model." In: *Journal of Applied Meteorology and Climatology* 31.7, pp. 708–721. DOI: 10.1175/1520-0450(1992)031<0708:NPINPI>2.0.CO;2.

Miller, Nathaniel B., Matthew D. Shupe, Christopher J. Cox, Von P. Walden, David D. Turner, and Konrad Steffen (2015). "Cloud Radiative Forcing at Summit, Greenland." In: *Journal of Climate* 28.15, pp. 6267–6280. DOI: 10.1175/JCLI-D-15-0076.1. URL: https://journals.ametsoc.org/view/journals/clim/28/15/jcli-d-15-0076.1.xml.

Moore, R. H., V. A. Karydis, S. L. Capps, T. L. Lathem, and A. Nenes (2013). "Droplet number uncertainties associated with CCN: an assessment using observations and a global model adjoint." In: *Atmospheric Chemistry and Physics* 13.8, pp. 4235–4251. DOI: 10.5194/acp-13-4235-2013. URL: https://acp.copernicus.org/articles/13/4235/2013/.

Motos, G., G. Freitas, P. Georgakaki, J. Wieder, G. Li, W. Aas, C. Lunder, R. Krejci, J. T. Pasquier, J. Henneberger, R. O. David, C. Ritter, C. Mohr, P. Zieger, and A. Nenes (2023). "Aerosol and dynamical contributions to cloud droplet formation in Arctic low-level clouds." In: *Atmospheric Chemistry and Physics* 23.21, pp. 13941–13956. DOI: 10.5194/acp-23-13941-2023. URL: https://acp.copernicus.org/articles/23/13941/2023/.

Noel, Vincent, Helene Chepfer, Guy Ledanois, Arnaud Delaval, and Pierre H. Flamant (2002). "Classification of particle effective shape ratios in cirrus clouds based on the lidar depolarization ratio." In: *Appl. Opt.* 41.21, pp. 4245–4257. DOI: 10.1364/AO.41.004245. URL: http://ao.osa.org/abstract.cfm?URI=ao-41-21-4245.

Pasquier, Julie T., Jan Henneberger, Fabiola Ramelli, Annika Lauber, Robert Oscar David, Jörg Wieder, Tim Carlsen, Rosa Gierens, Marion Maturilli, and Ulrike Lohmann (2022). "Conditions favorable for secondary ice production in Arctic mixed-phase clouds." In: *Atmospheric Chemistry and Physics* 22.23, pp. 15579–15601. DOI: 10.5194/acp-22-15579-2022. URL: https://acp.copernicus.org/articles/22/15579/2022/.

Peters, G. P., T. B. Nilssen, L. Lindholt, M. S. Eide, S. Glomsrød, L. I. Eide, and J. S. Fuglestvedt (2011). "Future emissions from shipping and petroleum activities in the Arctic." In: *Atmospheric Chemistry and Physics* 11.11, pp. 5305–5320. DOI: 10.5194/acp-11-5305-2011. URL: https://acp.copernicus.org/articles/11/5305/2011/.

Phillips, Vaughan T. J., Sachin Patade, Julie Gutierrez, and Aaron Bansemer (2018). "Secondary Ice Production by Fragmentation of Freezing Drops: Formulation and Theory." In: *Journal of the Atmospheric Sciences* 75.9, pp. 3031–3070. DOI: https://doi.org/10.1175/JAS-D-17-0190.1. URL: https://journals.ametsoc.org/view/journals/atsc/75/9/jas-d-17-0190.1.xml.

Phillips, Vaughan T. J., Jun-Ichi Yano, Marco Formenton, Eyal Ilotoviz, Vijay Kanawade, Innocent Kudzotsa, Jiming Sun, Aaron Bansemer, Andrew G. Detwiler, Alexander Khain, and Sarah A. Tessendorf (2017). "Ice Multiplication by Breakup in Ice–Ice Collisions. Part II: Numerical Simulations." In: *Journal of the Atmospheric Sciences* 74.9, pp. 2789–2811. DOI: https://doi.org/10.1175/JAS-D-16-0223.1. URL: https://journals.ametsoc.org/view/journals/atsc/74/9/jas-d-16-0223.1.xml.

Reutter, P., H. Su, J. Trentmann, M. Simmel, D. Rose, S. S. Gunthe, H. Wernli, M. O. Andreae, and U. Pöschl (2009). "Aerosol- and updraft-limited regimes of cloud droplet formation: influence of particle number, size and hygroscopicity on the activation of cloud condensation nuclei (CCN)." In: *Atmospheric Chemistry and Physics* 9.18, pp. 7067–7080. DOI: 10.5194/acp-9-7067-2009. URL: https://acp.copernicus.org/articles/9/7067/2009/.

Sassen, Kenneth (1991). "The polarization lidar technique for cloud research: A review and current assessment." In: *Bulletin of the American Meteorological Society* 72.12, pp. 1848–1866. DOI: 10.1175/1520-0477(1991)072<1848:TPLTFC>2.0.CO;2. URL: https://journals.ametsoc.org/view/journals/bams/2/12/1520-0477_1991_072_1848_tpltfc_2_0_co_2.xml.

Sassen, Kenneth and Sally Benson (2001). "A midlatitude cirrus cloud climatology from the Facility for Atmospheric Remote Sensing. Part II: Microphysical properties derived from lidar depolarization." In: *Journal of the Atmospheric Sciences* 58.15, pp. 2103–2112. DOI: 10.1175/1520-0469(2001)058<2103:AMCCCF>2.0.CO;2. URL: https://journals.ametsoc.org/view/journals/atsc/8/15/1520-0469_2001_058_2103_amcccf_2.0.co_2.xml.

Schär, Christoph, Christoph Frei, Daniel Lüthi, and Huw C. Davies (1996). "Surrogate climate-change scenarios for regional climate models." In: *Geophysical Research Letters* 23.6, pp. 669–672. DOI: https://doi.org/10.1029/96GL00265. URL: https://agupubs.onlinelibrary.wiley.com/doi/abs/10.1029/96GL00265.

Schneider, J., K. Höhler, P. Heikkilä, J. Keskinen, B. Bertozzi, P. Bogert, T. Schorr, N. S. Umo, F. Vogel, Z. Brasseur, Y. Wu, S. Hakala, J. Duplissy, D. Moisseev,

M. Kulmala, M. P. Adams, B. J. Murray, K. Korhonen, L. Hao, E. S. Thomson, D. Castarède, T. Leisner, T. Petäjä, and O. Möhler (2021). "The seasonal cycle of ice-nucleating particles linked to the abundance of biogenic aerosol in boreal forests." In: *Atmospheric Chemistry and Physics* 21.5, pp. 3899–3918. DOI: 10.5194/acp-21-3899-2021. URL: https://acp.copernicus.org/articles/21/3899/2021/.

Shi, Y., X. Liu, M. Wu, X. Zhao, Z. Ke, and H. Brown (2022). "Relative importance of high-latitude local and long-range-transported dust for Arctic ice-nucleating particles and impacts on Arctic mixed-phase clouds." In: *Atmospheric Chemistry and Physics* 22.4, pp. 2909–2935. DOI: 10.5194/acp-22-2909-2022. URL: https://acp.copernicus.org/articles/22/2909/2022/.

Shupe, Matthew D. and Janet M. Intrieri (2004). "Cloud Radiative Forcing of the Arctic Surface: The Influence of Cloud Properties, Surface Albedo, and Solar Zenith Angle." In: *Journal of Climate* 17.3, pp. 616–628. DOI: 10.1175/1520-0442(2004)017<0616:CRFOTA>2.0.CO;2. URL: https://journals.ametsoc.org/view/journals/clim/17/3/1520-0442_2004_017_0616_crfota_2.0.co_2.xml.

Sinclair, Victoria A., Dmitri Moisseev, and Annakaisa von Lerber (2016). "How dual-polarization radar observations can be used to verify model representation of secondary ice." In: *Journal of Geophysical Research: Atmospheres* 121.18, pp. 10, 954–10, 970. DOI: https://doi.org/10.1002/2016JD025381. URL: https://agupubs.onlinelibrary.wiley.com/doi/abs/10.1002/2016JD025381.

Skamarock, William C, Joseph B Klemp, Jimy Dudhia, David O Gill, Zhiquan Liu, Judith Berner, Wei Wang, Jordan G Powers, Michael G Duda, Dale M Barker, et al. (2019). "A description of the advanced research WRF model version 4." In: *National Center for Atmospheric Research: Boulder, CO, USA*, p. 145. URL: http://dx.doi.org/10.5065/1dfh-6p97.

Solomon, A., G. de Boer, J. M. Creamean, A. McComiskey, M. D. Shupe, M. Maahn, and C. Cox (2018). "The relative impact of cloud condensation nuclei and ice nucleating particle concentrations on phase partitioning in Arctic mixed-phase stratocumulus clouds." In: *Atmospheric Chemistry and Physics* 18.23, pp. 17047–17059. DOI: 10.5194/acp-18-17047-2018. URL: https://acp.copernicus.org/articles/18/17047/2018/.

Sotiropoulou, G., S. Sullivan, J. Savre, G. Lloyd, T. Lachlan-Cope, A. M. L. Ekman, and A. Nenes (2020). "The impact of secondary ice production on Arctic stratocumulus." In: *Atmospheric Chemistry and Physics* 20.3, pp. 1301–1316. DOI: 10.5194/acp-20-1301-2020. URL: https://acp.copernicus.org/articles/20/1301/2020/.

Sotiropoulou, G., É. Vignon, G. Young, H. Morrison, S. J. O'Shea, T. Lachlan-Cope, A. Berne, and A. Nenes (2021). "Secondary ice production in summer clouds over the Antarctic coast: an underappreciated process in atmospheric models." In: *Atmospheric Chemistry and Physics* 21.2, pp. 755–771. DOI: 10.5194/acp-21-755-2021. URL: https://acp.copernicus.org/articles/21/755/2021/.

Storelvmo, Trude (2017). "Aerosol Effects on Climate via Mixed-Phase and Ice Clouds." In: *Annual Review of Earth and Planetary Sciences* 45.1, pp. 199–222. DOI: 10.1146/annurev-earth-060115-012240. URL: https://doi.org/10.1146/annurev-earth-060115-012240.

Storelvmo, Trude and Ivy Tan (2015). "The Wegener–Bergeron–Findeisen process—Its discovery and vital importance for weather and climate." In: *Meteorologische Zeitschrift* 24.4, pp. 455–461. DOI: 10.1127/metz/2015/0626.

Stull, Ronald B (2015). *Practical meteorology: an algebra-based survey of atmospheric science*. University of British Columbia. Chap. 7. URL: https://openlibrary-repo.ecampusontario.ca/jspui/handle/123456789/405.

Tan, Ivy and Trude Storelvmo (2019). "Evidence of Strong Contributions From Mixed-Phase Clouds to Arctic Climate Change." In: *Geophysical Research Letters* 46.5, pp. 2894–2902. DOI: https://doi.org/10.1029/2018GL081871. eprint: https://agupubs.onlinelibrary.wiley.com/doi/pdf/10.1029/2018GL081871. URL: https://agupubs.onlinelibrary.wiley.com/doi/abs/10.1029/2018GL081871.

Tan, Ivy, Trude Storelvmo, and Yong-Sang Choi (2014). "Spaceborne lidar observations of the ice-nucleating potential of dust, polluted dust, and smoke aerosols in mixed-phase clouds." In: *Journal of Geophysical Research: Atmospheres* 119.11, pp. 6653–6665. DOI: https://doi.org/10.1002/2013JD021333. URL: https://agupubs.onlinelibrary.wiley.com/doi/abs/10.1002/2013JD021333.

Tan, Ivy, Trude Storelvmo, and Mark D. Zelinka (2016). "Observational constraints on mixed-phase clouds imply higher climate sensitivity." In: *Science* 352.6282, pp. 224–227. DOI: 10.1126/science.aad5300. URL: https://www.science.org/doi/abs/10.1126/science.aad5300.

Twomey, Sean (1977). "The influence of pollution on the shortwave albedo of clouds." In: *Journal of the atmospheric sciences* 34.7, pp. 1149–1152.

Vali, G., P. J. DeMott, O. Möhler, and T. F. Whale (2015). "Technical Note: A proposal for ice nucleation terminology." In: *Atmospheric Chemistry and Physics* 15.18, pp. 10263–10270. DOI: 10.5194/acp-15-10263-2015. URL: https://acp.copernicus.org/articles/15/10263/2015/.

Wandinger, Ulla (2005a). "Introduction to lidar." In: *Lidar: Range-Resolved Optical Remote Sensing of the Atmosphere*. Springer, pp. 1–18.

— (2005b). "Raman Lidar." In: *Lidar: Range-Resolved Optical Remote Sensing of the Atmosphere*. Springer, pp. 241–271.

Wegener, Alfred (1911). *Thermodynamik der Atmosphäre*. JA Barth.

Wieder, J., C. Mignani, M. Schär, L. Roth, M. Sprenger, J. Henneberger, U. Lohmann, C. Brunner, and Z. A. Kanji (2022). "Unveiling atmospheric transport and mixing mechanisms of ice-nucleating particles over the Alps." In: *Atmospheric Chemistry and Physics* 22.5, pp. 3111–3130. DOI: 10.5194/acp-22-3111-2022. URL: https://acp.copernicus.org/articles/22/3111/2022/.

Wilson, Theodore W., Luis A. Ladino, Peter A. Alpert, Mark N. Breckels, Ian M. Brooks, Jo Browse, Susannah M. Burrows, Kenneth S. Carslaw, J. Alex Huffman, Christopher Judd, Wendy P. Kilthau, Ryan H. Mason, Gordon McFiggans, Lisa A. Miller, Juan J. Nájera, Elena Polishchuk, Stuart Rae, Corinne L. Schiller, Meng Si, Jesús Vergara Temprado, Thomas F. Whale, Jenny P. S. Wong, Oliver Wurl, Jacqueline D. Yakobi-Hancock, Jonathan P. D. Abbatt, Josephine Y. Aller, Allan K. Bertram, Daniel A. Knopf, and Benjamin J. Murray (2015). "A marine biogenic source of atmospheric ice-

nucleating particles." In: *Nature* 525.7568, pp. 234–238. ISSN: 1476-4687. DOI: 10.1038/nature14986. URL: https://doi.org/10.1038/nature14986.

Winker, David M, Mark A Vaughan, Ali Omar, Yongxiang Hu, Kathleen A Powell, Zhaoyan Liu, William H Hunt, and Stuart A Young (2009). "Overview of the CALIPSO mission and CALIOP data processing algorithms." In: *Journal of Atmospheric and Oceanic Technology* 26.11, pp. 2310–2323. DOI: 10.1175/2009JTECHA1281.1.

Young, G., P. J. Connolly, H. M. Jones, and T. W. Choularton (2017). "Microphysical sensitivity of coupled springtime Arctic stratocumulus to modelled primary ice over the ice pack, marginal ice, and ocean." In: *Atmospheric Chemistry and Physics* 17.6, pp. 4209–4227. DOI: 10.5194/acp-17-4209-2017. URL: https://acp.copernicus.org/articles/17/4209/2017/.

Young, G., T. Lachlan-Cope, S. J. O'Shea, C. Dearden, C. Listowski, K. N. Bower, T. W. Choularton, and M. W. Gallagher (2019). "Radiative Effects of Secondary Ice Enhancement in Coastal Antarctic Clouds." In: *Geophysical Research Letters* 46.4, pp. 2312–2321. DOI: https://doi.org/10.1029/2018GL080551. URL: https://agupubs.onlinelibrary.wiley.com/doi/abs/10.1029/2018GL080551.

Zelinka, Mark D., Timothy A. Myers, Daniel T. McCoy, Stephen Po-Chedley, Peter M. Caldwell, Paulo Ceppi, Stephen A. Klein, and Karl E. Taylor (2020). "Causes of Higher Climate Sensitivity in CMIP6 Models." In: *Geophysical Research Letters* 47.1, e2019GL085782. DOI: https://doi.org/10.1029/2019GL085782. URL: https://agupubs.onlinelibrary.wiley.com/doi/abs/10.1029/2019GL085782.

Zhang, Yuanchong, William B. Rossow, Andrew A. Lacis, Valdar Oinas, and Michael I. Mishchenko (2004). "Calculation of radiative fluxes from the surface to top of atmosphere based on ISCCP and other global data sets: Refinements of the radiative transfer model and the input data." In: *Journal of Geophysical Research: Atmospheres* 109.D19. DOI: https://doi.org/10.1029/2003JD004457. URL: https://agupubs.onlinelibrary.wiley.com/doi/abs/10.1029/2003JD004457.

Zhao, X., X. Liu, V. T. J. Phillips, and S. Patade (2021). "Impacts of secondary ice production on Arctic mixed-phase clouds based on ARM observations and CAM6 single-column model simulations." In: *Atmospheric Chemistry and Physics* 21.7, pp. 5685–5703. DOI: 10.5194/acp-21-5685-2021. URL: https://acp.copernicus.org/articles/21/5685/2021/.

# List of Figures

# Part II

# Papers

# Paper I

# Observations of cold-cloud properties in the Norwegian Arctic using ground-based and spaceborne lidar

I

Atmos. Chem. Phys., 22, 9537–9551, 2022
https://doi.org/10.5194/acp-22-9537-2022


Atmospheric Chemistry and Physics
Open Access
EGU



# Observations of cold-cloud properties in the Norwegian Arctic using ground-based and spaceborne lidar

**Britta Schäfer[1], Tim Carlsen[1], Ingrid Hanssen[2], Michael Gausa[2], and Trude Storelvmo[1,3]**

[1]Department of Geosciences, University of Oslo, Oslo, Norway
[2]Andøya Space, Andenes, Norway
[3]Business School, Nord University, Bodø, Norway

**Correspondence:** Britta Schäfer (britta.schafer@geo.uio.no)

Received: 21 December 2021 – Discussion started: 18 February 2022
Revised: 6 June 2022 – Accepted: 1 July 2022 – Published: 25 July 2022

**Abstract.** The role of clouds in the surface radiation budget is particularly complex in the rapidly changing Arctic. However, despite their importance, long-term observations of Arctic clouds are relatively sparse. Here, we present observations of cold clouds based on 7 years (2011–2017) of ground-based lidar observations at the Arctic Lidar Observatory for Middle Atmosphere Research (ALOMAR) in Andenes in the Norwegian Arctic. In two case studies, we assess (1) the agreement between a co-located cirrus cloud observations from the ground-based lidar and the spaceborne lidar aboard the Cloud-Aerosol Lidar and Infrared Pathfinder Satellite Observation (CALIPSO) satellite and (2) the ground-based lidar's capability to determine the cloud phase in mixed-phase clouds from depolarization measurements. We then compute multiyear statistics of cold clouds from both platforms with respect to their occurrence, cloud top and base height, cloud top temperature, and thermodynamic phase for the 2011–2017 period. We find that satellite- and ground-based observations agree well with respect to the coincident cirrus measurement and that the vertical phase distribution within a liquid-topped mixed-phase cloud could be identified from depolarization measurements. On average, 8 % of all satellite profiles were identified as single-layer cold clouds with no apparent seasonal differences. The average cloud top and base heights, combining the ground-based and satellite measurements, are 9.1 and 6.9 km, respectively, resulting in an average thickness of 2.2 km. Seasonal differences between the average top and base heights are on the order of 1–2 km and are largest when comparing fall (highest) and spring (lowest). However, seasonal variations are small compared with the observed day-to-day variability. Cloud top temperatures agree well between both platforms, with warmer cloud top temperatures in summer. The presented study demonstrates the capabilities of long-term cloud observations in the Norwegian Arctic from the ground-based lidar at Andenes.

## 1 Introduction

Clouds play an important role in the Earth's radiative energy budget and hydrological cycle. While clouds cool the surface by scattering incoming shortwave (SW) radiation back to space, they also warm the surface by absorbing and emitting longwave (LW) radiation. The balance of these two processes determines the net effect of clouds on the surface radiation budget and is mainly determined by the cloud's macrophysical (e.g., occurrence, cloud altitude, vertical extent, and optical thickness) and microphysical (e.g., thermodynamic phase, water content, and particle size and shape) properties. Due to their high altitude and low temperature, cirrus clouds generally have a warming effect on the climate by reducing the emission of LW radiation to space, whereas low-level clouds contribute to cooling by reflecting incoming SW radiation. This has been quantified by Matus and L'Ecuyer (2017) on a global scale using satellite observations. They highlight the crucial role of a cloud's thermodynamic phase composition in their radiative properties (e.g., Sun and Shine, 1994). The amount of liquid droplets and ice crystals in a

cloud further controls the formation of precipitation and influences cloud lifetime (e.g., Korolev et al., 2017).

In a warming climate, cloud properties are expected to change and, in turn, influence changes in the climate system through feedback mechanisms. The latest report by the Intergovernmental Panel on Climate Change (IPCC) states that the net cloud feedback in a warming climate is positive – i.e., changes in clouds amplify future warming (Forster et al., 2021). This is due to an increase in the altitude of tropical high clouds and a reduction in the occurrence of subtropical low-level clouds (creating a warming effect), while changes in the composition of extratropical clouds – from ice to more liquid water content – have a counteracting but weaker cooling effect. A focus region for studying clouds and cloud changes is the Arctic, as this area is warming at a particularly high rate compared with the global average; this phenomenon is known as "Arctic amplification" (Serreze and Barry, 2011; Wendisch et al., 2017).

However, assessing how clouds influence the surface radiation budget is particularly complex in the high latitudes, where the dry atmosphere, the high surface albedo due to snow and ice cover, the lack of solar radiation in winter, and the strong temperature inversions strongly influence the clouds' radiative effect (Curry et al., 1996). Intrieri et al. (2002) found that Arctic clouds warm the surface for most of the year. Nevertheless, for a brief period in summer, they report a net cooling effect when the SW cooling outweighs the LW warming due to a lower surface albedo and larger solar elevation. While this has been observed in different regions of the Arctic, Miller et al. (2015) showed a continuous warming effect of clouds at Summit, Greenland, where the surface albedo is high throughout the year. The cloud radiative effect in the Arctic is dominated by clouds that contain liquid water (Shupe and Intrieri, 2004), and modeling studies suggest that the amount of liquid cloud water is essential for understanding Arctic climate change (Hofer et al., 2017, 2019). Nonetheless, using ground-based remote sensing, Ebell et al. (2020) showed that cirrus clouds can dominate the LW radiative effect in the Arctic in winter.

Besides their radiative impact, Arctic cirrus clouds also have the potential to dry the upper troposphere, contribute to chemical reactions affecting ozone, and redistribute trace gases and ice-nucleating particles (INPs), which, in turn, affects lower mixed-phase clouds (Kärcher, 2005).

To estimate the radiative impact of Arctic clouds, long-term observations of their macrophysical and microphysical properties are needed (e.g., Turner et al., 2018). However, continuous cloud observations in the harsh and remote Arctic are scarce. The weak contrast between clouds and the underlying bright snow and ice surfaces makes passive remote sensing from satellites difficult to evaluate. Active radar and lidar measurements from the CloudSat (Stephens et al., 2002) and Cloud-Aerosol Lidar and Infrared Pathfinder Satellite Observation (CALIPSO) (Winker et al., 2009) satellites provide valuable cloud observations in the Arctic, but their polar orbits limit their coverage to below 81° N and reduce the temporal resolution. Moreover, ground clutter can affect cloud detection, especially for low clouds. Thus, ground-based remote sensing sites are essential for long-term observations of Arctic clouds. Shupe et al. (2011) combined observations from six different Arctic sites and estimated the total annual cloud occurrence to be 58 %–83 %; they found that cloud ice occurred 60 %–70 % of the time at heights of up to 11 km and that ice clouds were more prevalent than mixed-phase clouds (Shupe, 2011).

Arctic observatories with permanent ground-based remote sensing measurements include, for example, the French–German Arctic Research Base AWIPEV in Ny-Ålesund, Svalbard (78.55° N, 11.56° E) (Hoffmann et al., 2009; Nomokonova et al., 2019; Nakoudi et al., 2021b), the Atmospheric Radiation Measurement (ARM) North Slope of Alaska (NSA) site near Utqiagvik, Alaska (71.3° N, 156.6° W) (Dong and Mace, 2003; Dong et al., 2010), Summit Station, Greenland (72.6° N, 38.5° W) (Shupe et al., 2013; Miller et al., 2015), and Eureka, Canada (80.0° N, 86.42° W) (de Boer et al., 2009).

Cirrus cloud occurrence shows strong variations across the Arctic sites as well as a strong seasonal cycle. Nomokonova et al. (2019) estimated the occurrence of single-layer ice clouds in Ny-Ålesund to be 15 %–20 % in winter and spring but less than 5 % in summer and fall. On the other hand, ice-cloud occurrence at Eureka varies between 35 % in summer and up to 70 % in winter (Shupe, 2011).

In addition to the permanent observatories, there have been intensive measurement campaigns with durations of several weeks to 1 year, including the Surface Heat Budget of the Arctic Ocean (SHEBA) project (Uttal et al., 2002), the Mixed-Phase Arctic Cloud Experiment (M-PACE) (Verlinde et al., 2007), and the Multidisciplinary drifting Observatory for the Study of Arctic Climate (MOSAiC) expedition (Shupe et al., 2022).

Here, we present the statistics of cold-cloud properties in the Norwegian Arctic, as observed by ground-based and spaceborne lidars for the 2011–2017 period. The cloud observations were conducted on Andøya (69.3° N, 16.0° E) and focus on the properties of mid- and high-level mixed-phase and cirrus clouds in this region (single-layer clouds with cloud base heights between 4000 and 12000 m and a cloud top temperature below −20 °C).

This paper is structured as follows: the instrumentation and methods (with a special focus on the ground-based lidar) are described in Sect. 2. In Sect. 3, we demonstrate the capabilities of the ground-based lidar with respect to observing cold clouds based on two case studies focused on (1) a cirrus cloud and (2) a mixed-phase cloud. For the cirrus cloud case, we compare the ground-based measurements with co-located observations from the spaceborne lidar aboard CALIPSO for validation. In Sect. 4, both platforms are used independently to compute cold-cloud statistics for cloud top temperature as well as cloud top and cloud base heights. We discuss the re-

sults from both case studies and the statistics in Sect. 5, and our conclusions are summarized in Sect. 6.

## 2 Instrumentation and methods

This section is split into a description of the ground-based lidar system (Sect. 2.1), including the methods for processing its raw data, and a short description of the satellite-based instruments and the data product used (Sect. 2.2).

### 2.1 Ground-based lidar

The lidar is part of the Arctic Lidar Observatory for Middle Atmosphere Research (ALOMAR) and is co-located with other lidars specialized for profiling the middle and upper atmosphere. It has been in operation since 2005, although the observatory itself was opened in 1994 (Skatteboe, 1996). The tropospheric lidar is part of the European Aerosol Research Lidar Network (EARLINET; Pappalardo et al., 2014) and participates in validation activities for satellite missions such as the Atmospheric Dynamics Mission – Aeolus (ADM-Aeolus) (Stoffelen et al., 2005).

The monostatic biaxial system operates with a pulsed Nd:YAG solid-state laser as an emitter (primary wavelength of 1064 nm; second and third harmonic of 532 and 355 nm, respectively; and laser repetition frequency of 30 Hz) and a Newtonian telescope as the receiver. The detection channels include the three emitted wavelengths for elastic scattering and one for Raman scattering at 387 nm. At 532 nm, the outgoing light is linearly polarized, and the receiver has been equipped with orthogonal and parallel polarization channels since 2011. Moreover, there are two simultaneous detection channels for every wavelength (except for 387 nm): the analogue mode for stronger signals, especially in the near range, and the photon-counting mode for weaker signals, mostly for the far range. The two channels can be joint through a gluing algorithm; however, as we only consider relatively high clouds in this study, we generally use the photon-counting signal only. The range resolution of the lidar is 7.5 m, and the time resolution used in this study is 67 s. A more detailed technical description of the instrument can be found in Frioud et al. (2006).

The collected raw data have to undergo several technical corrections before the signal can be physically interpreted. These include the following: (1) dead-time correction for the photon-counting channels (which accounts for the statistical loss of photons in photon-counting mode due to limitations in the detection speed), (2) background subtraction (we consider the signal above 40 km as background and subtract the average of this altitudinal region from the data), and (3) range correction (which accounts for the quadratic decrease in the signal with distance). The processed product is the total attenuated backscatter (in arbitrary units) which is then used in a cloud detection algorithm. In case studies, we additionally use lidar constants computed by the EARLINET Single Calculus Chain (D'Amico et al., 2015) to convert total attenuated backscatter from arbitrary units into units of per meter per steradian $(\mathrm{m\,sr})^{-1}$.

Besides statistically analyzing macroscopic cloud properties, we use the linear volume depolarization ratio to identify regions of different cloud thermodynamic phase and particle composition inside the cloud during the case studies. The linear volume depolarization ratio $\delta$ is defined as the ratio of cross-parallel polarized backscatter $\beta_\perp$ to parallel polarized backscatter $\beta_\parallel$:

$$\delta = \beta_\perp / \beta_\parallel. \tag{1}$$

To calibrate the polarization-filtered signals against each other, we use the $\pm 45°$ method described in Freudenthaler et al. (2009).

The cloud optical depth $\tau$ is another important property when considering a cloud's impact on radiative fluxes. The possibility to calculate cloud optical depth from lidar data is limited to optically thin clouds, and we follow a technique originally developed for the micropulse lidars of the ARM program at the US Department of Energy (Lo et al., 2006; Comstock and Sassen, 2001):

$$\beta_\mathrm{c}(z) = \frac{G(z_0, z)}{1 - \frac{2\eta}{k}\int_{z_0}^{z} G(z_0, z')\,\mathrm{d}z'} - \beta_\mathrm{m}(z), \tag{2}$$

$$\text{where } G(z_0, z) = \beta_\mathrm{m}(z_0)\,\frac{S(z)z^2}{S(z_0)z_0} \cdot \exp\left[2\left(\frac{8\pi}{3} - \frac{\eta}{k}\right)\int_{z_0}^{z} \beta_\mathrm{m}(z'')\mathrm{d}z''\right]. \tag{3}$$

Here, $\beta_\mathrm{c}(z)$ and $\beta_\mathrm{m}(z)$ are the cloud and molecular backscatter coefficients, respectively, as a function of the altitude $z$; $\eta$ is the multiple-scattering coefficient; $z_0$ is a boundary height below the cloud where the air is assumed to be cloud-free; $k$ is the backscatter-to-extinction ratio; and $S$ is the sum of the processed parallel and cross-parallel signals. There have been various approaches to determine the multiple-scattering coefficient for cirrus clouds, and these approaches have commonly used values that vary between 0.4 (Platt, 1973, proposed $0.41 \pm 0.15$ from observations) and 0.9 (upper maximum used by Comstock and Sassen, 2001). For this study, we decided to use $\eta = 0.8$, which is in agreement with Lo et al. (2006) and Comstock and Sassen (2001). The backscatter-to-extinction ratio $k$ is varied between 0.01 and 0.2 such that the total backscatter above the cloud is closest to the molecular backscatter. The latter is calculated using the air density profile of a modified US standard atmosphere (i.e., adjusted to the measured ground temperature and pressure). Afterwards, the optical depth $\tau$ of a cloud with cloud

base $z_b$ and cloud top $z_t$ is calculated as follows:

$$\tau = \frac{1}{k} \int_{z_b}^{z_t} \beta_c(z) dz. \quad (4)$$

The cloud detection is based on an algorithm developed by Gong et al. (2011). It uses only one wavelength and, due to the fact that is has the lowest Rayleigh scattering efficiency and, therefore, the highest penetration into a cloud, we apply it to the 1064 nm channel. After smoothing and noise level calculation, the signal is first simplified using the Douglas–Peucker algorithm (Douglas and Peucker, 1973), which identifies points with large gradient changes (vertices). A cloud base is detected if the gradient between two vertices exceeds a certain threshold and the signal is above noise level. The corresponding cloud top is identified as the first vertex with a lower signal strength than the base vertex. The threshold is empirically determined and set to $10^5$. Due to the fact that the calculated noise levels tend to be too low, there is a significant number of false identifications that do not actually stand out from the background noise, especially above 10 km altitude. To avoid these false identifications, all clouds detected by the algorithm are manually verified.

The cloud top temperatures (CTTs) for the clouds identified by the ground-based lidar are retrieved from nearby released radiosondes (Norwegian Meteorological Institute, 2021) and ERA5 reanalysis data (Hersbach et al., 2020). There have been two radiosonde releases daily in Andenes, which is only 5 km away from the ground-based lidar, since in October 2014. Before this, the closest releases were from Bodø (67.28° N, 14.45° E) which, at a great-circle distance of 240 km, were too far away to be considered relevant for routinely retrieving CTTs. Instead, we use ERA5 reanalysis data for the period before 2014 (downloaded from Hersbach et al., 2018). In order to compare both methods, we tested their correlation for the years from 2015 to 2017 (see Fig. 1). For ERA5 temperatures, we interpolate the cloud top temperature linearly between the two closest pressure levels. The rather coarse vertical resolution of the ERA5 reanalysis might omit details of the thermal structure around cirrus clouds. Nevertheless, with a correlation coefficient of 0.95, the agreement is generally good, although the interpolated temperatures from reanalysis data show a tendency to be higher than those measured by the radiosonde (by 1 K on average). These differences can be attributed to the horizontal displacement of the radiosondes and the uncertainties in the ERA5 reanalysis (30 km horizontal resolution and 37 pressure levels between the surface and 80 km altitude). Additionally, the average time lag between the retrieved ERA5 temperature (available on the hour) and the radiosonde release (twice a day) in Fig. 1 is 3 h and 20 min.

The available measurement record of observations, including depolarization-sensitive channels, spans from 2011 to the present with a maintenance break from April 2013 to July 2015. The lidar can be operated whenever there is no precipitation and the 10 min average wind speed does not exceed 12 m s$^{-1}$. The majority of measurements is made during daytime. Possible implications and biases of the measurement routines will be discussed in Sect. 4.

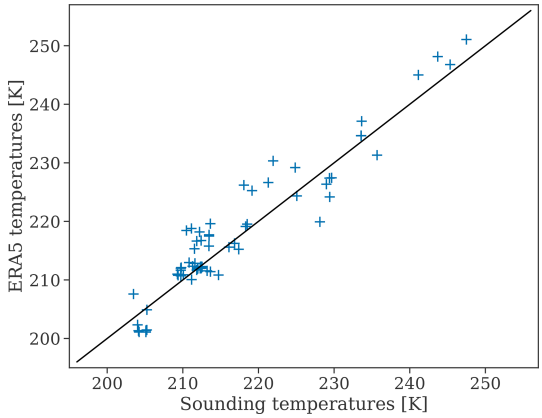


**Figure 1.** Cloud top temperature extracted from ERA5 scattered against cloud top temperature from the closest available radiosonde release (Andenes) for all detected cirrus clouds between 2015 and 2017. The black one-to-one line indicates exact agreement and shows a slight bias of ERA5 data towards warmer temperatures. The average difference is 1 K.

## 2.2 Spaceborne lidar and radar

We use data from the cloud profiling radar (CPR) aboard CloudSat (Stephens et al., 2002) and the Cloud-Aerosol Lidar with Orthogonal Polarization (CALIOP) aboard the Cloud-Aerosol Lidar and Infrared Pathfinder Satellite Observation (CALIPSO) satellite (Winker et al., 2009). For direct comparison with the ground-based lidar, we use CALIOP Level 1 (1B profile; NASA/LARC/SD/ASDC, 2016) and Level 2 (5 km cloud layer; NASA/LARC/SD/ASDC, 2018) data products for cloud properties such as backscatter, altitude, and optical depth. CALIOP operates on the same wavelengths (1064 and 532 nm) as the lidar at ALOMAR. Here, the vertical resolution in the relevant altitudinal region above 8 km is 60 m, and the horizontal resolution is 1 km. For the phase discrimination between cirrus, mixed-phase, and liquid clouds, we use the 2B-CLDCLASS-LIDAR data product (Sassen et al., 2008), which utilizes the different sensitivities of the radar and lidar to liquid droplets and ice crystals. Beside the cloud phase, we use the cloud top and base height information, and, for each cloudy profile, we retrieve the cloud top temperature from the ECMWF-AUX dataset (version $P_R05$), which uses ancillary European Centre for Medium-Range Weather Forecasts (ECMWF) state variable data interpolated to each CPR vertical bin.

We are aware that the use of different reanalysis products for temperature retrievals introduces uncertainties. However, as ECMWF-AUX has been specifically designed to provide profiles of temperature from atmospheric reanalysis interpo-

lated on the time and location of the CloudSat/CALIPSO overpass, this makes it the first choice for use in combination with the phase retrieval from the 2B-CLDCLASS-LIDAR product. To draw conclusions about the general CTT distribution of cold clouds without introducing a large bias from the choice of the reanalysis product, we choose a bin size of 2.5 K when showing the distributions in Fig. 7. The choice of 2.5 K is based on previous estimates of the validity of atmospheric reanalysis temperatures in the Arctic: Jakobson et al. (2012) found a bias of up to 2 K for the lowest 890 m when comparing tethersonde data from an Arctic drifting ice station with ERA-Interim reanalysis data. Moreover, Graham et al. (2019) compared ERA5 reanalysis data with radiosondes launched from two ship campaigns in the Fram Strait and found a vertically averaged absolute bias of 0.3 K. Other reanalysis products in their study also showed biases of less than 0.6 K. In addition, our own comparison of the radiosonde data from Andenes with ERA5 data yielded a bias of 1 K. This gives us confidence in the use of different reanalysis products for the spaceborne and ground-based retrievals of the CTT.

Apart from gaps in the satellite dataset (January 2011; January–April 2012; and June, July, and September 2017) we analyze the 2011–2017 period.

### 2.3 Comparison of ground-based and spaceborne observations

For the statistical analysis, we split the available data from the ground-based lidar into 30 min measurement intervals (shorter measurements also count as one interval), which results in a total number of 1366 measurements between 2011 and 2017. We include all satellite overpasses within a $2° \times 2°$ box around ALOMAR in the analysis. This corresponds to an extent of approximately 80 km in the zonal direction and 220 km in the meridional direction, and it results in 48 873 individual profiles being used for the statistical analysis of cold-cloud properties.

We limit this analysis to single-layer clouds in order to avoid attenuation by the lidar when penetrating multiple cloud layers, which would induce a bias in the statistics due to the opposite upward and downward viewing configurations of the two lidar systems. A cloud scene observed from the ground-based lidar is considered to be multilayer if there is a cloud-free region of at least 200 m vertical distance between two cloudy layers. Otherwise, the scene is regarded as a single-layer cloud.

## 3 Case study results

To demonstrate the capabilities of the ground-based lidar with respect to observing cold clouds, we present two case studies focusing on (1) a cirrus cloud and (2) a mixed-phase cloud. The cirrus cloud case provides the opportunity to directly compare the ground-based lidar with measurements from the spaceborne CALIOP lidar. For the mixed-phase cloud case, we use the lidar to distinguish between liquid droplets and ice crystals, providing insight into the vertical phase distribution of the cloud.

### 3.1 Cirrus cloud case

On 1 April 2011, CALIPSO passed over the ALOMAR lidar at 11:11 UTC (13:11 LT) while both lidars were measuring a cloud layer between 9.6 and 11.5 km altitude. The satellite ground track is shown in Fig. 2d, and it crosses the island of Andøya with a horizontal distance to ALOMAR of 2 km northeast of the mountain of Ramnan.

On the same day, the Norwegian west coast was located between a low-pressure system west of Iceland and a high-pressure system centered over Svalbard. The cirrus clouds observed here were located in a region between a warm front in the north, which had passed Andøya the day before, and a vanishing occluded front, which reached from the Atlantic east of Greenland to Southern Norway (Met Office, 2021).

The ground-based lidar was running from 09:53 to 11:20 UTC, followed by a depolarization calibration measurement. From the satellite, we use data from the time when the ground track was located in a geographical box of $2° \times 2°$ in the meridional and zonal direction around ALOMAR. This is the case from 11:11:09 until 11:11:37 UTC (i.e., for a total duration of 28 s).

The total attenuated backscatter from ground- and spaceborne lidar is shown in Fig. 2a and c, respectively. The total attenuated backscatter from the ground-based lidar ranges from $1 \times 10^{-6}$ to $2.5 \times 10^{-6}$ $(\mathrm{m\,sr})^{-1}$ in the cloud around the time of the CALIPSO overpass (black vertical line). In terms of vertical structure, the lowest backscatter values inside the cloud are found at around 11 km, and the layer intensifies from there towards both the cloud top and base. From the spaceborne lidar, the total attenuated backscatter ranges between $1 \times 10^{-6}$ and $4 \times 10^{-6}$ $(\mathrm{m\,sr})^{-1}$, and the vertical substructure is less clear, although still recognizable, especially at the latitude closest to ALOMAR until around 69.6° N. Here, the retrieved cirrus cloud base and top heights are 9.6 and 11.4 km, respectively. This is in good agreement with the ground-based lidar. Taking temperature data from the closest available radiosonde release into account (from Bodø; 67.28° N, 14.45° E; 11:10 UTC), we see that the temperature at this altitude was −60 °C or lower, i.e., well below the limit for homogeneous freezing (e.g., Heymsfield and Sabin, 1989). According to the World Meteorological Organization, the tropopause is defined as the lowest level at which the lapse rate decreases to 2 K km$^{-1}$ or less and where the average lapse rate between this level and all higher levels within 2 km does not exceed 2 K km$^{-1}$ (WMO, 1992). Applying this definition, we estimate the beginning of the tropopause to be located at about 11.0 km (from radiosonde data; see Fig. 2d) or 10.6 km (from reanalysis data) and at a temperature of −70 °C. Thus, the cirrus cloud is ex-

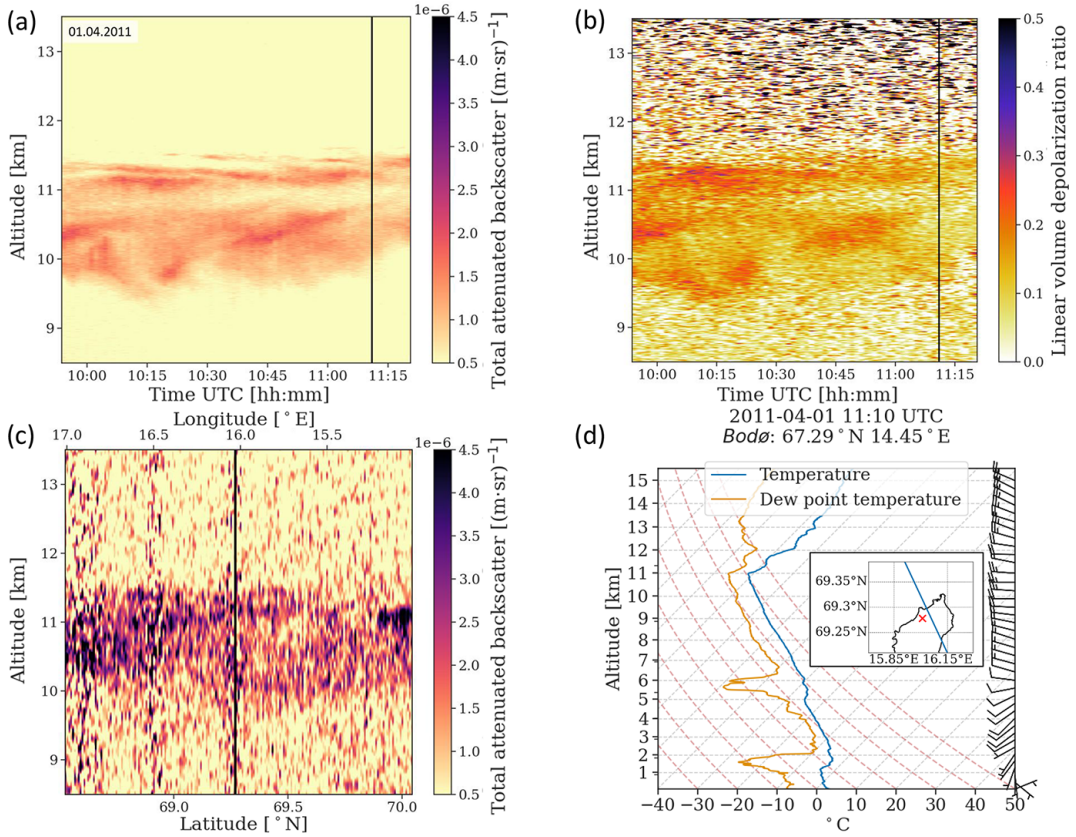


**Figure 2.** Cirrus cloud measurement on 1 April 2001, showing the total attenuated backscatter at 532 nm from the ALOMAR lidar **(a)** and CALIOP **(c)** as well as the linear volume depolarization ratio from the ground-based lidar **(b)**. The closest available radiosounding from Bodø is shown in panel **(d)**, along with a map showing the ground track of the satellite (blue line) and the position of the ground-based lidar (red cross). The black lines show the overpass time in panels **(a)** and **(b)** and the closest location during the overpass in panel **(c)**. The vertical and temporal resolutions of the ALOMAR lidar are 7.5 m and 67 s, respectively. The satellite resolution is 60 m in the vertical direction and 1 km in the horizontal direction. In addition, the satellite backscatter is smoothed by a Gaussian filter.

tending well into the tropopause, potentially dehumidifying the upper-troposphere–lower-stratosphere region through ice crystal growth and sedimentation (e.g., Kärcher, 2005). However, a quantification of dehydration in this case requires knowledge of further cloud parameters and is beyond the scope of this study.

The linear volume depolarization ratio from the ground-based lidar is shown in Fig. 2b and ranges from 0.2 to 0.3, indicating thin plate-like particles (shape ratio length / diameter $< 0.1$) and intermediate and irregular shapes with shape ratios of up to 0.5 (categories I and II in Noel et al., 2002). From the satellite products, the layer-integrated depolarization ratio is available and has values of between 0 and 0.4 over the displayed period (not shown), which covers the range observed by ground-based lidar. A more detailed comparison is not possible, as the noise level of the linear volume depolarization ratio from the satellite is too high.

To compare the cloud optical depths ($\tau$) retrieved from both platforms, we estimated the backscatter-to-extinction ratio to be $k = 0.2$, which yields the best agreement with molecular backscatter above the cloud. Averaging over the time interval from 09:55 to 11:20 UTC, the ground-based lidar gives an optical depth $\tau$ of $0.07 \pm 0.02$. At the location where the satellite ground track has the shortest distance to ALOMAR, the spaceborne lidar retrieves the same value of $\tau = 0.07 \pm 0.02$. Thus, the retrieved cloud optical depths show a very good agreement. The observed cloud is an optically thin cirrus cloud according to the classification by Sassen and Cho (1992) ($0.03 < \tau < 0.3$). This is also the most common cirrus category observed at Ny-Ålesund, Svalbard, with a 73 % occurrence (Nakoudi et al., 2021a), and at the subarctic site of Kuopio, Finland (62.74° N, 27.54° E), with a 71 % occurrence (Voudouri et al., 2020).

### 3.2 Mixed-phase cloud case

The second case that is selected for detailed analysis is an altocumulus mixed-phase cloud, as shown in the image in Fig. 3a. It was observed on 24 August 2017 from 10:10 to

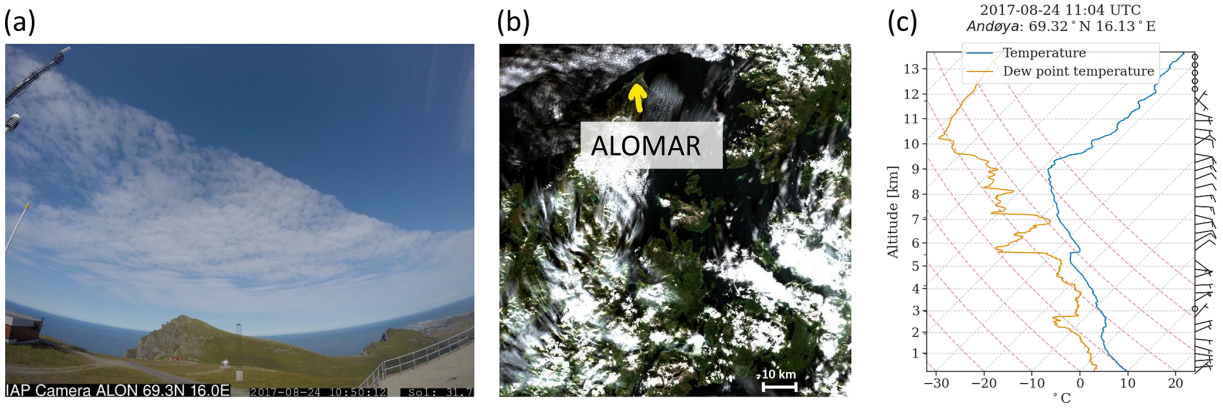


**Figure 3.** Images of the cloud field probed by lidar at 10:50 UTC, as seen **(a)** from inside the ALOMAR observatory and **(b)** from the Sentinel-2 satellite (true color image) (Drusch et al., 2012). In the satellite image, the northern tip of the island is marked by the yellow arrow, and the cloud field probed by the lidar is directly to the north of the island. The border between cloud and clear sky that is visible in both pictures moves through the lidar's field of view at around 10:40 UTC. Temperature, dew point, and wind profiles from a radiosonde released in Andenes at 11:04 UTC on 24 August 2017 are given in panel **(c)**.

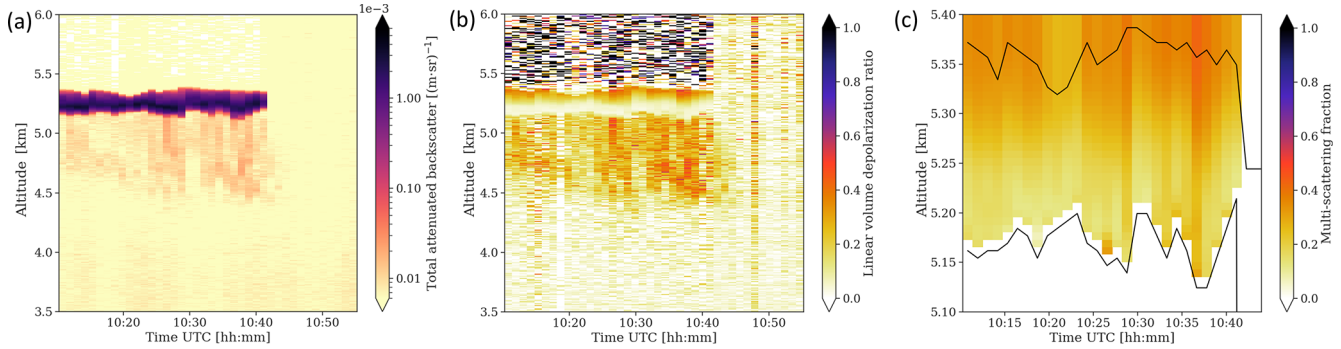


**Figure 4.** **(a)** Total attenuated backscatter (TAB), **(b)** the linear volume depolarization ratio at 532 nm, and **(c)** the accumulated multiple-scattering fraction inside the liquid cloud body. The black lines indicate the cloud base and top of the liquid cloud body, as identified from the combined parallel and cross-parallel signal. The multiple-scattering fraction is accumulated from cloud base.

10:40 UTC and was located at 5.2 to 5.4 km altitude. The general weather situation in Northern Norway that day was influenced by two high-pressure systems, one located over Greenland and the other over the Barents Sea extending over the Atlantic towards Iceland. At the same time, two low-pressure systems were located northwest of the British Isles and close to St Petersburg, Russia (Met Office, 2021). This synoptic situation resulted in fields of scattered clouds along the Norwegian coast, mostly of orographic origin over land (see Fig. 3b).

The radio sounding closest in time to the observation was released from Andenes at 11:04 UTC (i.e., ca. 25 min after the end of the cloud observation). Therefore, it did not penetrate the cloud but rather the air mass behind it. The pronounced cloud boundary can be seen in Fig. 3a. Nevertheless, the sounding profile reveals a temperature of −24 to −26 °C in the relevant altitudinal region (Fig. 3c). It increases 2 K right above 5.6 km, at the same altitude where the dew point temperature drops more than 10 K. This indicates a sudden decrease in humidity and marks the border between two air masses: the lower air mass is connected to the cloud, and the upper air mass is warmer and dry above the cloud top.

The total attenuated backscatter and the linear volume depolarization ratio from the ground-based lidar are shown in Fig. 4. From the backscatter signal, the distinct cloud boundaries at 5.2 and 5.4 km altitude with falling hydrometeors below become apparent. Differences in the linear volume depolarization ratio imply different shapes of the cloud particles (Noel et al., 2002), at least as long as single scattering is concerned. Hexagonal ice crystals typically lead to linear depolarization ratios of 0.2–0.5, depending on the aspect ratio, whereas single scattering from spherical water droplets does not induce any polarization change. The depolarization ratio in the mixed-phase cloud case shows a clear separation into three regions (see Fig. 4b): the center of the cloud around 5.2–5.3 km, with values below 0.1, can be clearly separated from the cloud top and a large area below that extends down to 4.5 km (both with values up to 0.4). Thus,

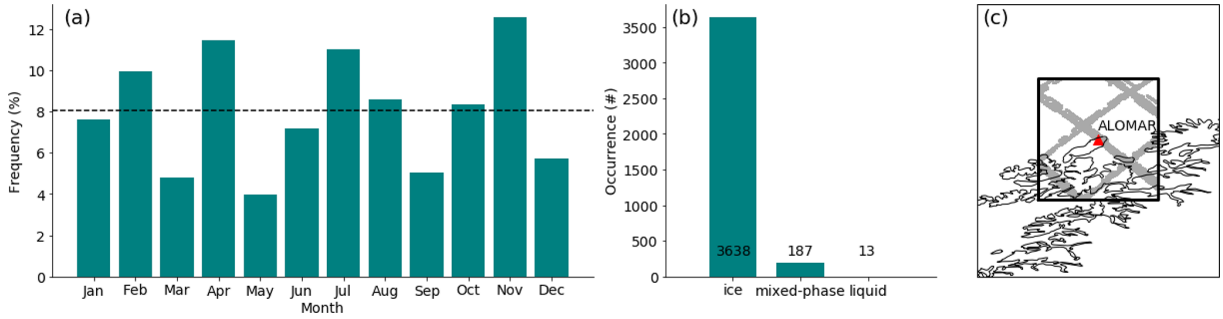


**Figure 5.** **(a)** Monthly single-layer cold-cloud occurrence from satellite. **(b)** The distribution of cloud phase, given as the number of observed single-layer cold clouds. **(c)** The spatial box from which cloud measurements are taken for the analysis: the ground-based lidar at ALOMAR is indicated by the red triangle, the box extends 2° around ALOMAR (1° in each direction), and satellite overpasses with cloud detection are indicated in gray.

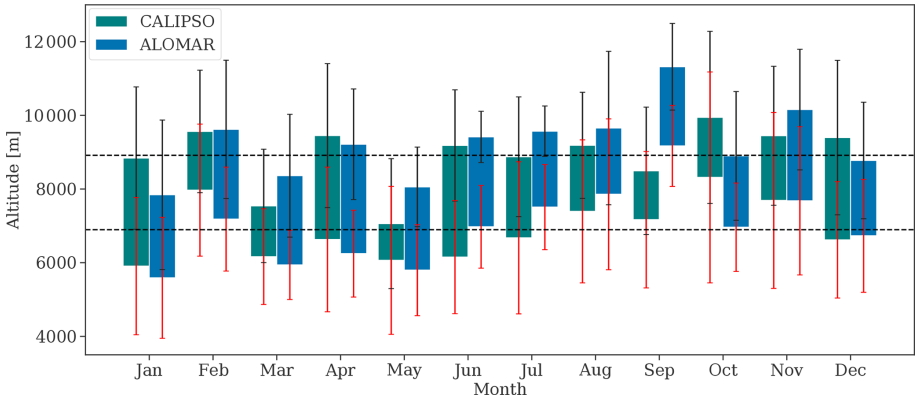


**Figure 6.** Monthly mean thickness of cirrus clouds observed from the ground-based lidar at ALOMAR (blue) and CALIOP (green). The error bars indicate the standard deviation of the computed cloud top and base heights. The dashed black lines show the multiyear annual average.

spherical liquid water droplets dominate in the region around 5.2 km, with $\delta < 0.1$, whereas the high depolarization values between 4.5 and 5.2 km altitude can be attributed to falling ice crystals (virga). The increasing depolarization ratio from the liquid cloud base towards the cloud top can be attributed to multiple scattering by liquid water droplets, as the cloud is optically thick, meaning that there is no signal coming back from above the cloud. Hu et al. (2006) presented a relationship between the accumulated multiple-scattering fraction in water clouds and the accumulated depolarization ratio $\delta_{\mathrm{acc}}$. We retrieve the altitude of the (assumed) liquid cloud base and top from the gradient in the attenuated backscatter signal, and we use this cloud base as a starting point for the accumulated depolarization and multiple-scattering ratios. Applying the formula $A_{\mathrm{S}} = 0.999 - 3.906\delta_{\mathrm{acc}} + 6.263\delta_{\mathrm{acc}}^2 - 3.554\delta_{\mathrm{acc}}^3$ from Hu et al. (2006) results in the profile of the multiple-scattering fraction within the cloud, as shown in Fig. 4c. The fraction of multiple scattering increases from around 15 % at cloud base to up to 40 % at cloud top. Note that this calculation assumes that the depolarization signal is entirely explained by multiple scattering from spherical water droplets. Hence, the multiple-scattering fraction of 15 % at cloud base indicates an additional influence from ice crystals within the predominantly liquid cloud layer. This is typical for a liquid-topped mixed-phase cloud, where small ice crystals are formed at the cloud top and then fall through the liquid part of the cloud. The observed structure is in accordance with, for example, in situ observations from aircraft by Barrett et al. (2020) and ground-based lidar observations by Engelmann et al. (2021). These studies found ice production within the supercooled layer at temperatures of −30 and −28.5 °C, respectively, and ice virgae below. Thus, we conclude that there are active ice-nucleating particles at temperatures around −25 °C, although in insufficient amounts for complete glaciation of the cloud.

## 4 Cold-cloud statistics

The statistical analysis of cold-cloud properties uses all data from the ground-based lidar at ALOMAR spanning from the installation of the depolarization channel in 2011 until 2017 as well as spaceborne lidar data for the same period.

**Table 1.** The seasonal and multiyear annual ("All-year") average of occurrence, temperature, and cloud height for the two datasets from the ground- and satellite-based lidar. The occurrence for the satellite is the total number of detections between 2011 and 2017 during the respective season.

| Variable and instrument | Winter (DJF) | Spring (MAM) | Summer (JJA) | Fall (SON) | All-year |
|---|---|---|---|---|---|
| Occurrence | | | | | |
| Satellite [no.] | 626 | 1064 | 1250 | 898 | 3838 |
| Satellite [%] | 7.8 | 6.9 | 8.8 | 8.0 | 8.0 |
| Cloud top temperature [K] | | | | | |
| Satellite (ECMWF) | 211.8 | 221.3 | 227.3 | 220.4 | 220.2 |
| Ground-based | 217.1 | 224.1 | 227.0 | 218.3 | 221.6 |
| Cloud base height [m] | | | | | |
| Satellite | 6832 | 6286 | 6740 | 7724 | 6896 |
| Ground-based | 6501 | 5995 | 7427 | 7938 | 6965 |
| Satellite and ground-based average | | | | | $6930 \pm 35$ |
| Cloud top height [m] | | | | | |
| Satellite | 9267 | 8017 | 9082 | 9295 | 8915 |
| Ground-based | 8746 | 8545 | 9527 | 10 125 | 9236 |
| Satellite and ground-based average | | | | | $9075 \pm 160$ |

We define cirrus clouds as all single-layer clouds with cloud base heights between 4000 and 12 000 m and a cloud top temperature below −20 °C (253.15 K). This is based on Sassen et al. (2008) and Heymsfield et al. (2017), who showed, using satellite observations, that cirrus clouds in the Arctic are mostly limited to an altitude range between 4 and 12 km.

To test this definition, we applied it to all 25 779 single-layer clouds detected by CloudSat/CALIPSO during the study period. Of these, 3838 clouds were identified as cirrus clouds. Figure 5c shows the location of these cirrus cloud profiles within the 2° × 2° box around ALOMAR. Using the additional phase information, we find that 95 % of these clouds were indeed pure ice clouds (3638 cases; see Fig. 5b). The remaining 5 % consisted of mixed-phase clouds (187 cases) and pure liquid clouds (13 cases). This confirms that the cirrus cloud definition captures mostly pure ice clouds; however, it cannot be ruled out that some of the cirrus cloud cases identified by the ground-based lidar might include some mixed-phase clouds. A further phase discrimination from the ground-based lidar for this possible mixed-phase cloud influence is beyond the scope of this study. Due to this slight ambiguity, we hereafter refer to these predominantly ice clouds as cold clouds. Furthermore, we conclude that INP concentrations are generally high enough to glaciate single-layer clouds at temperatures below −20 °C.

As can be seen from Fig. 5a, the monthly occurrence of single-layer cold clouds varied between 4 % and 13 %, showing no clear seasonal dependence. On average, 8 % of all satellite profiles were identified as single-layer cold clouds. With a total occurrence of 51 % for single-layer clouds of all heights and phase compositions, this corresponds to 15.4 % of all single-layer clouds being cold clouds according to our definition. This fraction of 15.4 % is less than the 1 : 4 ratio reported by Nomokonova et al. (2019) for Ny-Ålesund, Svalbard (36 % total occurrence of single-layer clouds, thereof 9 % pure ice clouds). The number of cirrus cloud observations from the ground-based lidar also shows no seasonal trend. However, the ground-based record is not continuous due to the hours of operation and weather limitations: measurements are not possible in the case of precipitation or when average wind speeds exceed 13 m s$^{-1}$ due to local instrument safety restrictions. Thus, the cold-cloud occurrence as seen from the ground-based lidar has a bias towards higher values, and it is not shown here because it cannot be compared to the spaceborne lidar.

Nevertheless, the macroscopic cold-cloud properties (cloud top and base height) for both the ground-based and satellite observations can be compared, and they are displayed in Fig. 6. The corresponding seasonal averages can be found in Table 1. The ground-based lidar records cloud top heights between 5045 and 13 130 m (mean of 9240 m) and cloud base heights between 4040 and 11 090 m (mean of 6970 m) with a pronounced annual cycle. There are distinct increases in height from January to February, from May to June, and from August to September as well as decreases from February to March and from September to October. In general, there is a trend towards higher cold clouds in summer and fall compared with winter and spring. The highest monthly average altitudes (both cloud base and top) are

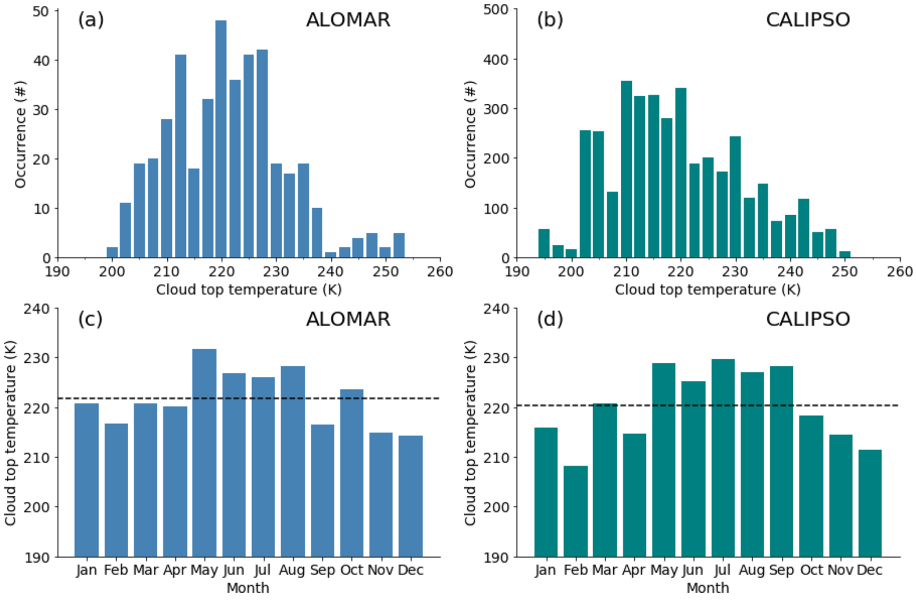


**Figure 7.** **(a, b)** Histogram of cloud top temperatures for all cirrus detections from **(a)** the ground-based lidar and **(b)** the spaceborne lidar between 2011 and 2017. The bin width is 2.5 K. For the ground-based lidar, the temperatures are interpolated from reanalysis data (ERA5) on pressure levels until 2014 and taken from radiosondes thereafter. **(c, d)** Monthly average cloud top temperature from **(c)** ground-based and **(d)** spaceborne lidar.

recorded in September, whereas the lowest monthly average altitudes are seen in January. The general trend of higher cold clouds in fall than in winter and spring is also apparent in the results from the spaceborne observations (see Fig. 6). However, the monthly variability is less pronounced than for the ground-based measurements, indicating an influence of the irregular observation times on the ground-based lidar. Cloud top heights as retrieved from the satellite are also slightly lower (4150–12 490 m, mean of 8915 m) than for the ground-based lidar. The cloud base height from satellite varies between 4030 and 11 890 m (mean of 6895 m), which is more similar to the ground-based observations. However, this is expected due to the cloud-type detection algorithm being dependent on the cloud base height. The large standard deviations for cloud top and base heights (as visible in Fig. 6) indicate a larger case-to-case variability than monthly variability for both platforms. Moreover, the average vertical extents of the cold clouds are similar: 2270 m for ground-based measurements and 2020 m for spaceborne measurements.

We show histograms and the monthly averages of the cloud top temperatures from both lidars in Fig. 7. The distributions of observed cloud top temperatures are similar from both platforms: the registered cold clouds showed CTTs between 201 and 253 K (ground-based) and between 196 and 252 K (spaceborne) with a pronounced maximum of cold-cloud occurrence at around 220 K (ground-based) and 210 K (satellite). The distribution from ground-based lidar has a second (lower) maximum at 212 K, closer to the maximum observed from the satellite. Likewise, the second highest peak in the distribution from satellite measurements at 220 K corresponds to the maximum of the ground-based distribution. The main difference between both distributions is the total number of measurements, which leads to the more patchy histogram for the ground-based observations, especially towards the high-temperature end of the distribution. Furthermore, the observed cold-cloud CTTs show a similar annual cycle from both platforms (see Fig. 7c and d). The highest CTTs were registered in summer (between May and August), with values of up to 230 K, whereas CTTs are lowest in the winter months (214 K in December for ground-based measurements and 208 K in February for spaceborne measurements). For the satellite measurements, this low CTT in February coincides with the high mean cloud top height (CTH) in February (see Fig. 6). However, even though the cold clouds in December show the coldest CTTs from the ground-based lidar, their corresponding CTH is not the highest throughout the year. This can partly be explained by the lower temperatures throughout the troposphere in the winter. However, similarly low CTTs in September correspond well to the highest CTHs registered in that month (see Fig. 6).

## 5 Discussion

First, we put our results into the context of long-term ground-based observations of clouds in the Arctic, and we then compare them to spaceborne instrument studies. The multiyear annual average total cloud occurrence at 4 km altitude varies between around 15 % (Utqiagvik, Alaska) and 30 % (SHEBA, ship-based observatory in the western Arc-

tic Ocean) and decreases with altitude to less than 1 % above 10 km altitude (Shupe, 2011). These values are higher than our finding of 8 % cold-cloud occurrence, and the difference can be explained by the restriction to single-layer clouds (Shupe, 2011, also accounted for multilayer clouds). On the other hand, our result is still larger than the annual mean cirrus occurrence of $2.7 \pm 1.8$ % reported from Ny-Ålesund by Nakoudi et al. (2021a); this is meaningful, as, according to the authors, their value is negatively biased due to the very strict criteria for reliable detection. Nakoudi et al. (2021a) also find a mean thickness of 2 km and higher cloud bases during summer and fall than during winter and spring. Relatively large variations in geometrical thickness with a tendency towards thicker layers in winter seem to be common in the Northern Hemisphere high latitudes (Nakoudi et al., 2021a; Devasthale et al., 2011).

In the following, we compare our results for cold-cloud occurrence with the earlier estimates of cirrus cloud frequency at high latitudes from CALIPSO and CloudSat by Mace et al. (2009), Nazaryan et al. (2008), and Gasparini et al. (2018). The analyses by Mace et al. (2009) and Nazaryan et al. (2008) are restricted to the first year of observations from CALIPSO and CloudSat. However, whereas Mace et al. (2009) address hydrometeor layers of all altitudes and compositions, Nazaryan et al. (2008) focus on cirrus clouds. They find values of cirrus cloud occurrence of less than 20 % to nearly 30 %, depending on the season and how multilayer clouds are treated in the analysis. These occurrences are more than double the satellite values presented in our study. Nevertheless, it is important to note that all of these studies include observations with multiple layers. For the "single-layer" statistics in Nazaryan et al. (2008), only the top cloud layer is considered, whereas only single-layer observations are considered in our study.

## 6 Conclusions

We use the record of the tropospheric lidar at the ALOMAR observatory on Andøya in the Norwegian Arctic to retrieve macroscopic (cloud top and base height) and microphysical cloud properties. In analyzing (1) a cirrus cloud and (2) a mixed-phase cloud case, we demonstrate the capabilities of the ground-based lidar with respect to observing cold-cloud properties. Co-located observations from the spaceborne lidar aboard CALIPSO allow for a direct comparison of both lidars for the cirrus cloud case. We then compare the statistics of cold-cloud properties in the Norwegian Arctic as observed from the ground-based and spaceborne instruments between 2011 and 2017. To this end, we define cold clouds as all single-layer clouds with cloud base heights between 4000 and 12 000 m and a cloud top temperature below −20 °C. Applying this definition to the satellite profiles, we find that 95% of these clouds were pure ice clouds. This result suggests that ice formation via homogeneous freezing or (at temperatures above −38 °C) heterogeneous freezing via ice-nucleating particles is mostly sufficient to completely glaciate single-layer clouds at the given temperatures.

The main conclusions of this work are as follows:

1. Observations of an optically thin cirrus cloud agree well between ground-based and spaceborne lidar instruments in terms of the cloud height and optical depth. Cloud height deviations are on the order of 100 m or less, and the difference in the retrieved optical depth is below 10 %.

2. Polarization-sensitive measurements in combination with multiple-scattering considerations from the ground-based lidar can be used to determine cloud structure and vertical phase composition, as demonstrated for a mixed-phase altocumulus cloud.

3. Between 2011 and 2017, 8 % of all satellite profiles were identified as single-layer cold clouds on average (corresponding to 15.4 % of all single-layer clouds). Their average thickness was 2.0 km. No clear seasonal cycle for the cold-cloud occurrence could be identified from the satellite measurements.

4. The ground-based lidar records mean cold-cloud top and base heights of 9.2 and 7.0 km, respectively, with a trend towards higher clouds in summer and fall compared with winter and spring. The mean cold-cloud top and base heights as retrieved from the spaceborne lidar are 8.9 and 6.9 km and are, thus, slightly lower than those from the ground-based lidar. The seasonal variability in cloud thickness and height is smaller than the case-to-case variability.

5. Cold clouds in the Norwegian Arctic are between 1 and 2 km higher in fall than in spring on average, while winter and summer show intermediate values. This is confirmed by both ground-based and spaceborne observations.

6. For both platforms, the retrieved cloud top temperatures show similar distributions and a good agreement in their annual cycle with warmer CTTs in summer.

7. Cold-cloud properties in the Norwegian Arctic agree well with observations from other Arctic sites. Geometrical properties are very similar to Ny-Ålesund, Svalbard, and occurrence is within the range found at sites in Alaska, Canada, the Arctic Ocean, and Svalbard.

Limitations on the applicability of the lidar for mixed-phase cloud research are mainly connected to the restriction to elastic-scattering channels during daylight measurements. When using a lidar with a single field of view and elastic channels only, a more detailed study of the microphysical processes requires complementary observational data from radiosondes and sensitivity studies with radiative transfer

simulations in order to account for multiple-scattering effects.

The ground-based lidar at ALOMAR is still in operation, and its long-term installation provides an opportunity to study changes in cold-cloud properties in the rapidly changing Arctic.

**Data availability.** The satellite data used in this study are available from the CloudSat Data Processing Center (https://www.cloudsat.cira.colostate.edu/, Cooperative Institute for Research in the Atmosphere, 2022; CloudSat and CALIPSO data products, version R05: 2B-CLDCLASS-LIDAR and ECMWF-AUX) and the NASA Langley Research Center – Atmospheric Science Data Center (https://asdc.larc.nasa.gov/, NASA Langley Research Center, 2022; CALIOP Level 1 and Level 2 data products). ERA5 temperature data are available from the Copernicus Climate Data Store (https://cds.climate.copernicus.eu/; https://doi.org/10.24381/cds.bd0915c6, Hersbach et al., 2018), and radiosounding profiles are available from the Norwegian Meteorological Institute (https://thredds.met.no/thredds/catalog/remotesensingradiosonde/catalog.html; Norwegian Meteorological Institute, 2021). Ground-based lidar data can be made available upon request.

**Author contributions.** BS, TS, and TC designed the study. IH and MG provided the raw ground-based lidar data. IH provided the framework for the analysis of the raw data. BS performed the data analysis and interpretation for the case studies as well as the statistical analysis of the ground-based lidar. MG contributed to the interpretation of the results. TC performed the statistical analysis of the spaceborne lidar data. BS and TC prepared the manuscript with input from TS.

**Competing interests.** The contact author has declared that none of the authors has any competing interests.

**Disclaimer.** Publisher's note: Copernicus Publications remains neutral with regard to jurisdictional claims in published maps and institutional affiliations.

**Acknowledgements.** The authors wish to thank all of the lidar operators who contributed to the ground-based dataset. They also gratefully acknowledge the donation of lasers for the tropospheric lidar system at ALOMAR from the Leibniz Institute of Atmospheric Physics (IAP) at the University of Rostock and thank Jens Fiedler and Götz von Cossart for their technical support. Moreover, we are grateful to Gerd Baumgarten (IAP) for providing the cloud image in Fig. 3a and to Malin Abrahamsen (Andøya Space) for her work on the code for cloud detection.

**Financial support.** This research has been supported by the European Research Council (grant no. StG758005) and EEARO-NO-2019-0423/IceSafari (contract no. 31/2020) under the NO grants 2014–2021 of EEA Grants/Norway Grants.

**Review statement.** This paper was edited by Rolf Müller and reviewed by three anonymous referees.

## References

NASA Langley Research Center: Atmospheric Science Data Center, https://asdc.larc.nasa.gov/, last access: 21 July 2022.

Barrett, P. A., Blyth, A., Brown, P. R. A., and Abel, S. J.: The structure of turbulence and mixed-phase cloud microphysics in a highly supercooled altocumulus cloud, Atmos. Chem. Phys., 20, 1921–1939, https://doi.org/10.5194/acp-20-1921-2020, 2020.

Comstock, J. M. and Sassen, K.: Retrieval of Cirrus Cloud Radiative and Backscattering Properties Using Combined Lidar and Infrared Radiometer (LIRAD) Measurements, J. Atmos. Ocean. Tech., 18, 1658–1673, https://doi.org/10.1175/1520-0426(2001)018<1658:ROCCRA>2.0.CO;2, 2001.

Cooperative Institute for Research in the Atmosphere: CloudSat Data Processing Center, Colorado State University, Fort Collins, https://www.cloudsat.cira.colostate.edu/, last access: 21 July 2022.

Curry, J. A., Schramm, J. L., Rossow, W. B., and Randall, D.: Overview of Arctic Cloud and Radiation Characteristics, J. Climate, 9, 1731–1764, https://doi.org/10.1175/1520-0442(1996)009<1731:OOACAR>2.0.CO;2, 1996.

D'Amico, G., Amodeo, A., Baars, H., Binietoglou, I., Freudenthaler, V., Mattis, I., Wandinger, U., and Pappalardo, G.: EARLINET Single Calculus Chain –overview on methodology and strategy, Atmos. Meas. Tech., 8, 4891–4916, https://doi.org/10.5194/amt-8-4891-2015, 2015.

de Boer, G., Eloranta, E. W., and Shupe, M. D.: Arctic Mixed-Phase Stratiform Cloud Properties from Multiple Years of Surface-Based Measurements at Two High-Latitude Locations, J. Atmos. Sci., 66, 2874–2887, https://doi.org/10.1175/2009JAS3029.1, 2009.

Devasthale, A., Tjernström, M., Karlsson, K.-G., Thomas, M. A., Jones, C., Sedlar, J., and Omar, A. H.: The vertical distribution of thin features over the Arctic analysed from CALIPSO observations, Tellus B, 63, 77–85, https://doi.org/10.1111/j.1600-0889.2010.00516.x, 2011.

Dong, X. and Mace, G. G.: Arctic Stratus Cloud Properties and Radiative Forcing Derived from Ground-Based Data Collected at Barrow, Alaska, J. Climate, 16, 445–461, https://doi.org/10.1175/1520-0442(2003)016<0445:ASCPAR>2.0.CO;2, 2003.

Dong, X., Xi, B., Crosby, K., Long, C. N., Stone, R. S., and Shupe, M. D.: A 10 year climatology of Arctic cloud fraction and radiative forcing at Barrow, Alaska, J. Geophys. Res.-Atmos., 115, D17, https://doi.org/10.1029/2009JD013489, 2010.

Douglas, D. H. and Peucker, T. K.: Algorithms for the reduction of the number of points required to represent a digitized line or its caricature, Cartographica, 10, 112–122, 1973.

Drusch, M., Del Bello, U., Carlier, S., Colin, O., Fernandez, V., Gascon, F., Hoersch, B., Isola, C., Laberinti, P., Martimort, P., Meygret, A., Spoto, F., Sy, O., Marchese, F., and

Bargellini, P.: Sentinel-2: ESA's Optical High-Resolution Mission for GMES Operational Services, Remote Sens. Environ., 120, 25–36, https://doi.org/10.1016/j.rse.2011.11.026, 2012.

Ebell, K., Nomokonova, T., Maturilli, M., and Ritter, C.: Radiative effect of clouds at Ny-Ålesund, Svalbard, as inferred from ground-based remote sensing observations, J. Appl. Meteorol. Clim., 59, 3–22, 2020.

Engelmann, R., Ansmann, A., Ohneiser, K., Griesche, H., Radenz, M., Hofer, J., Althausen, D., Dahlke, S., Maturilli, M., Veselovskii, I., Jimenez, C., Wiesen, R., Baars, H., Bühl, J., Gebauer, H., Haarig, M., Seifert, P., Wandinger, U., and Macke, A.: Wildfire smoke, Arctic haze, and aerosol effects on mixed-phase and cirrus clouds over the North Pole region during MOSAiC: an introduction, Atmos. Chem. Physics, 21, 13397–13423, https://doi.org/10.5194/acp-21-13397-2021, 2021.

Forster, P., Storelvmo, T., Armour, K., Collins, W., Dufresne, J.-L., Frame, D., Lunt, D. J., Mauritsen, T., Palmer, M. D., Watanabe, M., Wild, M., and Zhang, X.: The Earth's Energy Budget, Climate Feedbacks, and Climate Sensitivity, in: Climate Change 2021: The Physical Science Basis, Contribution of Working Group I to the Sixth Assessment Report of the Intergovernmental Panel on Climate Change, edited by: Masson-Delmotte, V., Zhai, P., Pirani, A., Connors, S. L., Péan, C., Berger, S., Caud, N., Chen, Y., Goldfarb, L., Gomis, M. I., Huang, M., Leitzell, K., Lonnoy, E., Matthews, J. B. R., Maycock, T. K., Waterfield, T., Yelekçi, Ö., Yu, R., and Zhou, B., Cambridge University Press, 923–1054, https://www.ipcc.ch/report/ar6/wg1/downloads/report/IPCC_AR6_WGI_Chapter07.pdf (last access: 21 July 2022), 2021.

Freudenthaler, V., Esselborn, M., Wiegner, M., Heese, B., Tesche, M., Ansmann, A., Müller, D., Althausen, D., Wirth, M., Fix, A., Ehret, G., Knippertz, P., Toledano, C., Gasteiger, J., Garhammer, M., and Seefeldner, M.: Depolarization ratio profiling at several wavelengths in pure Saharan dust during SAMUM 2006, Tellus B, 61, 165–179, https://doi.org/10.1111/j.1600-0889.2008.00396.x, 2009.

Frioud, M., Gausa, M., Baumgarten, G., Kristjansson, J. E., and Føre, I.: New tropospheric lidar system in operation at ALOMAR (69° N, 16° E), in: Reviewed and Revised Papers of the 23rd International Laser Radar Conference (ILRC), 24–28 July 2006, Nara, Japan, ISBN4-9902916-0-3, 2006.

Gasparini, B., Meyer, A., Neubauer, D., Münch, S., and Lohmann, U.: Cirrus Cloud Properties as Seen by the CALIPSO Satellite and ECHAM-HAM Global Climate Model, J. Climate, 31, 1983 – 2003, https://doi.org/10.1175/JCLI-D-16-0608.1, 2018.

Gong, W., Mao, F., and Song, S.: Signal simplification and cloud detection with an improved Douglas-Peucker algorithm for single-channel lidar, Meteorol. Atmos. Phys., 113, 89–97, 2011.

Graham, R. M., Hudson, S. R., and Maturilli, M.: Improved Performance of ERA5 in Arctic Gateway Relative to Four Global Atmospheric Reanalyses, Geophys. Res. Lett., 46, 6138–6147, https://doi.org/10.1029/2019GL082781, 2019.

Hersbach, H., Bell, B., Berrisford, P., Biavati, G., Horányi, A., Muñoz Sabater, J., Nicolas, J., Peubey, C., Radu, R., Rozum, I., Schepers, D., Simmons, A., Soci, C., Dee, D., and Thépaut, J.-N.: ERA5 hourly data on pressure levels from 1979 to present, Copernicus Climate Change Service (C3S) Climate Data Store (CDS) [data set], https://doi.org/10.24381/cds.bd0915c6, 2018.

Hersbach, H., Bell, B., Berrisford, P., Hirahara, S., Horányi, A., Muñoz-Sabater, J., Nicolas, J., Peubey, C., Radu, R., Schepers, D., Simmons, A., Soci, C., Abdalla, S., Abellan, X., Balsamo, G., Bechtold, P., Biavati, G., Bidlot, J., Bonavita, M., De Chiara, G., Dahlgren, P., Dee, D., Diamantakis, M., Dragani, R., Flemming, J., Forbes, R., Fuentes, M., Geer, A., Haimberger, L., Healy, S., Hogan, R. J., Hólm, E., Janisková, M., Keeley, S., Laloyaux, P., Lopez, P., Lupu, C., Radnoti, G., de Rosnay, P., Rozum, I., Vamborg, F., Villaume, S., and Thépaut, J.-N.: The ERA5 global reanalysis, Q. J. Roy. Meteorol. Soc., 146, 1999–2049, https://doi.org/10.1002/qj.3803, 2020.

Heymsfield, A. J. and Sabin, R. M.: Cirrus Crystal Nucleation by Homogeneous Freezing of Solution Droplets, J. Atmos. Sci., 46, 2252–2264, https://doi.org/10.1175/1520-0469(1989)046<2252:CCNBHF>2.0.CO;2, 1989.

Heymsfield, A. J., Krämer, M., Luebke, A., Brown, P., Cziczo, D. J., Franklin, C., Lawson, P., Lohmann, U., McFarquhar, G., Ulanowski, Z., and Tricht, K. V.: Cirrus Clouds, Meteorol. Monogr., 58, 2.1–2.26, https://doi.org/10.1175/AMSMONOGRAPHS-D-16-0010.1, 2017.

Hofer, S., Tedstone, A. J., Fettweis, X., and Bamber, J. L.: Decreasing cloud cover drives the recent mass loss on the Greenland Ice Sheet, Sci. Adv., 3, 6, https://doi.org/10.1126/sciadv.1700584, 2017.

Hofer, S., Tedstone, A. J., Fettweis, X., and Bamber, J. L.: Cloud microphysics and circulation anomalies control differences in future Greenland melt, Nat. Clim. Change, 9, 523–528, https://doi.org/10.1038/s41558-019-0507-8, 2019.

Hoffmann, A., Ritter, C., Stock, M., Shiobara, M., Lampert, A., Maturilli, M., Orgis, T., Neuber, R., and Herber, A.: Ground-based lidar measurements from Ny-Ålesund during ASTAR 2007, Atmos. Chem. Phys., 9, 9059–9081, https://doi.org/10.5194/acp-9-9059-2009, 2009.

Hu, Y., Liu, Z., Winker, D., Vaughan, M., Noel, V., Bissonnette, L., Roy, G., and McGill, M.: Simple relation between lidar multiple scattering and depolarization for water clouds, Opt. Lett., 31, 1809–1811, 2006.

Intrieri, J., Fairall, C., Shupe, M., Persson, P., Andreas, E., Guest, P., and Moritz, R.: An annual cycle of Arctic surface cloud forcing at SHEBA, J. Geophys. Res.-Oceans, 107, SHE 13-1–SHE 13-14, https://doi.org/10.1029/2000JC000439, 2002.

Jakobson, E., Vihma, T., Palo, T., Jakobson, L., Keernik, H., and Jaagus, J.: Validation of atmospheric reanalyses over the central Arctic Ocean, Geophys. Res. Lett., 39, 10, 2012.

Kärcher, B.: Supersaturation, dehydration, and denitrification in Arctic cirrus, Atmos. Chem. Phys., 5, 1757–1772, https://doi.org/10.5194/acp-5-1757-2005, 2005.

Korolev, A., McFarquhar, G., Field, P. R., Franklin, C., Lawson, P., Wang, Z., Williams, E., Abel, S. J., Axisa, D., Borrmann, S., Crosier, J., Fugal, J., Krämer, M., Lohmann, U., Schlenczek, O., Schnaiter, M., and Wendisch, M.: Mixed-Phase Clouds: Progress and Challenges, Meteorol. Monogr., 58, 5.1–5.50, https://doi.org/10.1175/AMSMONOGRAPHS-D-17-0001.1, 2017.

Lo, C., Comstock, J. M., and Flynn, C.: An atmospheric radiation measurement value-added product to retrieve optically thin

cloud visible optical depth using micropulse lidar, Rep. DOE/SC-ARM/TR, 77, https://www.arm.gov/publications/tech_reports/doe-sc-arm-tr-077.pdf?id=34 (last access: 18 July 2022), 2006.

Mace, G. G., Zhang, Q., Vaughan, M., Marchand, R., Stephens, G., Trepte, C., and Winker, D.: A description of hydrometeor layer occurrence statistics derived from the first year of merged Cloudsat and CALIPSO data, J. Geophys. Res.-Atmos., 114, D8, https://doi.org/10.1029/2007JD009755, 2009.

Matus, A. V. and L'Ecuyer, T. S.: The role of cloud phase in Earth's radiation budget, J. Geophys. Res.-Atmos., 122, 2559–2578, https://doi.org/10.1002/2016JD025951, 2017.

Met Office, U. K.: Digital Library and Archive, Forecast Data and Analysis. Crown Copyright [2011,2017], Information provided by the National Meteorological Library and Archive, Met Office, UK, https://digital.nmla.metoffice.gov.uk/SO_a3062731-4abc-43b4-8a8a-477c76231d31/ (last access: 18 July 2022), 2021.

Miller, N. B., Shupe, M. D., Cox, C. J., Walden, V. P., Turner, D. D., and Steffen, K.: Cloud Radiative Forcing at Summit, Greenland, J. Climate, 28, 6267–6280, https://doi.org/10.1175/JCLI-D-15-0076.1, 2015.

Nakoudi, K., Ritter, C., and Stachlewska, I. S.: Properties of Cirrus Clouds over the European Arctic (Ny-Ålesund, Svalbard), Remote Sens., 13, 22, https://doi.org/10.3390/rs13224555, 2021a.

Nakoudi, K., Stachlewska, I. S., and Ritter, C.: An extended lidar-based cirrus cloud retrieval scheme: first application over an Arctic site, Opt. Express, 29, 8553–8580, https://doi.org/10.1364/OE.414770, 2021b.

NASA/LARC/SD/ASDC: CALIPSO Lidar Level 1B profile data, V4-10, https://doi.org/10.5067/CALIOP/CALIPSO/LID_L1-STANDARD-V4-10, 2016.

NASA/LARC/SD/ASDC: CALIPSO Lidar Level 2 5 km Cloud Layer, V4-20, https://doi.org/10.5067/CALIOP/CALIPSO/LID_L2_05KMCLAY-STANDARD-V4-20, 2018.

Nazaryan, H., McCormick, M. P., and Menzel, W. P.: Global characterization of cirrus clouds using CALIPSO data, J. Geophys. Res.-Atmos., 113, D16, https://doi.org/10.1029/2007JD009481, 2008.

Noel, V., Chepfer, H., Ledanois, G., Delaval, A., and Flamant, P. H.: Classification of particle effective shape ratios in cirrus clouds based on the lidar depolarization ratio, Appl. Optics, 41, 4245–4257, https://doi.org/10.1364/AO.41.004245, 2002.

Nomokonova, T., Ebell, K., Löhnert, U., Maturilli, M., Ritter, C., and O'Connor, E.: Statistics on clouds and their relation to thermodynamic conditions at Ny-Ålesund using ground-based sensor synergy, Atmos. Chem. Phys., 19, 4105–4126, https://doi.org/10.5194/acp-19-4105-2019, 2019.

Norwegian Meteorological Institute: MET Norway Thredds Service, Radiosonde archive, Norwegian Meteorological Institute [data set], https://thredds.met.no/thredds/catalog/remotesensingradiosonde/catalog.html (last access: 28 August 2020), 2021.

Pappalardo, G., Amodeo, A., Apituley, A., Comeron, A., Freudenthaler, V., Linné, H., Ansmann, A., Bösenberg, J., D'Amico, G., Mattis, I., Mona, L., Wandinger, U., Amiridis, V., Alados-Arboledas, L., Nicolae, D., and Wiegner, M.: EARLINET: towards an advanced sustainable European aerosol lidar network, Atmos. Meas. Tech., 7, 2389–2409, https://doi.org/10.5194/amt-7-2389-2014, 2014.

Platt, C. M. R.: Lidar and Radiometric Observations of Cirrus Clouds, J. Atmos. Sci., 30, 1191–1204, https://doi.org/10.1175/1520-0469(1973)030<1191:LAROOC>2.0.CO;2, 1973.

Sassen, K. and Cho, B. S.: Subvisual-Thin Cirrus Lidar Dataset for Satellite Verification and Climatological Research, J. Appl. Meteorol. Clim., 31, 1275–1285, https://doi.org/10.1175/1520-0450(1992)031<1275:STCLDF>2.0.CO;2, 1992.

Sassen, K., Wang, Z., and Liu, D.: Global distribution of cirrus clouds from CloudSat/Cloud-Aerosol Lidar and Infrared Pathfinder Satellite Observations (CALIPSO) measurements, J. Geophys. Res.-Atmos., 113, D8, https://doi.org/10.1029/2008JD009972, 2008.

Serreze, M. C. and Barry, R. G.: Processes and impacts of Arctic amplification: A research synthesis, Global Planet. Change, 77, 85–96, https://doi.org/10.1016/j.gloplacha.2011.03.004, 2011.

Shupe, M. D.: Clouds at Arctic Atmospheric Observatories. Part II: Thermodynamic Phase Characteristics, J. Appl. Meteorol. Clim., 50, 645–661, https://doi.org/10.1175/2010JAMC2468.1, 2011.

Shupe, M. D. and Intrieri, J. M.: Cloud radiative forcing of the Arctic surface: The influence of cloud properties, surface albedo, and solar zenith angle, J. Climate, 17, 616–628, 2004.

Shupe, M. D., Walden, V. P., Eloranta, E., Uttal, T., Campbell, J. R., Starkweather, S. M., and Shiobara, M.: Clouds at Arctic Atmospheric Observatories. Part I: Occurrence and Macrophysical Properties, J. Appl. Meteorol. Clim., 50, 626–644, https://doi.org/10.1175/2010JAMC2467.1, 2011.

Shupe, M. D., Turner, D. D., Walden, V. P., Bennartz, R., Cadeddu, M. P., Castellani, B. B., Cox, C. J., Hudak, D. R., Kulie, M. S., Miller, N. B., Neely, R. R., Neff, W. D., and Rowe, P. M.: High and Dry: New Observations of Tropospheric and Cloud Properties above the Greenland Ice Sheet, B. Am. Meteorol. Soc., 94, 169–186, https://doi.org/10.1175/BAMS-D-11-00249.1, 2013.

Shupe, M. D., Rex, M., Blomquist, B., Persson, P. O. G., Schmale, J., Uttal, T., Althausen, D., Angot, H., Archer, S., Bariteau, L., Beck, I., Bilberry, J., Bucci, S., Buck, C., Boyer, M., Brasseur, Z., Brooks, I. M., Calmer, R., Cassano, J., Castro, V., Chu, D., Costa, D., Cox, C. J., Creamean, J., Crewell, S., Dahlke, S., Damm, E., de Boer, G., Deckelmann, H., Dethloff, K., Dütsch, M., Ebell, K., Ehrlich, A., Ellis, J., Engelmann, R., Fong, A. A., Frey, M. M., Gallagher, M. R., Ganzeveld, L., Gradinger, R., Graeser, J., Greenamyer, V., Griesche, H., Griffiths, S., Hamilton, J., Heinemann, G., Helmig, D., Herber, A., Heuzé, C., Hofer, J., Houchens, T., Howard, D., Inoue, J., Jacobi, H.-W., Jaiser, R., Jokinen, T., Jourdan, O., Jozef, G., King, W., Kirchgaessner, A., Klingebiel, M., Krassovski, M., Krumpen, T., Lampert, A., Landing, W., Laurila, T., Lawrence, D., Lonardi, M., Loose, B., Lüpkes, C., Maahn, M., Macke, A., Maslowski, W., Marsay, C., Maturilli, M., Mech, M., Morris, S., Moser, M., Nicolaus, M., Ortega, P., Osborn, J., Pätzold, F., Perovich, D. K., Petäjä, T., Pilz, C., Pirazzini, R., Posman, K., Powers, H., Pratt, K. A., Preußer, A., Quéléver, L., Radenz, M., Rabe, B., Rinke, A., Sachs, T., Schulz, A., Siebert, H., Silva, T., Solomon, A., Sommerfeld, A., Spreen, G., Stephens, M., Stohl, A., Svensson, G., Uin, J., Viegas, J., Voigt, C., von der Gathen, P., Wehner, B., Welker, J. M., Wendisch, M., Werner, M., Xie, Z., and Yue, F.: Overview

of the MOSAiC expedition – Atmosphere, Elementa, 10, 1, https://doi.org/10.1525/elementa.2021.00060, 00060, 2022.

Skatteboe, R.: ALOMAR: atmospheric science using lidars, radars and ground based instruments, J. Atmos. Terr. Phys., 58, 1823–1826, 1996.

Stephens, G. L., Vane, D. G., Boain, R. J., Mace, G. G., Sassen, K., Wang, Z., Illingworth, A. J., O'connor, E. J., Rossow, W. B., Durden, S. L., Miller, S. D., Austin, R. T., Benedetti, A., Mitrescu, C., and the CloudSat Science Team: The CloudSat mission and the A-Train: A new dimension of space-based observations of clouds and precipitation, B. Am. Meteorol. Soc., 83, 1771–1790, 2002.

Stoffelen, A., Pailleux, J., Källén, E., Vaughan, J. M., Isaksen, L., Flamant, P., Wergen, W., Andersson, E., Schyberg, H., Culoma, A., Meynart, R., Endemann, M., and Ingmann, P.: The atmospheric dynamics mission for global wind field measurement, B. Am. Meteorol. Soc., 86, 73–88, 2005.

Sun, Z. and Shine, K. P.: Studies of the radiative properties of ice and mixed-phase clouds, Q. J. Roy. Meteorol. Soc., 120, 111–137, 1994.

Turner, D. D., Shupe, M. D., and Zwink, A. B.: Characteristic Atmospheric Radiative Heating Rate Profiles in Arctic Clouds as Observed at Barrow, Alaska, J. Appl. Meteorol. Clim., 57, 953–968, https://doi.org/10.1175/JAMC-D-17-0252.1, 2018.

Uttal, T., Curry, J. A., McPhee, M. G., Perovich, D. K., Moritz, R. E., Maslanik, J. A., Guest, P. S., Stern, H. L., Moore, J. A., Turenne, R., Heiberg, A., Serreze, M. C., Wylie, D. P., Persson, O. G., Paulson, C. A., Halle, C., Morison, J. H., Wheeler, P. A., Makshtas, A., Welch, H., Shupe, M. D., Intrieri, J. M., Stamnes, K., Lindsey, R. W., Pinkel, R., Pegau, W. S., Stanton, T. P., and Grenfeld, T. C.: Surface Heat Budget of the Arctic Ocean, B. Am. Meteorol. Soc., 83, 255–276, https://doi.org/10.1175/1520-0477(2002)083<0255:SHBOTA>2.3.CO;2, 2002.

Verlinde, J., Harrington, J. Y., McFarquhar, G., Yannuzzi, V., Avramov, A., Greenberg, S., Johnson, N., Zhang, G., Poellot, M., Mather, J. H., Turner, D. D., Eloranta, E. W., Zak, B. D., Prenni, A. J., Daniel, J. S., Kok, G. L., Tobin, D. C., Holz, R., Sassen, K., Spangenberg, D., Minnis, P., Tooman, T. P., Ivey, M. D., Richardson, S. J., Bahrmann, C. P., Shupe, M., DeMott, P. J., Heymsfield, A. J., and Schofield, R.: The mixed-phase Arctic cloud experiment, B. Am. Meteorol. Soc., 88, 205–222, 2007.

Voudouri, K. A., Giannakaki, E., Komppula, M., and Balis, D.: Variability in cirrus cloud properties using a Polly$^{XT}$ Raman lidar over high and tropical latitudes, Atmos. Chem. Phys., 20, 4427–4444, https://doi.org/10.5194/acp-20-4427-2020, 2020.

Wendisch, M., Brückner, M., Burrows, J., Crewell, S., Dethloff, K., Ebell, K., Lüpkes, C., Macke, A., Notholt, J., Quaas, J., Rinke, A., and Tegen, I.: Understanding causes and effects of rapid warming in the Arctic, Eos Trans. Am. Geophys. Union, 98, https://doi.org/10.1029/2017EO064803, 2017.

Winker, D. M., Vaughan, M. A., Omar, A., Hu, Y., Powell, K. A., Liu, Z., Hunt, W. H., and Young, S. A.: Overview of the CALIPSO mission and CALIOP data processing algorithms, J. Atmos. Ocean. Tech., 26, 2310–2323, https://doi.org/10.1175/2009JTECHA1281.1, 2009.

World Meteorological Organization (WMO): International meteorological vocabulary, 2nd edn., WMO-No. 182, ISBN 978-92-63-02182-3, https://library.wmo.int/doc_num.php?explnum_id=4712 (last access: 19 July 2022), 1992.

# Paper II

# The Ny-Ålesund Aerosol Cloud Experiment (NASCENT): Overview and First Results

II

# Paper III

# Simulations of primary and secondary ice production during an Arctic mixed-phase cloud case from the NASCENT campaign

III

III

Revised manuscript accepted for ACP on 2 May 2024, https://doi.org/10.5194/egusphere-2023-2907

# Simulations of primary and secondary ice production during an Arctic mixed-phase cloud case from the NASCENT campaign

Britta Schäfer[1], Robert Oscar David[1], Paraskevi Georgakaki[2], Julie Thérèse Pasquier[3], Georgia Sotiropoulou[4,2], and Trude Storelvmo[1,5]

[1]University of Oslo, Postbox 1022, Blindern, 0315 Oslo, Norway
[2]Laboratory of Atmospheric Processes and their Impacts, School of Architecture, Civil and Environmental Engineering, École Polytechnique Fédérale de Lausanne, Lausanne 1015, Switzerland
[3]Meteomatics AG, St. Gallen, Switzerland
[4]National and Kapodistrian University of Athens, Greece
[5]Nord University, Bodø, Norway

**Correspondence:** Britta Schäfer (britta.schafer@geo.uio.no)

**Abstract.** The representation of Arctic clouds and their phase distribution, i.e. the amount of ice and supercooled water, influences predictions of future Arctic warming. Therefore, it is essential that cloud phase is correctly captured by models in order to accurately predict the future Arctic climate. Ice crystal formation in clouds happens through ice nucleation (primary ice production) and ice multiplication (secondary ice production). In common weather and climate models, rime-splintering is the only secondary ice production process included. In addition, prescribed number concentrations of cloud condensation nuclei or cloud droplets and ice-nucleating particles are often overestimated in Arctic environments by standard model configurations. This can lead to a misrepresentation of the phase distribution and precipitation formation in Arctic mixed-phase clouds, with important implications for the Arctic surface energy budget. During the Ny-Ålesund Aerosol Cloud Experiment (NASCENT) a holographic probe mounted on a tethered balloon took in-situ measurements of ice crystal and cloud droplet number and mass concentrations in Svalbard, Norway, during fall 2019 and spring 2020. In this study, we choose one case study from this campaign showing evidence of strong secondary ice production and use the Weather Research and Forecasting (WRF) model to simulate it at a high vertical and spatial resolution. We test the performance of different microphysical parametrizations and apply a new state-of-the-art secondary ice parametrization. We find that the agreement with observations highly depends on the prescribed cloud condensation nuclei/cloud droplet and ice-nucleating particle concentration and requires an enhancement of secondary ice production processes. Lowering mass mixing ratio thresholds for rime splintering inside the Morrison microphysics scheme is crucial for enabling secondary ice production and thereby matching observations for the right reasons. In our case, rime-splintering is required to kick off collisional break-up. The simulated contribution from collisional break-up is larger than that from droplet shattering. Simulating ice production correctly for the right reasons is a prerequisite for reliable simulations of Arctic mixed-phase cloud responses to future temperature- or aerosol perturbations.

## 1 Introduction

Given the Arctic being the fastest warming region on Earth, understanding the drivers of Arctic climate change and in particular the role of clouds in this warming has been of special interest (e.g. Serreze and Barry, 2011; Wendisch et al., 2017, 2019). Cloud phase is an important parameter in Arctic clouds as it influences both their radiative properties and lifetime, and thereby controls their climatic impact (e.g. Morrison et al., 2012). Mixed-phase clouds, i.e. clouds consisting of both ice crystals and supercooled liquid water droplets, can form at temperatures between approximately -38 and 0 °C. In the Arctic, these clouds frequently occur in every season and are especially common at low and mid-levels (Shupe et al., 2006; de Boer et al., 2009; Shupe, 2011; Gierens et al., 2020). In order for ice to form in the mixed-phase cloud temperature regime, a special subset of aerosol known as ice-nucleating particles (INPs) is required. INPs act as a catalyst for water to freeze at temperatures above -38 °C (the homogeneous freezing temperature of water, Vali et al. (2015)). Previous studies suggest that ice formation and thereby also the phase partitioning between liquid and ice are strongly affected by the availability of INPs (Jackson et al., 2012; Solomon et al., 2018; Norgren et al., 2018; Carlsen and David, 2022; Creamean et al., 2022). However, to which degree the phase composition is determined by INPs is still an ongoing topic of research and investigated in field campaigns (e.g. Pasquier et al., 2022a).

There are different mechanisms through which INPs can nucleate ice, namely immersion, contact, condensation and deposition freezing (Vali et al., 2015). Immersion freezing occurs when an INP is immersed in a liquid droplet and initiates freezing (Vali et al., 2015). Condensation freezing is similar to immersion freezing except that the INP acts as a cloud condensation nuclei (CCN) and nucleates ice as soon as bulk water condenses on its surface. Contact freezing occurs when an INP triggers a supercooled cloud droplet to freeze upon collision (Diehl et al., 2002; Yang et al., 2020). Lastly, deposition freezing occurs when water vapor directly nucleates into ice on an INP (Vali et al., 2015), however more recent studies have shown that deposition freezing may actually occur due to bulk water condensed in nano-scale cracks or pores i.e. pore condensation and freezing (e.g. David et al., 2019b, 2020; Marcolli, 2014; Campbell and Christenson, 2018). Although condensation freezing is considered a separate ice nucleation process, it is debatable whether it is microphysically different from deposition/pore condensation and freezing and immersion freezing (Kanji et al., 2017).

While these heterogeneous ice nucleation processes together with homogeneous nucleation are commonly summarized as primary ice production processes, there has long been evidence for the existence of additional processes enhancing the number of ice crystals in clouds. Field measurements show that ice crystal number concentrations (ICNC) can significantly exceed INP concentrations (INPC) in clouds by up to five orders of magnitude (e.g. Auer et al., 1969; Beard, 1992; Cantrell and Heymsfield, 2005; Korolev and Leisner, 2020; Wieder et al., 2022a; Järvinen et al., 2022; Ladino et al., 2017). To explain this discrepancy, a number of so-called secondary ice production (SIP) processes for the multiplication of ice from existing frozen particles have been proposed. These processes include the collisional breakup of ice crystals (BR), rime splintering (RS, also called Hallett-Mossop process), droplet shattering when freezing (DS) and sublimation fragmentation in subsaturated cloud regions (SF) (e.g. Field et al., 2017; Korolev and Leisner, 2020). The existence of additional SIP processes has been proposed but these have yet to be named and confirmed Knight (2012). RS occurs when liquid droplets (diameter < 13 $\mu$m) or drops

(>25 $\mu$m) rime on ice crystals but is only believed to be active in the temperature range between -8 °C and -3 °C (Hallett and Mossop, 1974; Mossop, 1978; Field et al., 2017). BR, caused by ice-ice collisions, and DS, i.e. splinter production during the freezing of large droplets, as well as SF have been observed outside of this temperature range (Lauber et al., 2018; Korolev and Leisner, 2020; Keinert et al., 2020; Lauber et al., 2021, and references therein), and thus, have the potential to significantly increase ICNC throughout the entire mixed-phase temperature range (Karalis et al., 2022).

Nevertheless, RS is generally the only SIP process that is part of standard microphysics schemes available for both numerical weather prediction and climate models (e.g. Field et al., 2017; Zhao et al., 2021; Atlas et al., 2022). Many previous studies of model-observation comparisons therefore do not include additional SIP processes (Prenni et al., 2007; Luo et al., 2008; Barton et al., 2012; Young et al., 2017; Schemann and Ebell, 2020). These include e.g. the extensive modeling of Arctic stratocumulus clouds performed by Solomon et al. (2009) for cases from the M-PACE campaign that took place in 2004 (Verlinde et al., 2007). They tested several one- and two-moment schemes, all without SIP apart from RS, inside the Weather Research and Forecasting model (WRF) (Skamarock et al., 2019), and found an underestimation of the number of small ice crystals. However, more recent studies have started including DS and BR to address the lack of SIP processes in models. E.g., Fu et al. (2019) studied a case from the same campaign using the Milbrandt and Yau microphysics scheme (Milbrandt and Yau, 2005) with different SIP configurations including tests for DS and BR. They found that BR did not contribute significantly in their case while DS enhanced ICNC by roughly a factor of 2. Also, Sotiropoulou et al. (2021) and Georgakaki et al. (2022) implemented BR and DS, respectively, into the Morrison microphysics scheme (Morrison et al., 2009) in the WRF model following the parametrizations by Phillips et al. (2017, 2018). Sotiropoulou et al. (2021) found that including BR improved the representation of ICNC in the model considerably compared to field observations of Antarctic clouds. Georgakaki et al. (2022) found that including BR increases the simulated ICNC also in Alpine mixed-phase clouds and thereby leads to a better agreement with observations, while DS did not significantly contribute to the simulated ICNC.

In our study, we use the WRF model including the modified Morrison microphysics scheme from Sotiropoulou et al. (2021) and Georgakaki et al. (2022) for a case study from a campaign at the Svalbard archipelago where information about the presence of SIP is available from field measurements (Pasquier et al., 2022b). The Ny-Ålesund Aerosol Cloud Experiment (NASCENT) study took place from September 2019 to August 2020 in Ny-Ålesund, Svalbard (78.9°N, 11.9°E) (Pasquier et al., 2022a). One of its central objectives was to determine under which conditions either INPs or secondary ice production (SIP) dominantly affect the phase partitioning inside Arctic mixed-phase clouds. For a deeper understanding of this dependency, here we complement the performed observations with a regional modeling study. The main objective of this study is to simulate ice production that is in agreement with observations, both in terms of numbers and processes. We are particularly interested in whether the model can simulate an ICNC as high as observed when using measured INPC and added SIP processes.

A description of the used observations is given in Section 2, while modeling methods follow in Section 3. Section 4 comprises results and discussion before the conclusions are presented in Section 5.

## 2 Observations

We first present the relevant measurements from the campaign and then describe the meteorological situation of the chosen case study.

### 2.1 Instruments and measurements

In this study we utilize the extensive suite of aerosol and cloud measurements conducted during the NASCENT campaign (Pasquier et al., 2022a), which took place over an entire year (fall 2019-2020) in and around the Norwegian research village, Ny-Ålesund (78.9° N, 11.9° E). The measurements we use here are concentrations of aerosols suitable to act as CCN and INPs, measured at the ground, as well as ice crystal and cloud droplet number and mass concentrations, measured in-cloud from the holographic imager HOLIMO onboard the tethered balloon system HoloBalloon (Ramelli et al., 2020).

The CCN concentration (CCNC) was assessed from the concentration of aerosols larger than 70 nm as particles of these sizes can be used as a proxy for CCN (Koike et al., 2019; Pasquier et al., 2022a).

To quantify the INP concentrations, aerosols were sampled through an inlet in a container installed at the balloon launch site, using 1) the Horizontal Ice Nucleating Chamber (HINC; Lacher et al. (2017); Mahrt et al. (2018)) and 2) a high-flow rate liquid impinger (Bertin Coriolis-u) with subsequent analysis using the DRoplet Ice Nuclei Counter Zurich (DRINCZ; David et al. (2019a); Wieder et al. (2022b)). Both techniques measure INPs in the immersion mode (Li et al., 2022). It is important to note that due to the efficiency of the liquid-impinger, only aerosols larger than 500 nm could be assessed for their ice nucleating ability in DRINCZ. However, previous studies have shown that aerosols larger than 500 nm make up the largest fraction of the INP population (DeMott et al., 2010; Mason et al., 2015). HoloBalloon itself, or more precisely HOLIMO3B onboard it, provides hydrometeor number and size concentrations measured at altitudes up to 850 m. The technical setup and pixel size restrict the detection of small particles to diameters larger than 6 $\mu$m and up to 2 mm (Ramelli et al., 2020). The holographic imager sampled a 15.5 $cm^3$ volume of cloud at a rate of 6 Hz during the flights (Pasquier et al., 2022a, supplement). For this study, we use the hydrometeor number and size concentrations accumulated over 30 s, 60 s or 300 s, published in Pasquier et al. (2022c). All of the recorded hydrometeors larger than 25 $\mu$m were classified as either liquid droplets or ice particles using supervised machine learning (Touloupas et al., 2020). Meanwhile, all particles smaller than 25 $\mu$m were automatically classified as liquid droplets as a reliable phase classification based on particle shape from HoloBalloon is limited to particles larger than this threshold (Lauber, 2020). Therefore, the retrieved ICNC is strictly speaking a lower estimate. The phase separated number-size distributions were used to calculate the liquid water content (LWC) and ice water content (IWC). For the IWC, the effective mass-dimensional relationship reported in Cotton et al. (2013) was used. The associated uncertainties when using this approach are discussed in Heymsfield et al. (2010).

### 2.2 Case study

In this study we focus on the 12 November 2019 cloud event from the NASCENT campaign, when there was observational evidence for a large contribution of secondary ice production to the overall ice formation in the cloud (Pasquier et al., 2022a, b).

Pasquier et al. (2022a, b) determined this by following the approach presented in Korolev et al. (2020) where the concentration of small pristine ice crystals with diameters <100 $\mu$m is used as a measure to identify regions where recent ice formation occurred. If the observed concentration of the newly formed ice crystals is larger than the INPC, it is likely that SIP was occurring. Still, this assumption includes the caveat that the actual INPC might be larger than measured since INPs in the contact mode were not assessed. For a more detailed description of the application during the NASCENT campaign see Pasquier et al. (2022b).

On 12 November, a warm front influenced the weather around Ny-Ålesund (Fig. A1). The surface temperature varied between -3 °C and 0 °C, the dominant wind direction was southwesterly and there was a persistent mixed-phase cloud lasting until around 21 UTC. As the cloud top rose from ca. 1300 m to 2000 m a.s.l. during the day, the cloud top temperature decreased from around -11 to -14 °C. The cloud base varied between 200 m and 600 m a.s.l. and there were several periods of precipitation, resulting in about 2.4 mm of total precipitation (Pasquier et al., 2022a).

HoloBalloon performed three flights during 12 November 2019: 10:00-11:00, 12:15-14:00 and 14:45-17:00 UTC. The HoloBalloon measurement time spent at a certain altitude was not uniformly distributed, rather, the majority of the sampling time was spent close to the maximum altitude of the flight leading to the highest robustness of the measurements inside the main body of the cloud. The estimated CCNC on 12 November of around 9 $\mathrm{cm}^{-3}$ is within a factor of two of the observed cloud droplet number concentration (CDNC) varying between 5 and 15 $\mathrm{cm}^{-3}$, indicating that droplet formation was CCN limited (Motos et al., 2023). Such low concentrations were also commonly observed in earlier studies of CDNC in aerosol-limited regions (e.g. Mauritsen et al., 2011; Moore et al., 2013). The INP measurements made by DRINCZ during the day were fitted and reported as a function of temperature in Eq. 1 (Pasquier et al., 2022a, Fig. 7).

$$n_{\mathrm{INP}}(T)[\mathrm{m}^3] = 1000 \cdot \exp(-0.4146 \cdot (T[\mathrm{K}] - 273.15) - 12.4059) \quad (1)$$

The fit is several orders of magnitude lower than other parametrizations commonly used in weather and climate models that are often developed based on mineral dust or measurements from urban mid-latitude areas (e.g. Tobo et al., 2020), but on a similar order of magnitude to the INPC on other days during the NASCENT campaign (Li et al., 2022) as well as results from field campaigns in other Arctic and remote coastal sites (e.g. Hartmann et al., 2020; McCluskey et al., 2018; DeMott et al., 2016; Sze et al., 2023).

The reported CCNC and INP fit are used to replace default values in the model. This permits a better quantification of heterogeneous cloud particle formation and also guides towards accomplishing an agreement of the modeled cloud particle concentrations with observations through the correct processes. Details about the model setup and implementation of measured aerosol properties follow in the next section.

## 3 Modeling setup and methods

All of the simulations presented here were conducted with the WRF model. To account for the different microphysics schemes investigated, two model versions were used, namely version 4.2.1 for simulations with the Milbrandt and Yau (MY) microphysics scheme (Milbrandt and Yau, 2005) and version 4.0.1 for simulations with the Morrison (Morr) microphysics scheme (Morrison et al., 2009; Skamarock et al., 2019). The simulations with the Morr scheme were conducted with this version of WRF so that the modified Morr scheme with the secondary ice production processes implemented by Sotiropoulou et al. (2021) and Georgakaki et al. (2022) could be used. We used a nested setup with three domains, where the outermost domain had a resolution of 15 km, the middle domain had 5 km and the inner domain had 1 km resolution. The geographical extent of the domains is shown in Fig. 1, where the innermost domain spans 100 x 100 km. The number of vertical levels between the surface and 50 hPa was set to 172, whereof 93 are below 3 km altitude. This high vertical resolution was chosen to ensure that processes at cloud top and base are resolved in sufficient detail. All of the simulations were initiated on 11 Nov 2019 at 12 UTC, and had a duration of 36 h with a timestep of 30 s. The first 12 h of the simulations were used as spin-up. We initialized and nudged the model using reanalysis data from ERA5 on pressure levels at 00, 06, 12, and 18 UTC on the two outermost domains (Hersbach et al., 2018a, b). Grid nudging was performed for the two horizontal wind components, temperature and specific humidity. No nudging was performed at the surface. As by default in WRF, the nudging strength was $0.0003\,s^{-1}$ and nudging lasted for 60 min with a ramp-down at the end of the period. Longwave and shortwave radiation are treated by the CAM scheme (NCAR community atmosphere model, Collins et al. (2004)), and for boundary layer processes we use the YSU scheme (Yonsei University, Hong et al. (2006)). The cumulus parametrization for deep and shallow convection on subgrid scales was only turned on in the largest domain and here we used the scale aware Grell-Freitas ensemble scheme (Grell and Freitas, 2014).

The described settings for domain size, resolution, run duration, time step, nudging, radiation and convection parametrizations are the same for all runs. Changes are only made inside the microphysics schemes and will be explained in the following.

### 3.1 Microphysics parametrizations

To investigate the sensitivity of cloud properties such as CDNC, ICNC, LWC and IWC to both different microphysical parametrizations and to prescribed CCN and INPC, we perform similar sets of simulations with two different microphysics schemes that are described in more detail in the following subsections. Both schemes are double-moment schemes, but only the MY scheme predicts the CDNC from a prescribed CCNC and ambient supersaturation, while the Morr double-moment scheme uses a prescribed CDNC and therefore is actually only single-moment for cloud droplets. Additionally, MY has the largest number of hydrometeor classes, including cloud droplets, cloud ice, rain, snow, graupel and hail while Morr, in its default setup, does not include hail. The reasons for focusing most of the study on simulations with the Morr scheme were that the MY scheme failed to produce a suitable control simulation due to excessive graupel production when CCN/INP concentrations were adapted to observed values (see Section 4.3), and, more importantly, that we wanted to apply and test the new SIP implementation recently developed for the Morr scheme by Sotiropoulou et al. (2021) and Georgakaki et al. (2022).

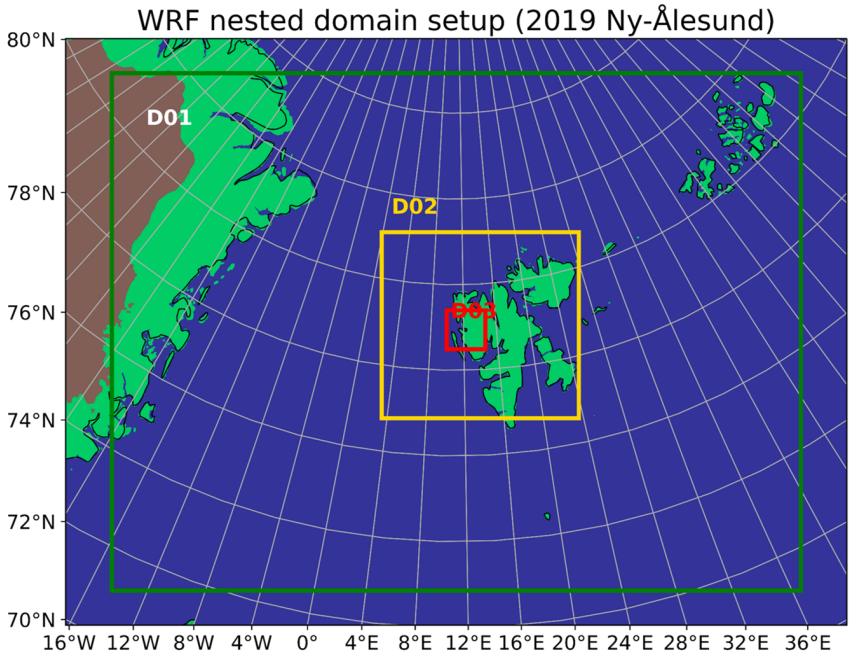


**Figure 1.** The three nested domains D01, D02 and D03 in the WRF model are shown by the green, yellow and red box, respectively. The associated horizontal resolutions are 15 km, 5 km and 1 km.

### Milbrandt and Yau scheme

In the MY scheme, CCNC and INPC are characterized individually. The default CCNC when there are negligible vertical motions or downdrafts is 200 $cm^{-3}$ for continental aerosol and 80 $cm^{-3}$ when maritime aerosol is selected. By default, continental aerosol is assumed and the corresponding value is used across the entire domain. During updrafts, the number of activated CCN is parametrized following Cohard and Pinty (2000), which takes into account local temperature, updraft speed and pressure.

The three possible pathways for primary ice production are heterogeneous ice nucleation, homogeneous freezing of cloud droplets, and freezing of rain drops (parametrized after Bigg (1953)). For heterogeneous ice nucleation, a switch enables either 1) the empirical parametrization from Meyers et al. (1992) for deposition and condensation-freezing and contact freezing parametrized following Young (1974) or 2) the parametrization from Cooper (1986) for deposition nucleation and no contact nucleation. As a default, option 1 (Meyers condensation/deposition nucleation and Young contact freezing) is active. Once primary ice is formed, the only SIP process included is RS (Hallett and Mossop, 1974). Ice mass may also increase from riming.

To assess the effect of changing the given aerosol parametrizations towards a more realistic representation of the environmental conditions in our case, we compare two simulations performed with the MY scheme. The first simulation uses the default parametrizations only ($MY_{def}$). In the second simulation, both the CCNC and INPC are adapted to match the estimated val-

| | CCNC [$cm^{-3}$] when $w \leq 0$ | CCNC [$cm^{-3}$] when $w > 0$ | deposition/sorption nucleation | immersion freezing | contact nucleation | rain freezing |
|---|---|---|---|---|---|---|
| $MY_{def}$ | 200 | Cohard and Pinty (2000) | Meyers et al. (1992) | off | Young (1974) | Bigg (1953) |
| $MY_{adap}$ | 9 | 9 | off | Pasquier et al. (2022a) | Young (1974) | off |

**Table 1.** Overview over simulations for 12 Nov 2019 with the Milbrandt and Yau microphysics (MY) scheme: The default scheme has two parametrizations for CCNC depending on the ambient vertical velocity $w$.

ues during 12 November ($MY_{adap}$) as follows: The CCNC is set to $9\,cm^{-3}$ during updrafts, negligible vertical motion and downdrafts. Regarding heterogeneous ice nucleation, we chose to stick with the default option (option 1) as it includes contact nucleation, which previous studies have shown is more important in Arctic mixed-phase clouds than deposition freezing (Morrison et al., 2005b, e.g.), and is not active in option 2. We replace the formula for deposition/condensation freezing by Meyers et al. (1992) with the fit for INPC in the immersion mode given in Eq. 1 (Pasquier et al., 2022a). This is because immersion freezing is generally seen as the most common process for ice nucleation in mixed-phase clouds in the Arctic and in general in supercooled layers warmer than -27 °C (de Boer et al., 2010; Westbrook and Illingworth, 2011; de Boer et al., 2011). For contact freezing, we use the parametrization by Young (1974), as no measurements of INPs in the contact freezing mode were conducted. For a further discussion of the treatment of contact nucleation, see the following section on the Morr scheme. Additionally, we turn off the freezing of rain drops in the model, as this process should only happen either because of an immersed INP or upon collisions with an ice particle (both already accounted for). All important parameter differences between the two simulations are given in Table 1.

**Morrison scheme**

The Morr scheme is described in Morrison et al. (2009) and builds on an older version published in 2005 (Morrison et al., 2005a). It is a double-moment scheme for the hydrometeor species rain, ice, snow and graupel, but only single-moment for cloud droplets as the CDNC is a predefined number. It also contains a switch to include hail as a separate category but this is not applied in this study.

In order for the Morr scheme to accurately represent the observed cloud properties for the correct physical reasons, several adaptations to the Morr scheme were tested and combined. The entire sequence of adaptations is shown in Fig 2 and Table 3. First, we adjusted the CDNC from the default value of $250\,cm^{-3}$ ($Morr_0$) to $9\,cm^{-3}$ ($Morr_1$), to match the observations within a factor of 2 (5-15 $cm^{-3}$ observed) (Pasquier et al., 2022a). Next, we adjusted primary ice production ($Morr_2$). Regarding processes involving INPs, the scheme contains the following: contact freezing parametrized after Meyers et al. (1992), deposition nucleation after Cooper (1986) and immersion freezing of cloud droplets and rain as parameterized by Bigg (1953). It is important to clarify here that Meyers et al. (1992) presented different parametrizations for deposition/condensation freezing and for contact freezing and the formula used here is not the one mentioned during the description of the MY scheme above for

condensation/deposition freezing. As the INP concentration during the NASCENT campaign was measured in the immersion mode, we use Eq. 1 retrieved in Ny-Ålesund (Pasquier et al., 2022a) to replace the formula by Bigg (1953) for the immersion freezing of cloud droplets. Along with this change, we introduce the following condition to limit ice nucleation by INPC: New ice crystals are only nucleated if supercooled cloud droplets are present and the number of INPs at the given temperature exceeds the number of ice particles present. This limitation is necessary to prevent infinite ice nucleation as the scheme is not aerosol aware and INPs nucleated earlier in the cloud are not removed (Kärcher and Marcolli, 2021). Before, i.e. in the default scheme ($\text{Morr}_0$), the maximum number of newly formed ice crystals through immersion freezing was only limited by the number of available droplets. However, a limitation based on the number of ice crystals existed for deposition nucleation in the default scheme. As such, we effectively combine these two limitations (ice crystal and cloud droplet number) now for immersion freezing.

Based on the same rationale as for MY, we disable immersion freezing of rain and deposition nucleation, but keep the default formula by Meyers et al. (1992) active for contact nucleation. Even though it is questionable to which extent contact freezing is actually occurring in the atmosphere (Ladino Moreno et al., 2013; Marcolli et al., 2016; Nagare et al., 2016), a sensitivity test with the Morr scheme (not shown) revealed that without contact freezing active and with immersion freezing parametrized after Pasquier et al. (2022a) as the only heterogeneous ice nucleation process, simulated ice crystal concentrations were far lower than observed. An agreement could not be achieved by adding SIP the way it is done in this study. Therefore, we decided to keep contact freezing active (see also Sect. 4.5). In summary, $\text{Morr}_2$ and $\text{MY}_{\text{adap}}$ contain comparable microphysical adjustments.

In $\text{Morr}_3$ we keep all of the previous adjustments from $\text{Morr}_2$ and add the SIP processes BR and DS following the parametrizations by Phillips et al. (2017, 2018) implemented into the Morr scheme for WRF by Sotiropoulou et al. (2021) and Georgakaki et al. (2022). As a result of implementing the BR parametrization following Phillips et al. (2017), the rimed fraction of snow and ice particles has to be prescribed and here we use a rimed fraction of 0.4 in all simulations that include BR ($\text{Morr}_3$, $\text{Morr}_4$ and $\text{Morr}_5$). This corresponds to heavily rimed particles and was found to give reasonable results in Sotiropoulou et al. (2021) even though the value in nature is highly variable. We also note that in the scheme by Georgakaki et al. (2022), DS was also allowed to be triggered by the freezing of rain drops in addition to during freezing induced by ice/snow/graupel-rain collisions (true SIP). Here, as we do not allow for immersion freezing of rain (but only cloud droplets), DS only includes events triggered by collisions.

Motivated by the results from $\text{Morr}_3$, we continued by adjusting the mixing ratio thresholds required for RS to occur ($\text{Morr}_4$) and finally the numbers of splinters created per RS event ($\text{Morr}_5$). We found that RS was not active in $\text{Morr}_3$, because the required mixing ratios for RS were never exceeded, and none of the newly implemented SIP mechanisms were triggered in a sufficient amount to increase ICNC either (see Sect. 4.4, Appendix C). However, the required mixing ratios for BR and DS used by Sotiropoulou et al. (2021) and Georgakaki et al. (2022) were actually much lower than the ones given by Morrison et al. (2009) for RS. In that light, we adapted the thresholds for RS to occur. In particular, we lowered the snow and graupel water mixing ratio thresholds to match those required for BR during snow-snow and graupel-graupel collisions ($10^{-8}$ kg/kg) and lowered the cloud liquid and rain water mixing ratios to those required for DS induced by rain-ice crystal collisions

| | | Snow - liquid | | | Graupel - liquid | |
|---|---|---|---|---|---|---|
| | $q_{\text{snow}}$ | $q_{\text{cloud liquid}}$ | $q_{\text{rain}}$ | $q_{\text{graupel}}$ | $q_{\text{cloud liquid}}$ | $q_{\text{rain}}$ |
| Default ($\text{Morr}_0$-$\text{Morr}_3$) | $10^{-4}$ | $0.5 \cdot 10^{-3}$ | $10^{-4}$ | $10^{-4}$ | $0.5 \cdot 10^{-3}$ | $10^{-4}$ |
| $\text{Morr}_4$, $\text{Morr}_5$ | $10^{-8}$ | $10^{-6}$ | $10^{-6}$ | $10^{-8}$ | $10^{-6}$ | $10^{-6}$ |
| Sinclair et al. (2016); | $10^{-4}$ | removed ($\approx 0$) | removed ($\approx 0$) | $10^{-4}$ | removed ($\approx 0$) | removed ($\approx 0$) |
| Young et al. (2019) | | | | | | |
| Atlas et al. (2020, 2022) | removed ($\approx 0$) | removed ($\approx 0$) | removed ($\approx 0$) | removed ($\approx 0$) | removed ($\approx 0$) | removed ($\approx 0$) |

**Table 2.** Mixing ratio thresholds in kg/kg that have to be overcome in order for rime splintering to happen in the Morrison microphysics scheme.

| | CDNC [$\text{cm}^{-3}$] | contact freezing | heterogeneous nucleation | immersion freezing | rime splintering | add. SIP |
|---|---|---|---|---|---|---|
| $\text{Morr}_0$ | 250 | Meyers et al. (1992) | Cooper (1986) | Bigg (1953) | on | no |
| $\text{Morr}_1$ | 9 | Meyers et al. (1992) | Cooper (1986) | Bigg (1953) | on | no |
| $\text{Morr}_2$ | 9 | Meyers et al. (1992) | off | Pasquier et al. (2022a) | on | no |
| $\text{Morr}_3$ | 9 | Meyers et al. (1992) | off | Pasquier et al. (2022a) | on | yes |
| $\text{Morr}_4$ | 9 | Meyers et al. (1992) | off | Pasquier et al. (2022a) | mod.thr. | yes |
| $\text{Morr}_5$ | 9 | Meyers et al. (1992) | off | Pasquier et al. (2022a) | mod. thr., no. splinters*20 | yes |

**Table 3.** Overview of runs for 12 Nov 2019 with the Morrison double-moment microphysics scheme (Morr). The parameters changed during different model runs are CDNC, INPC in primary ice production processes, and lower threshold values for mixing ratios during rime splintering. In addition, we implement the secondary ice processes in the Morr microphysics scheme introduced by Sotiropoulou et al. (2021) (BR) and Georgakaki et al. (2022) (DS).

($10^{-6}$ kg/kg). Earlier high-resolution modeling studies over the Southern Ocean and the Antarctic showed an improvement in the representation of low-level mixed-phase clouds in models when removing the RS thresholds in the Morr scheme (Sinclair et al., 2016; Young et al., 2019; Atlas et al., 2020, 2022; Sotiropoulou et al., 2021). Sinclair et al. (2016) and Young et al. (2019) only removed thresholds for liquid mixing ratios, while Atlas et al. (2022) explicitly recommend to completely remove all mass thresholds. The mixing ratio threshold values used in the different studies are given in Table 2.

A further discussion of the changes in RS efficiency follows in Sect. 4.5.

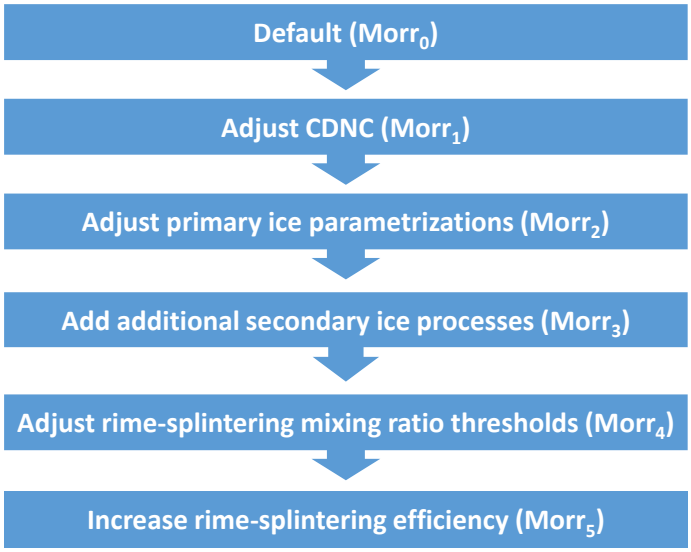


**Figure 2.** From default to final simulation: The different rows illustrate the steps from the default version of the Morrison scheme towards a version that represents cloud ice correctly. Adjusting CDNC and primary ice parametrizations is done by matching concentrations to observed values of CCNC and INPC. The modifications regarding secondary ice processes are necessary in order to make SIP as efficient in the model as it has been observed in this case.

### 3.2 Model-observation comparison methodology

Before comparing observed and simulated cloud properties, we test the model's ability to simulate the observed environment by comparing meteorological variables. For that, ambient and dew point temperature from the three radiosondes launched on 12 November are compared with the simulations at the closest grid point and time step. To then compare the observed and simulated hydrometeor concentrations, we take the model grid point that is closest to the location of HoloBalloon and average the simulated cloud properties over the given flight. To ensure that our results were robust, we also calculated these averages including a few neighboring grid points, but this did not alter the results (not shown). To match the data acquisition from HoloBalloon, we only distinguish between liquid and ice and sum up cloud and rain droplets into one liquid category (Pasquier et al., 2022a). Hence, hereafter the total LWC and CDNC always refer to the combined liquid category. Similarly, all ice particles are merged into one ice category characterized by total IWC and ICNC: these include ice crystals, snow and graupel in the Morr and MY schemes, as well as hail in MY. When comparing LWC, IWC, CDNC and ICNC with the values measured in-situ, we bin the observational data into 100 m intervals between 0 and 800 m altitude, centered around 50 m, 150 m, etc.. The cloud extended to higher altitudes than the tethered balloon was able to reach, therefore a direct comparison is limited to the part of the cloud below 800 m. Finally, we compare the simulated and observed precipitation accumulated over the 24 h of 12 Nov 2019 as well as downward longwave radiation at the surface. Total precipitation was measured using a single-fenced gauge, while the downward longwave radiation measurements were performed and provided by the French-German AWIPEV Research Base (Maturilli, 2019). As solid and mixed-phase precipitation is known to be underestimated when using single-fenced gauges (Wolff et al., 2015; Kochendorfer et al., 2017; Nitu et al., 2018), we adjust for this under-catch. In a simple estimate, we add 24% to the measured total precipitation which is the average under-catch reported for single-Alter-shielded gauges by Kochendorfer et al. (2017).

## 4 Results and Discussion

Before comparing the influence of the various microphysical parameterization changes in the model, we verify the performance of the model nudging by comparing the simulated meteorological conditions with radiosonde observations (Fig. 3). It should be noted that the radiosonde observations are incorporated into the Global Telecommunication System and thus ERA5 data, so no large differences should be expected. The simulated temperature profiles over Ny-Ålesund from the $\mathrm{MY}_{\mathrm{def}}$ and $\mathrm{Morr}_{0}$ simulations match the 11, 14 and 17 UTC radiosonde temperatures very well (mean deviation of 0.76 °C for both MY and Morr, see Fig. 3). The simulations also capture the dew point temperature profile well (mean deviation of 2.56 °C for MY and 2.55 °C for Morr), especially at lower altitudes up to 750 hPa where the cloud was present during the simulations (0.97 °C mean deviation for MY, 0.90 °C for Morr). With the simulated meteorological conditions validated when using the two microphysics schemes, we now assess the simulated macrophysical structure of the cloud before comparing the results from the MY and Morrison schemes against each other. Finally, we discuss the impact of the changes within the respective microphysics schemes.

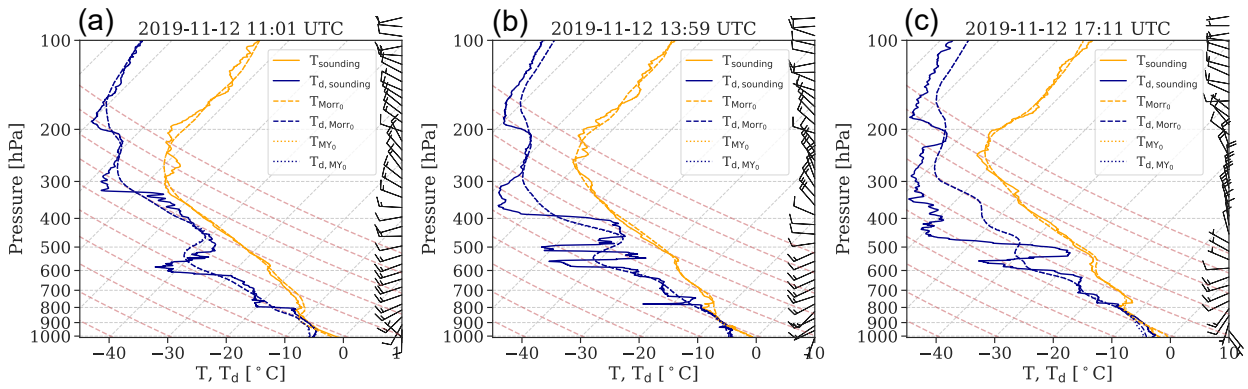


**Figure 3.** Simulated and radiosonde profiles of temperature (orange) and dew point temperature (blue) over Ny-Ålesund: Here the radiosoundings at (a) 11, (b) 14 and (c) 17 UTC (solid lines) are shown along with the simulations $MY_{def}$ (dotted) and $Morr_0$ (dashed) at the same given times. During the majority of altitudes and times, the profiles for $MY_{def}$ are not distinguishable as its values are identical with $Morr_0$. For illustration of the meteorological situation, we show the wind barbs from the sounding observations in addition.

### 4.1 Cloud macrophysics

Before diving into the analysis of microphysical cloud properties, we show that the macroscopic evolution of the cloud on Nov 12 agrees well between simulations and radar observations (Fig. 4). Throughout the day, the observed and simulated cloud top rises from ca. 1300 m at 6 UTC to around 2000 m at 18 UTC. This is true for simulations with both microphysics schemes and, relative to the increase in cloud top height throughout the day, variations in cloud top height between the different simulations are small (Figs. 5,6). This indicates that the changes in cloud microphysical properties discussed in subsequent sections are primarily caused by differences in the specific microphysics scheme and not by accompanying changes in cloud structure.

The simulated IWC and ICNC extend to higher altitudes than LWC (and CDNC) during all flights, indicating an ice-topped mixed-phase cloud (liquid only below ca. 1300 m vs. ice until 1450 m during the first and ca. 1800 m vs. 2000 m during the third flight, see Figs. 5,6). This result is in agreement with the Cloudnet classification (available from the Cloudnet data portal) that also identifies the cloud as ice-topped (Ebell et al., 2022). Previous observational studies have frequently observed liquid-topped mixed-phase clouds in the Arctic (de Boer et al., 2009; Morrison et al., 2012, e.g.). Therefore, the ice at cloud top in this case study may be a result of local effects (e.g. orography) or the synoptic situation.

### 4.2 Microphysics scheme intercomparison

In order to assess the influence of the MY and Morr schemes on the simulated cloud microphysics, we compare the results of the simulations using the two schemes in their default configurations ($MY_{def}$ and $Morr_0$, as described in Section 3.1). When comparing with the HoloBalloon measurements, it becomes clear that near the maximum flight altitude of HoloBalloon, the LWC is well captured by both simulations (see Fig. 5d and 6c). However, both $MY_{def}$ and $Morr_0$ are unable to reproduce the

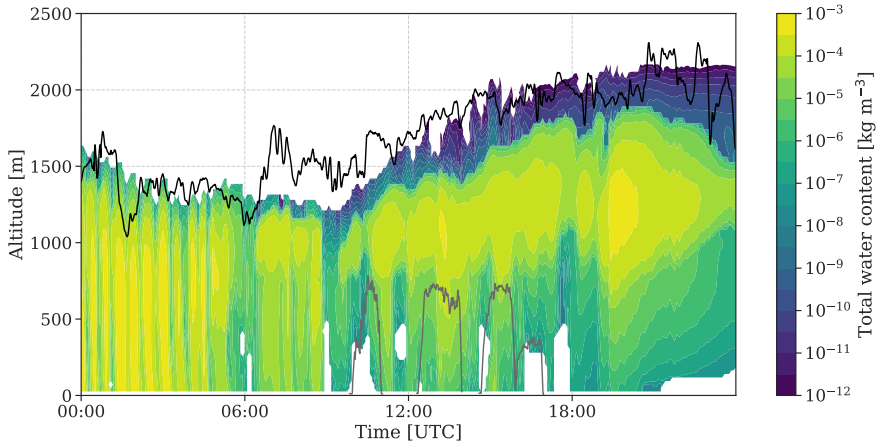


**Figure 4.** Total water content on 12 November as modeled by the final simulation $\text{Morr}_5$. The macrophysical shape of the cloud agrees well with observations of radar reflectivity (see Pasquier et al. (2022b, Fig. 3c)). The black lines show the observed cloud top as retrieved from radar measurements (Ebell et al., 2022) while the three flights performed by HoloBalloon are shown as grey lines.

LWC below 650 m, except for $\text{MY}_{\text{def}}$ during flight 1 (Fig. 5d, 6c) while $\text{MY}_{\text{def}}$ also underestimates CDNC in this altitude region (Fig. 5c). Simultaneously, $\text{MY}_{\text{def}}$ and $\text{Morr}_0$ underestimate IWC, particularly during the first flight. While the IWC magnitude is wrong in the simulations, they both have an almost constant value throughout the atmospheric layer considered, which is consistent with the observations. $\text{MY}_{\text{def}}$ is in slightly better agreement with the observed ICNC than $\text{Morr}_0$ but both simulations maintain too few ice crystals near the surface. This comparison suggests that relative to the observations the ice crystal aggregation may be too efficient in the default schemes, $\text{MY}_{\text{def}}$ and $\text{Morr}_0$, as evidenced by the near constant IWC and rapid decrease in ICNC towards the surface relative to the observations (Fig. 5a,b, 6a,b). The influence of constraining these two microphysical parametrizations with aerosol observations and the cause for these systematic biases in the default versions are discussed in the following sections.

### 4.3 Simulations using the Milbrandt and Yau microphysics scheme

As described in the previous section, $\text{MY}_{\text{def}}$ struggles to maintain enough LWC and CDNC below 650 m (Fig. 5c,d). The underestimation of liquid at lower altitudes is not overcome when the CCNC is adapted to observed values in $\text{MY}_{\text{adap}}$, but the representation is improved slightly, especially during flight 1. Meanwhile, the agreement between observed and simulated LWC is good around 750 m (Fig. 5d). Additionally taking the lowest part of the sounding comparison below 900 hPa into account (Fig. 3), this indicates that, at least during parts of the day, the simulated water vapor pressure is too low just above the surface. Thereby, the lifting condensation level, where dew point and absolute temperature are equal, is located too high in the model, which is visible from the soundings at 11 and 17 UTC (Fig. 3a,c). Nonetheless, at 14 UTC, there is no such discrepancy between simulated and observed dew point at the lowest altitudes (Fig. 3b).

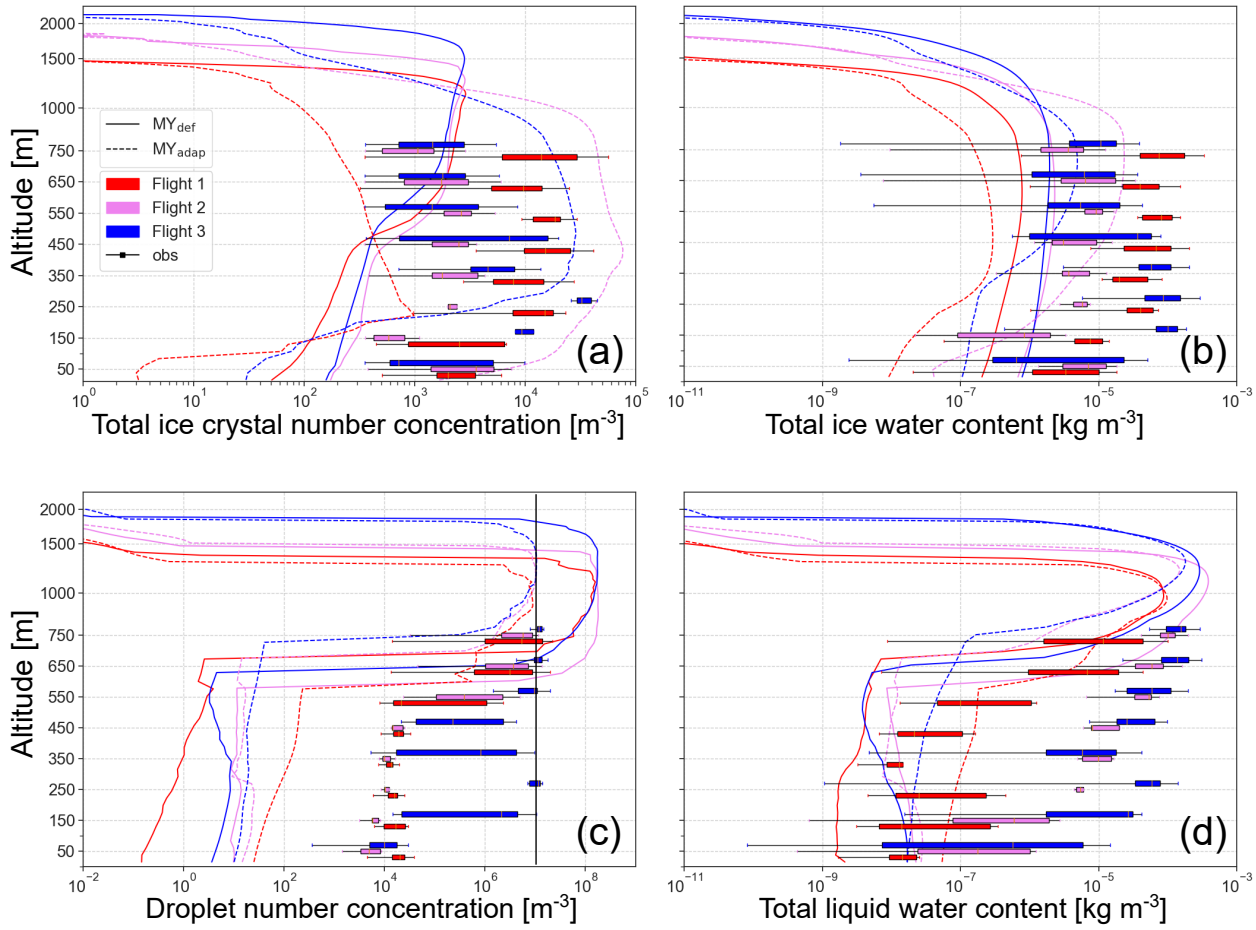


**Figure 5.** (a) Total ICNC, (b) IWC, (c) CDNC and (d) LWC on 12 Nov 2019 from the two simulations with the MY microphysics scheme. The different colors indicate the different balloon flights: flight 1 (10:00-11:00 UTC) in red, flight 2 (12:15-14:00 UTC) in violet, flight 3 (14:45-17:00 UTC) in blue. The different line styles indicate different simulations (solid line for $MY_{def}$, dashed line for $MY_{adap}$). The bar diagrams show observations put together in 100 m-bins between 0 and 800 m altitude, centered around 50 m, 150 m, etc.. Note that the y-axis is linear from the surface up to 800 m and logarithmic above to highlight the region where measurements are available. The black vertical line in (c) illustrates the constant CDNC used in the Morr simulations.

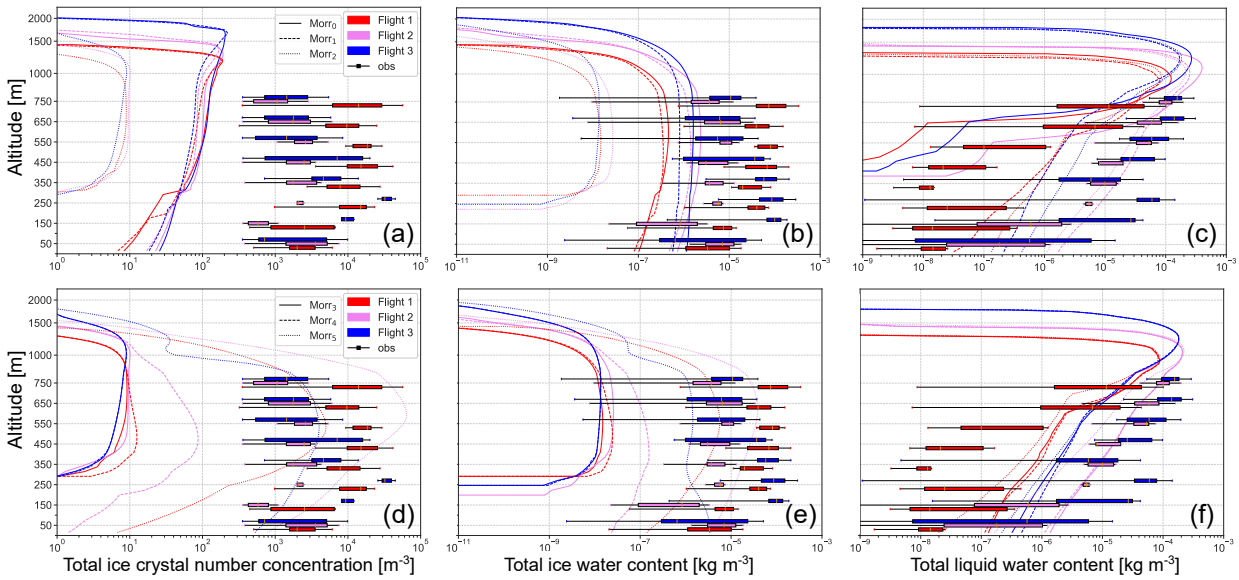


**Figure 6.** Same as Fig. 5, but for the simulations with the Morrison microphysics scheme and without showing droplet number concentration as this was predefined in the Morr scheme. Panels (a)-(c) show the simulations $\mathrm{Morr}_0$-$\mathrm{Morr}_2$, while (d)-(f) show the simulations $\mathrm{Morr}_3$-$\mathrm{Morr}_5$. The three balloon flights are marked by different colors, the simulations are distinguishable by linestyle. The profiles from $\mathrm{Morr}_2$ (upper row, dotted line) and $\mathrm{Morr}_3$ (lower row, solid line) look identical.

Compared to CDNC and LWC, variations in ICNC and IWC are much larger between the two simulations. In $\mathrm{MY}_{\mathrm{adap}}$, the ICNC increases from $\mathrm{MY}_{\mathrm{def}}$ and even surpasses the observed ICNC (Fig. 5a). This is quite surprising, as the INPC is significantly reduced in $\mathrm{MY}_{\mathrm{adap}}$ relative to $\mathrm{MY}_{\mathrm{def}}$. Upon further investigation, we find that the majority of the ICNC (and IWC) in $\mathrm{MY}_{\mathrm{adap}}$ is comprised of graupel (see Fig. B1), which is similar to the simulation in Pasquier et al. (2022a), but was not observed. To determine the major cause for this increase in graupel concentrations between $\mathrm{MY}_{\mathrm{def}}$ and $\mathrm{MY}_{\mathrm{adap}}$, we systematically performed simulations with only certain changes included at a time and found that the change in CCNC during updrafts is the determining factor for the increase in graupel number. We therefore conclude that the CCNC changes lead to changes in the cloud droplet size distribution that make riming more efficient. In a simulation where all adaptions given in Table 1 are included, except the CCNC during updrafts, which is kept parameterized following Cohard and Pinty (2000), the ICNC decreases and is lower than in $\mathrm{MY}_{\mathrm{def}}$, consistent with what we expected from lowering INP concentrations. In that case, the ICNC is two to three orders of magnitude lower than observed and not dominated by graupel (Fig. B2). These results show that $\mathrm{MY}_{\mathrm{def}}$ simulated the observed ICNC reasonably well, but for the wrong reasons, i.e. because of higher CCNC and INPC than observed. Instead, we expect SIP to be the missing process needed to simulate the cloud microphysical properties correctly and for the right reasons. Before an assessment of the effectiveness of SIP in the next section using the Morr scheme, we elaborate on the relevance of looking at the differences between flights as well as at the agreement between simulated and observed

precipitation and radiation.

Both the observations and simulations show variations in hydrometeor concentrations between flights, representing different environmental conditions throughout the day. This increases the credibility of the study's results even though the scope is limited to one day. The inter-flight spread in $\mathrm{MY}_{\mathrm{adap}}$, however, reveals that this simulation does not capture the change in ICNC, IWC and LWC between flight 1 and the subsequent flights correctly.

In addition to hydrometeor profiles, we assess precipitation accumulated over 24 h. The lack of simulated CDNC near the surface and the stronger reduction in ICNC and IWC towards the surface than observed lead to a strong underestimation of precipitation in both simulations (Fig. 7a).

Downward longwave radiation at the surface during the balloon flight times (10-17 UTC) is lower than observed in both simulations and lower in $\mathrm{MY}_{\mathrm{adap}}$ than in $\mathrm{MY}_{\mathrm{def}}$ (Fig. 7b). The overall underestimation of downward longwave radiation may be explained by a stronger simulated reduction in cloud water content towards the surface and thereby on average a higher and colder cloud base, but the detailed explanation remains uncertain.

Overall, our results show that the simulations with the MY scheme struggle to represent observed precipitation as well as observed CDNC and LWC at lower altitudes. Even though simulated ICNC and IWC agree better with observations, this is due to a higher CCNC and INPC than observed in $\mathrm{MY}_{\mathrm{def}}$ and due to a too high simulated graupel production in $\mathrm{MY}_{\mathrm{adap}}$, whereas we expect a strong SIP to be the missing element.

### 4.4 Simulations using the Morrison microphysics scheme

In this section, we show the results from six simulations with the Morr scheme, starting with the default version, $\mathrm{Morr}_0$. Regarding ICNC, the maximum simulated value in $\mathrm{Morr}_0$ is around $200\,\mathrm{m}^{-3}$ and thereby, depending on flight number and altitude, at least one order of magnitude below the observations (Fig. 6a). Also, the liquid part of the cloud has a base at ca. 400 m in contrast to the observations measuring liquid hydrometeors all the way to the surface (see Fig. 6c). This disagreement in LWC towards the surface is fixed by adapting the CDNC to the observed value of $9\,\mathrm{cm}^{-3}$, as done in simulation $\mathrm{Morr}_1$, which apart from the updated CDNC, has the same settings as $\mathrm{Morr}_0$. The reduced CDNC also results in an increase in the liquid precipitation simulated by $\mathrm{Morr}_1$, from 0.12 mm in $\mathrm{Morr}_0$ to 0.59 mm during 24 h on 12 Nov (Fig. 7a). This can be explained by fewer and larger droplets that more rapidly are converted to rain and fall out. However, it is important to note that in both $\mathrm{Morr}_0$ and $\mathrm{Morr}_1$, the majority of the precipitation is simulated during the early morning hours of Nov 12 and not during daytime when the balloon flights took place (not shown). Meanwhile, as expected, the IWC and ICNC are not impacted and remain on the same order of magnitude as in $\mathrm{Morr}_0$. Adapting the CDNC to the observed value results in a slight decrease in snowfall, but not by as much as the rainfall increases, leading to an increase in total precipitation (Fig. 7a).

When adapting the primary ice production via the INP concentration fit retrieved from the campaign measurements (as described in Section 3.1) in $\mathrm{Morr}_2$, the total ICNC and IWC decrease substantially, as expected. Ice (number and mass) no longer reaches the surface and even above ca. 300 m the ICNC and IWC decrease by approximately one and two orders of magnitude, respectively. This results in the suppression of the simulated snowfall at the surface, but also in a slight decrease in the total accumulated precipitation to 0.48 mm (Fig. 7a).

We expect that the decrease in ICNC from modifying heterogeneous nucleation will be counteracted by increasing SIP in $Morr_3$ following Sotiropoulou et al. (2021) and Georgakaki et al. (2022). However, this does not reduce the large discrepancy between the simulated and observed ICNC and the results of $Morr_3$ are in fact very similar to those of $Morr_2$ (Fig. 6a,d). To understand why implementing SIP in the simulation does not lead to substantial differences between $Morr_2$ and $Morr_3$, we examined the process tendencies from the model output in $Morr_3$ (similar to Fig. 8 where this is shown for $Morr_4$ and $Morr_5$). This allows us to quantify the contribution of the different processes, i.e. primary and secondary ice production processes, to the number of ice crystals formed.

In $Morr_3$ as well as the following simulations, we see that immersion freezing is mainly active at cloud top where the coldest temperatures occur, while contact freezing dominates inside the cloud (shown for $Morr_5$ in Fig. 8a). Meanwhile, in terms of SIP, RS did not occur in $Morr_3$ over Ny-Ålesund, even though a large portion of the cloud was within the RS temperature range and riming was occurring. BR occurred occasionally in $Morr_3$ but produced less ice crystals than primary ice production and DS occurred only sporadically but did not yield a substantial contribution to ice production (not shown).

Even though additional processes were implemented in $Morr_3$, they did not increase the ICNC compared to $Morr_2$ and the simulated ICNC still differed from the observations, as evidence of SIP was observed by HoloBalloon (Pasquier et al., 2022b). To investigate this discrepancy, we first adapted the required mixing ratio thresholds for RS to occur and then increased the number of splinters produced during RS in the following Section (Sect. 4.5).

### 4.5 Role of secondary ice

Contrary to our expectations, activating the SIP processes added in the Morr scheme by Sotiropoulou et al. (2021) did not immediately increase the ICNC. To investigate this surprising finding, we first lowered the thresholds required for RS to occur. Specifically, we set the cloud liquid/rain water and snow/graupel water mixing ratio thresholds to $10^{-8}$ and $10^{-6}$ kg/kg, respectively (see Tab. 2). The impact of lowering these thresholds is investigated in $Morr_4$ and results in a flight dependent change in the ICNC. Because graupel concentrations were negligible compared to snow in simulations with the Morr scheme, we focus on splintering events involving snow. Then, for RS to be able to occur in the model at a given time and altitude, the temperature must be within the given range (-8 °C < T < -3 °C), the snow water mixing ratio threshold must be overcome and, in addition, either the cloud liquid or rain water mixing ratio threshold must be overcome. In which altitude region and during which flight the individual conditions and the joint condition are fulfilled is given in Table C1. This overview explains the differences in the simulated impact of the RS process during different flights well. We find that the simulated snow water mixing ratio and the temperature are most influential in defining the RS active region, whereas the liquid water mixing ratio thresholds do not substantially limit the region further. As a result, during flight 1 and 2, the simulated ICNC increases by a factor of up to 2 and up to 10, respectively, while during flight 3 hardly any change in ICNC is simulated (see Fig. 6d, simulations $Morr_3$ and $Morr_4$). The latter is because the simulated snow water mixing ratio does not overcome the threshold at any altitude during the third flight. It should be noted that this is in contradiction with the observations, as HOLIMO measured the most SIP during flight 3. Along with RS, BR also became active during flight 1 and 2. Meanwhile, $Morr_4$ only showed a very minor contribution

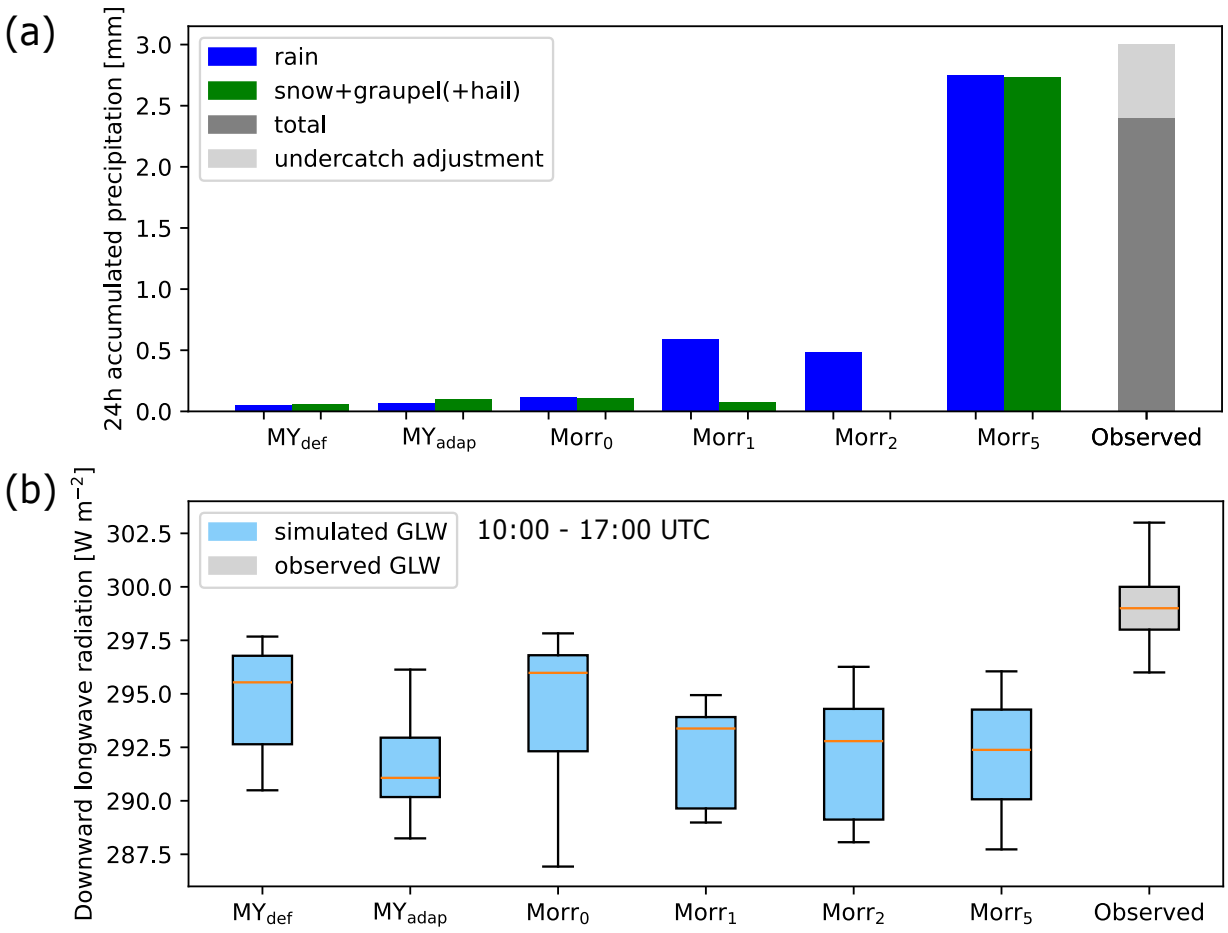


**Figure 7.** (a) Accumulated precipitation on 12 November (24 h), divided into liquid (blue) and frozen fraction (green) and (b) downward longwave radiation at the surface (GLW) between 10 and 17 UTC: Values are shown for the two simulations with the MY scheme, $MY_{def}$ and $MY_{adap}$, selected simulations with the Morr scheme, and observations (total precipitation shown in grey). As the observed precipitation was measured using a single-fenced gauge, there is likely an under-catch in the amount. Here, we adjust for that by adding 24% following Kochendorfer et al. (2017) (see Sect. 3.2). In the radiation panel (b), the orange lines illustrate the median, the boxes extend from the first to the third quartile of the data and the whisker end points mark the farthest point inside 1.5-times the inter-quartile range from the box. The observed GLW was measured from the French-German AWIPEV Research Base (Maturilli, 2019).

to the increase in ICNC from DS, and only during flight 2 (Fig. 8c). We discuss the relative importance of the different SIP mechanisms after presenting the results of the last adaption made in the scheme regarding the number of splinters produced during RS.

Previous studies have shown that the efficiency of the RS process increases in the presence of large cloud droplets (e.g. Mossop, 1978). As relatively large cloud droplets were observed during this case (Pasquier et al., 2022b, a), here we assess the impact of increasing the number of splinters produced by the RS process by a factor of 20 in the $\text{Morr}_5$ simulation (see Sect. 3.1). We justify this step by considering that cloud droplets in Arctic pristine conditions may be larger and lead to more splinters.

Even though the mixing ratio thresholds are not modified between $\text{Morr}_4$ and $\text{Morr}_5$, increasing the number of splinters generated influences the total ICNC during all flights. This increase in ICNC leads to a subsequent increase in BR, which in combination with the initial increase in ICNC from RS leads to a total increase in ICNC by up to three orders of magnitude, with BR making up a large share of that increase (Fig. 8b). This effectively leads to a "cascading" process of ice production as observed in field observations (Lawson et al., 2015; Pasquier et al., 2022b).

When comparing the observed and simulated SIP mechanisms, the observations indicate a more prominent contribution of SIP from DS (Pasquier et al., 2022a). In contrast, $\text{Morr}_5$ simulates that DS is not a determining factor in the increase in ICNC and only active at altitudes below 500 m/near cloud base (Fig. 8b). However, as the in-situ observations were made near cloud base, the fact that $\text{Morr}_5$ also simulates a contribution from DS in this region indicates that even though the model underestimates the contribution from DS, it is simulating it in the correct place. Additionally, it should be noted that near cloud base, where DS was observed and simulated, the temperatures were within the RS range. This, in combination with the observed frozen/fragmented droplets and rimed columns/lollipop ice (Pasquier et al., 2022a), makes it difficult to disentangle the true contributions from RS and DS from the measurements.

Nevertheless, our result that DS had a minor effect on the simulated ICNC is in agreement with the modelling study of wintertime alpine mixed-phase clouds by Georgakaki et al. (2022), which was conducted with the same modified Morrison microphysics scheme in WRF. This suggests a bias toward low DS activity in this scheme. As a possible key to alter this bias, two studies using the Morr microphysics scheme in global models suggest that, if a different size representation, i.e. a bin representation for the radius instead of a bulk representation of the particle mass, is used for cloud droplets during the treatment of DS, the magnitude of DS increases (Zhao et al., 2021; Sotiropoulou et al., 2022).

BR played the largest role in increasing ICNC not only in our case, but also in Georgakaki et al. (2022) and Sotiropoulou et al. (2021). However, Georgakaki et al. (2022) found that in their case falling ice crystals from aloft were important in initiating BR, which was not the case here. Sotiropoulou et al. (2021) also found that even with RS completely deactivated, BR alone could represent the observed ICNCs in Antarctic summer clouds. At the same time they admit that primary ice production might have been overestimated in their setup.

In our simulations with constrained CCNC and INPC, and thus a more realistic representation of primary ice production, we chose to reduce the thresholds for RS instead of removing them, as Sotiropoulou et al. (2021) hypothesized that removing all mass thresholds for RS overestimated RS. As previously stated, when the number of splinters is in addition increased relative to the default parametrization, our simulation results match the observed ICNC very well (Fig. 6d). This result is in accordance

with Young et al. (2019) who also found the best agreement between model and observations when removing the RS liquid mixing ratio threshold and making RS ten times more efficient in Arctic clouds. This may be due to the high concentration of large droplets observed in this case and typically found in the Arctic. When comparing the patterns in spatial and temporal extent of the SIP active regions for BR, RS and DS (Fig. 8b,c), it becomes clear that the higher number of splinters from RS in $\text{Morr}_5$ also strongly affects the activity of BR and DS. For example, during flight 3 where RS was not simulated in $\text{Morr}_4$ (Fig. 8c), SIP still became active enough to represent the observed ICNC in $\text{Morr}_5$ after increasing the number of splinters produced (Fig. 6f, blue dotted line). Overall, the activity of RS, BR and DS in time changes, e.g. due to the advection of ice particles between grid boxes, and a higher ICNC is maintained, in turn again favoring more SIP. Finally, our results show that in situations with constrained CCNC and INPC, maintaining some thresholds for RS works well when the number of splinters is also increased relative to the default parametrization.

As for the MY simulations, we assess the accumulated precipitation over 24 h and, here, we find a clear improvement in the representation in $\text{Morr}_5$, especially of solid precipitation (Fig. 7a). While highly underestimated in $\text{Morr}_0$, now total precipitation is even overestimated, likely due to a too high amount of supercooled drizzle. However, the phase assessment of precipitation from observations is uncertain and of qualitative type only, as it is based on the notes of the campaign crew, which do not cover the whole 24 h period. Looking at the downward longwave radiation during the flights, the variations in the median are small between the simulations $\text{Morr}_1$, $\text{Morr}_2$ and $\text{Morr}_5$, which all show lower values than $\text{Morr}_0$ (Fig. 7b). This hints to that the CDNC modification is influencing the radiation the most in our case. However, the reason for the underestimation compared to observations remains unclear.

Overall, $\text{Morr}_5$ clearly represents the best match with observations of ICNC and IWC even though the relative importance of BR and DS does not necessarily reflect the observations. It should also be noted that contact freezing is still active in this simulation. Assuming that this process is not as important in nature as simulated, the strength of SIP would need to be further increased. $\text{Morr}_5$ is the only simulation that produces an as high ICNC as observed and still represents LWC well and better than the default Morr scheme ($\text{Morr}_0$). In addition, it performs best in simulating enough precipitation. The combination of implemented and enhanced SIP processes is able to reproduce the observed ICNC and IWC during all flights, although the environmental conditions and the amount of IWC produced through primary ice production vary. Therefore we consider $\text{Morr}_5$ a successful attempt to represent an Arctic mixed-phase cloud with a realistic distribution of primary and secondary ice production.

## 5 Conclusions

This study shows that generalized out-of-the-box cloud microphysics schemes, i.e. MY and Morr, fail to correctly represent the vertical structure of ice and liquid water content of Arctic mixed-phase clouds. While these schemes do reproduce the observed maximum values reasonably well, we find that this occurs for the wrong reasons due to compensating errors. In the default schemes, the number of available aerosols for nucleating cloud particles is often unrealistically high for Arctic conditions

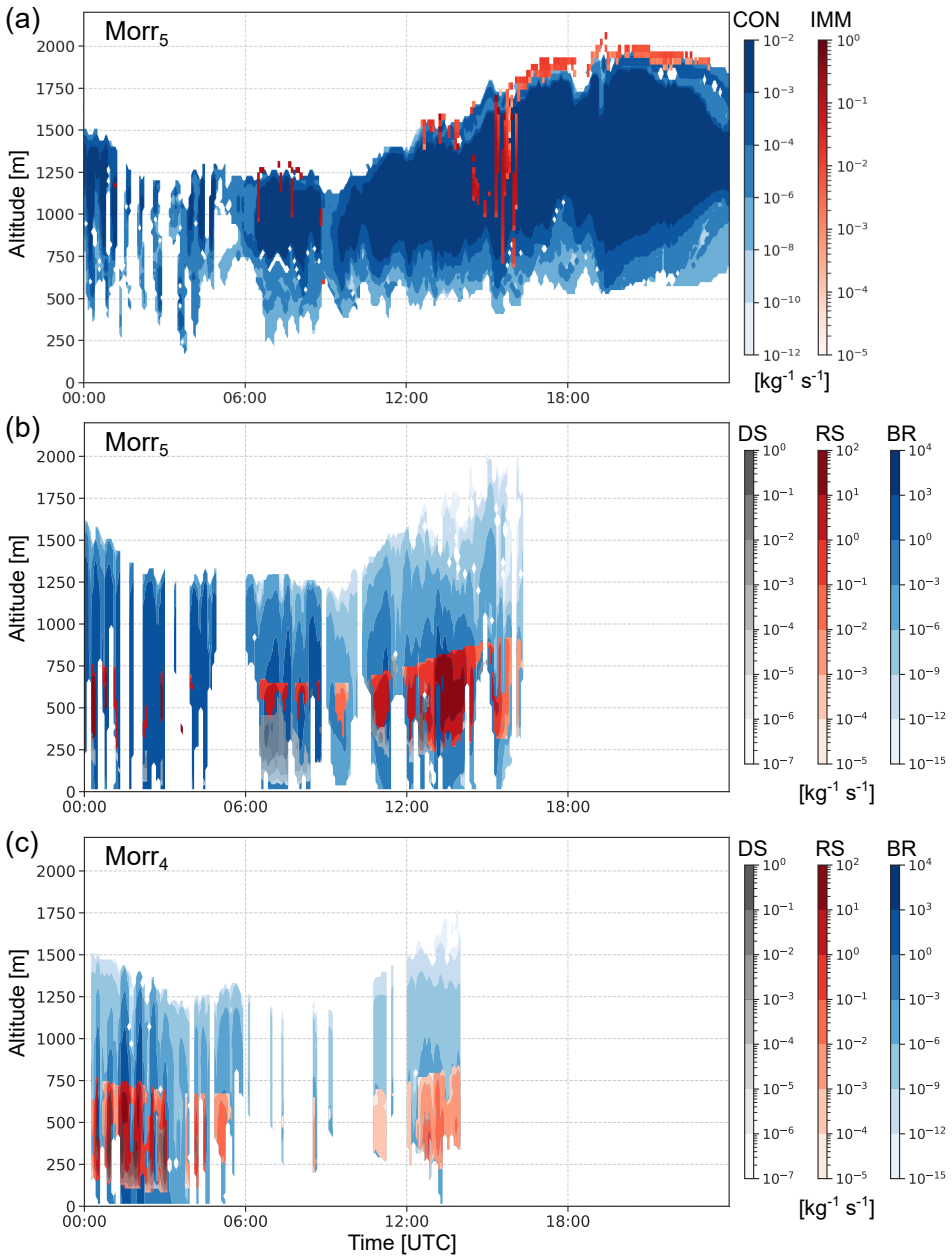


**Figure 8.** Ice crystal number concentration tendencies of (a) contact (CON, in blue) and immersion freezing (IMM, on top in red) and (b,c) collisional breakup (BR, in blue), rime splintering (RS, on top in red) and droplet shattering (DS, on top in grey): DS is shown partly transparent to visualize that BR is generally active simultaneously. The panels (a) and (b) show simulation $Morr_5$ while the lowermost panel (c) shows the SIP tendencies for simulation $Morr_4$.

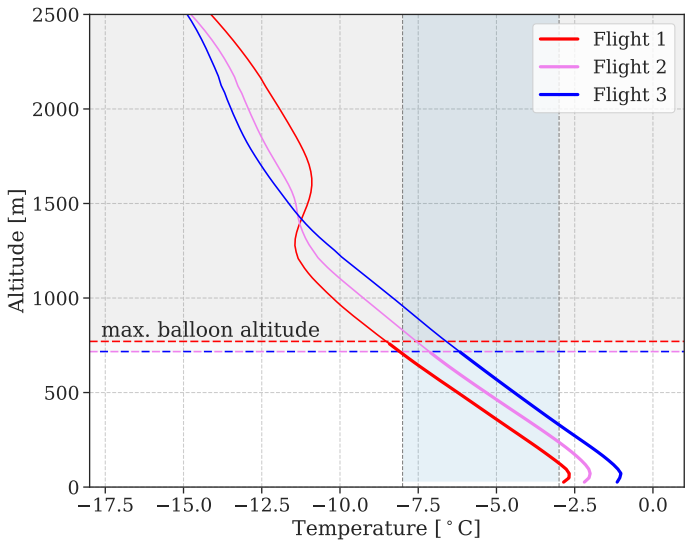


**Figure 9.** Temperature profiles from the model simulations averaged over the three flight times on 12 November. Here, the profiles from simulation $Morr_4$ are shown, but the choice of simulation does not play a role as the profiles don't vary across simulations. Temperatures below -38 °C, i.e. suitable for homogeneous freezing are reached above ca. 6300 m (not shown). The vertical dashed lines and shading indicate the temperature range where rime splintering is permitted (-8 to -3 °C), the colored horizontal dashed lines indicate the maximum flight altitudes.

and the overly efficient primary ice production compensates for the lack of secondary ice production. As shown here, in the pristine Arctic environment of Ny-Ålesund, Svalbard, the low-level mixed-phase cloud observed on 12 November 2019 is well represented in the WRF model with the default MY and Morr schemes in terms of macrophysical shape and water content, but the ICNC and the amount of precipitation from the cloud are underestimated. When the concentrations of aerosols suitable to nucleate cloud particles are adapted to observed values in the MY scheme, the ICNC increases, but is dominated by graupel which was not observed, but already pointed out in Pasquier et al. (2022a). This increase in graupel is caused by the lowered CCNC during updrafts, indicating that the MY scheme fails to represent ice production accurately in environments with very low CCNC. Meanwhile, the underestimation of liquid water towards the surface and of precipitation is not altered when aerosol concentrations are changed. In the Morr scheme, however, the simulation matches the observed ICNC and precipitation well, when the concentrations of cloud nucleating aerosols are adapted to observed values, rime splintering is made more efficient and further secondary ice processes are added. As the simulated primary ice production includes contact freezing, which is not observationally constrained and generally thought to be of limited importance, it must be considered an upper bound for the plausible primary ICNC contribution in this case. If we instead assume that contact freezing was significantly less important in our case than presumed in the simulations, or even not active at all, the already greatly enhanced secondary ice production

would have to be even further enhanced in order for agreement between simulated and observed ICNC to be achieved.

The lack of modeled secondary ice production in the default Morr scheme is both due to missing processes (in our case mainly collisional breakup) and too high snow, cloud liquid and rain water mixing ratio thresholds required for rime splintering to occur. Based on the earlier studies by Atlas et al. (2020, 2022); Sotiropoulou et al. (2021, 2020) and the finding in our case that the snow, cloud liquid and rain water mixing ratio never reached the thresholds required for rime splintering to happen in the default scheme, we recommend to lower these mixing ratio thresholds. The fact that the occurrence of rime splintering was needed in order to activate further SIP processes and ultimately represent observed ICNC further supports this recommendation. Otherwise, the thresholds restrict the occurrence of rime splintering to clouds with a higher ice and liquid water content than often observed in the Arctic. Additionally, we increase the number of splinters produced and find that an increase by a factor of 20 yields good agreement with observed ice crystal number concentrations. Based on this and the findings of Young et al. (2019), we hypothesize that this is justified in clean Arctic environments with relatively large droplets, but further laboratory and field studies relating the number of splinters produced by rime splintering to both mixing ratios and droplet sizes are required to confirm or reject this hypothesis. In addition to the ICNC profiles, also the simulated precipitation is considerably improved when aerosols and SIP processes are represented more realistically. The adapted schemes show a lower downward longwave radiation than default schemes, and the changes are likely mainly related to CCNC/CDNC changes. Thus, the misrepresentation of ice production might not lead to a bias in how much heat is trapped between the cloud and the surface, but due to an overall underestimation compared to observations, conclusions regarding downward longwave radiation remain uncertain.

Even though the changes made between the default simulation $\text{Morr}_0$ and the final simulation $\text{Morr}_5$ have been validated using the case study on 12 November with observational evidence for strong SIP, the applied modifications are meant to be of a general nature and should not hinder the application to cases where no SIP was observed. Also, the performance across different microphysical conditions between the flights already suggests that the modified scheme is applicable in different conditions. The correct representation of hydrometeor profiles as well as precipitation for the right reason is a prerequisite for model simulations to be used as baselines to investigate cloud responses to aerosol perturbations and future warming.

*Code and data availability.* The HoloBalloon data is available from Pasquier et al. (2022c). Cloudnet data is provided by the Finnish Meteorological Institute and available under https://cloudnet.fmi.fi. Radiosounding observations are available from https://thredds.met.no and PANGAEA (Maturilli, 2020). Observations of surface radiation from Ny-Ålesund are available from the World Radiation Monitoring Center - Baseline Surface Radiation Network (https://bsrn.awi.de). The modified Morrison scheme is available on request.

## Appendix A: Weather map

The following figure taken from Pasquier et al. (2022a, Fig. S2) illustrates the meteorological situation around Svalbard in the morning of 12 November 2019.

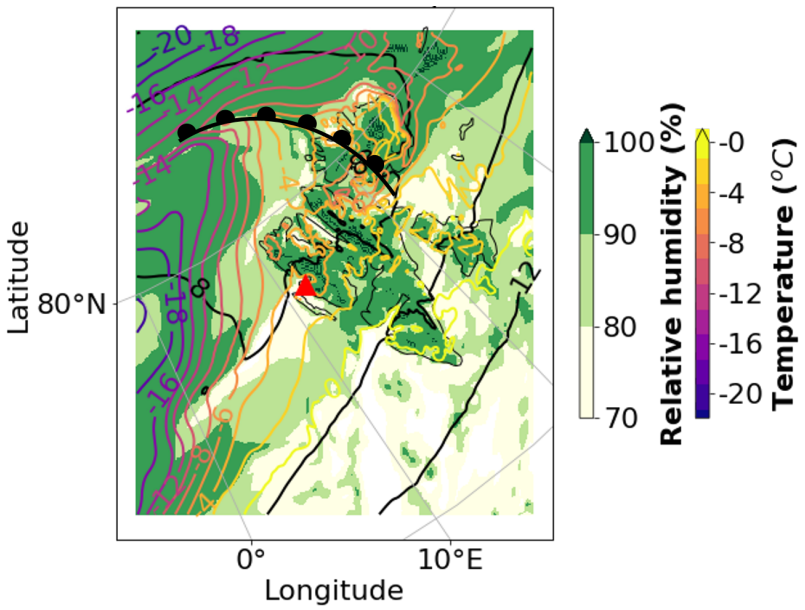


**Figure A1.** Map showing the synoptic situation with the estimated location of the warm front on 12 November at 06 UTC (figure taken from Pasquier et al. (2022a, Fig. S2), produced using MEPS model data (Hellmuth and Hofer, 2019)): The relative humidity and the temperature at 1000 hPa are indicated by green shading and colored lines, respectively. The red triangle shows the location of Ny-Ålesund.

## Appendix B: Impact of adapting updraft CCNC in the MY scheme

As mentioned in Section 4.3, the surprisingly high amount of graupel in $\mathrm{MY}_{\mathrm{adap}}$ (see Fig. B1) was not produced when all changes between $\mathrm{MY}_{\mathrm{def}}$ and $\mathrm{MY}_{\mathrm{adap}}$ were made except fixing the CCNC during updrafts to the observed value. Instead, the default parametrization by Cohard and Pinty (2000) was used here. The results of this simulation are marked by $\mathrm{MY}_{\mathrm{CP00}}$ in Fig. B2.

## Appendix C: Impact of RS mixing ratio threshold changes on simulated ICNC

Whether the lowering of required mixing ratio thresholds from simulation $\mathrm{Morr}_3$ to $\mathrm{Morr}_4$ has an effect on the simulated ICNC during one flight, depends on whether the new thresholds were overcome during the time of this flight. To reveal the regions where the lowered mixing ratio thresholds for RS in $\mathrm{Morr}_4$ actually enable RS, we show the altitude regions where the individual thresholds are overcome and where the joint condition (see Sect. 4.5) is met in Tab. C1. During flight 1, the flight time-averaged snow mixing ratio in $\mathrm{Morr}_4$ just overcame the updated threshold (by less than 50%) at altitudes between 350 and 620 m. At the same time, the temperature criterion was met between 100 and 700 m altitude and the rain mixing ratio exceeded the threshold above 370 m. Thus, the altitude region where RS involving snow and rain was active during flight 1 is located

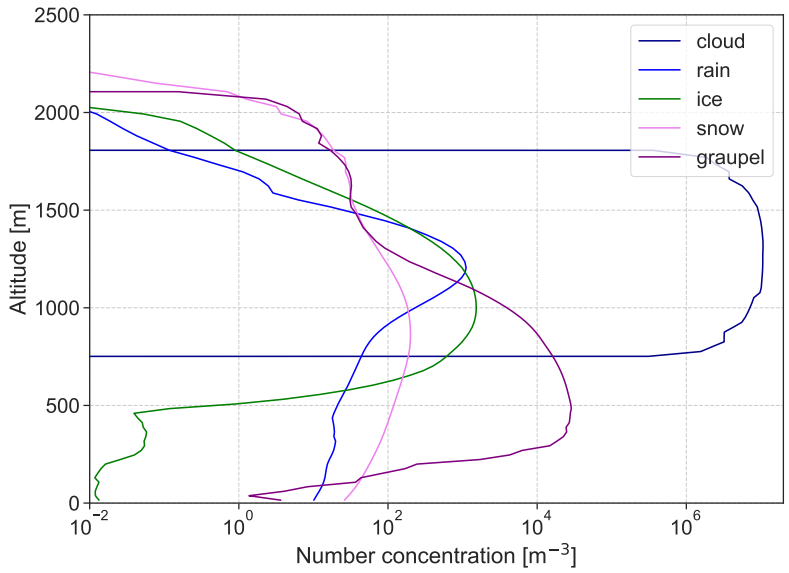


**Figure B1.** Number concentrations of individual hydrometeor categories in simulation $\mathrm{MY}_{\mathrm{adap}}$ during the third flight.

between 370 and 620 m. RS involving snow and cloud droplets was not occurring during flight 1 as the cloud liquid mixing ratio threshold was not overcome in the altitude region where the amount of snow was sufficiently high. During flight 2, both the snow and rain mixing ratio clearly exceeded the thresholds at all altitudes. Therefore, the impact of lowering the required mixing ratio thresholds is mostly captured during the second flight. The ice part of the cloud now extends to the surface as observed. Similar to during flight 1, the temperature profile leads to RS primarily increasing the ICNC towards cloud base where the cloud is warm enough for RS to be active (Fig. 9). During the third flight, however, the flight-averaged snow water mixing ratio was even lower than in the first flight and did not reach the threshold. This explains the lack of difference in ICNC between $\mathrm{Morr}_3$ and $\mathrm{Morr}_4$ for the third flight.

*Author contributions.* BS performed all model simulations, led the analysis and wrote the manuscript. RD and TS contributed to the manuscript and took part in the development of the methods and the discussion of the results. GS and PG provided the code for added SIP in the Morr scheme and assisted in setting it up. JP provided the measurement data and RD also participated in the measurement campaign. PG, JP and GS commented on the final version of the manuscript.

*Competing interests.* The authors declare that they have no conflict of interests.

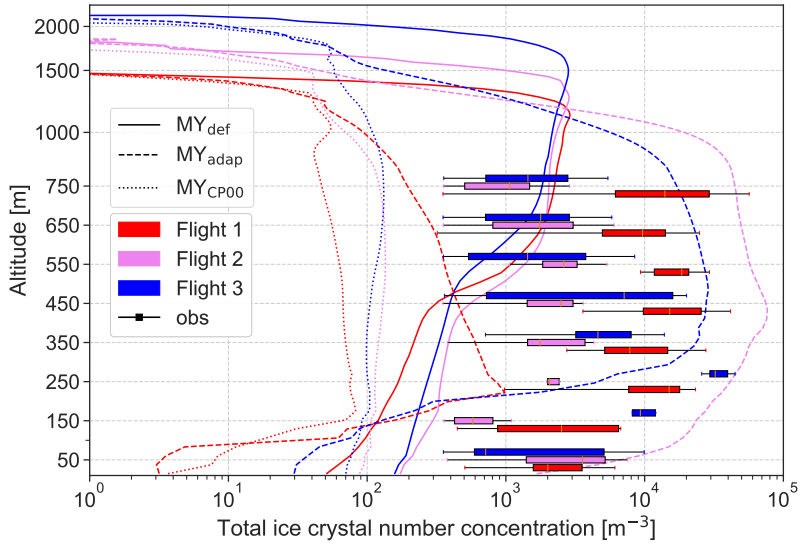


**Figure B2.** ICNC for the simulations $MY_{def}$, $MY_{adap}$ and $MY_{CP00}$ which is identical to $MY_{adap}$ apart from the CCNC during updrafts: The ICNC is much lower when CCNC during updrafts is parametrized by Cohard and Pinty (2000) than when it is set to 9 $cm^{-3}$.

| | Flight 1 | Flight 2 | Flight 3 |
|---|---|---|---|
| $q_{snow}$>$10^{-8}$ kg/kg | 350-620 m | all altitudes | no altitudes |
| $q_{cloud\ liquid}$>$10^{-6}$ kg/kg | above 640 m | above 570 m | above 610 m |
| $q_{rain}$>$10^{-6}$ kg/kg | above 370 m | all altitudes | above 200 m |
| -8 °C < T < -3 °C | 100-700 m | 250-800 m | 350-1000 m |
| RS active region | 370-620 m | 250-800 m | no altitudes |

**Table C1.** Regions where criteria for RS are met in $Morr_4$: In order for RS to happen, the threshold for the snow mixing ratio $q_{snow}$ has to be overcome, the temperature must be inside the given range and the cloud water mixing ratio $q_{cloud\ liquid}$ and/or rain water mixing ratio $q_{rain}$ must overcome the threshold. The combination of these limitations results in the RS active region given in the lowest row.

*Acknowledgements.* We gratefully acknowledge the funding by the European Research Council (ERC) through Grant StG758005 and CoG101045273. We would also like to acknowledge EEARO-NO-2019-0423/IceSafari, contract no. 31/2020, under the NO grants 2014–2021 of EEA Grants/Norway Grants and funding from the European Union's Horizon research and innovation programme under Grant Agreement 821205 (FORCeS). The simulations were performed on resources provided by Sigma2 - the National Infrastructure for High Performance Computing and Data Storage in Norway. We would like to thank everyone from ETH Zürich and other institutions who were part of the NASCENT campaign for sharing their dataset. We acknowledge ACTRIS and Finnish Meteorological Institute for providing the cloud clas-

sification which is available for download from https://cloudnet.fmi.fi. The cloud radar data for Ny-Ålesund was provided by the University of Cologne, the ceilometer and microwave radiometer data by the Alfred Wegener Institute, Helmholtz Centre for Polar and Marine Research.

## References


Atlas, R. L., Bretherton, C. S., Blossey, P. N., Gettelman, A., Bardeen, C., Lin, P., and Ming, Y.: How Well Do Large-Eddy Simulations and Global Climate Models Represent Observed Boundary Layer Structures and Low Clouds Over the Summertime Southern Ocean?, Journal of Advances in Modeling Earth Systems, 12, e2020MS002 205, https://doi.org/https://doi.org/10.1029/2020MS002205, e2020MS002205 10.1029/2020MS002205, 2020.

Atlas, R. L., Bretherton, C. S., Khairoutdinov, M. F., and Blossey, P. N.: Hallett-Mossop Rime Splintering Dims Cumulus Clouds Over the Southern Ocean: New Insight From Nudged Global Storm-Resolving Simulations, AGU Advances, 3, e2021AV000 454, https://doi.org/https://doi.org/10.1029/2021AV000454, e2021AV000454 2021AV000454, 2022.

Auer, A. H., Veal, D. L., and Marwitz, J. D.: Observations of Ice Crystal and Ice Nuclei Concentrations in Stable Cap Clouds, Journal of the Atmospheric Sciences, 26, 1342–1343, 1969.

Barton, N. P., Klein, S. A., Boyle, J. S., and Zhang, Y. Y.: Arctic synoptic regimes: Comparing domain-wide Arctic cloud observations with CAM4 and CAM5 during similar dynamics, Journal of Geophysical Research: Atmospheres, 117, https://doi.org/https://doi.org/10.1029/2012JD017589, 2012.

Beard, K. V.: Ice initiation in warm-base convective clouds: An assessment of microphysical mechanisms, Atmospheric Research, 28, 125–152, https://doi.org/https://doi.org/10.1016/0169-8095(92)90024-5, 1992.

Bigg, E.: The formation of atmospheric ice crystals by the freezing of droplets, Quarterly Journal of the Royal Meteorological Society, 79, 510–519, 1953.

Campbell, J. M. and Christenson, H. K.: Nucleation- and Emergence-Limited Growth of Ice from Pores, Phys. Rev. Lett., 120, 165 701, https://doi.org/10.1103/PhysRevLett.120.165701, 2018.

Cantrell, W. and Heymsfield, A.: Production of Ice in Tropospheric Clouds: A Review, Bulletin of the American Meteorological Society, 86, 795 – 808, https://doi.org/https://doi.org/10.1175/BAMS-86-6-795, 2005.

Carlsen, T. and David, R. O.: Spaceborne Evidence That Ice-Nucleating Particles Influence High-Latitude Cloud Phase, Geophysical Research Letters, 49, e2022GL098 041, https://doi.org/https://doi.org/10.1029/2022GL098041, e2022GL098041 2022GL098041, 2022.

Cohard, J.-M. and Pinty, J.-P.: A comprehensive two-moment warm microphysical bulk scheme. I: Description and tests, Quarterly Journal of the Royal Meteorological Society, 126, 1815–1842, https://doi.org/https://doi.org/10.1002/qj.49712656613, 2000.

Collins, W. D., Rasch, P. J., Boville, B. A., Hack, J. J., McCaa, J. R., Williamson, D. L., Kiehl, J. T., Briegleb, B., Bitz, C., Lin, S.-J., et al.: Description of the NCAR community atmosphere model (CAM 3.0), NCAR Tech. Note NCAR/TN-464+ STR, 226, 2004.

Cooper, W. A.: Ice Initiation in Natural Clouds, pp. 29–32, American Meteorological Society, Boston, MA, https://doi.org/10.1007/978-1-935704-17-1_4, 1986.

Cotton, R. J., Field, P. R., Ulanowski, Z., Kaye, P. H., Hirst, E., Greenaway, R. S., Crawford, I., Crosier, J., and Dorsey, J.: The effective density of small ice particles obtained from in situ aircraft observations of mid-latitude cirrus, Quarterly Journal of the Royal Meteorological Society, 139, 1923–1934, https://doi.org/https://doi.org/10.1002/qj.2058, 2013.

Creamean, J. M., Barry, K., Hill, T. C. J., Hume, C., DeMott, P. J., Shupe, M. D., Dahlke, S., Willmes, S., Schmale, J., Beck, I., Hoppe, C. J. M., Fong, A., Chamberlain, E., Bowman, J., Scharien, R., and Persson, O.: Annual cycle observations of aerosols capable of ice formation in central Arctic clouds, Nature Communications, 13, 3537, https://doi.org/10.1038/s41467-022-31182-x, 2022.

David, R. O., Cascajo-Castresana, M., Brennan, K. P., Rösch, M., Els, N., Werz, J., Weichlinger, V., Boynton, L. S., Bogler, S., Borduas-Dedekind, N., Marcolli, C., and Kanji, Z. A.: Development of the DRoplet Ice Nuclei Counter Zurich (DRINCZ): validation and applica-

tion to field-collected snow samples, Atmospheric Measurement Techniques, 12, 6865–6888, https://doi.org/10.5194/amt-12-6865-2019, 2019a.

David, R. O., Marcolli, C., Fahrni, J., Qiu, Y., Sirkin, Y. A. P., Molinero, V., Mahrt, F., Brühwiler, D., Lohmann, U., and Kanji, Z. A.: Pore condensation and freezing is responsible for ice formation below water saturation for porous particles, Proceedings of the National Academy of Sciences, 116, 8184–8189, https://doi.org/10.1073/pnas.1813647116, 2019b.

David, R. O., Fahrni, J., Marcolli, C., Mahrt, F., Brühwiler, D., and Kanji, Z. A.: The role of contact angle and pore width on pore condensation and freezing, Atmospheric Chemistry and Physics, 20, 9419–9440, https://doi.org/10.5194/acp-20-9419-2020, 2020.

de Boer, G., Eloranta, E. W., and Shupe, M. D.: Arctic Mixed-Phase Stratiform Cloud Properties from Multiple Years of Surface-Based Measurements at Two High-Latitude Locations, Journal of the Atmospheric Sciences, 66, 2874 – 2887, https://doi.org/https://doi.org/10.1175/2009JAS3029.1, 2009.

de Boer, G., Hashino, T., and Tripoli, G. J.: Ice nucleation through immersion freezing in mixed-phase stratiform clouds: Theory and numerical simulations, Atmospheric Research, 96, 315–324, https://doi.org/https://doi.org/10.1016/j.atmosres.2009.09.012, 15th International Conference on Clouds and Precipitation, 2010.

de Boer, G., Morrison, H., Shupe, M. D., and Hildner, R.: Evidence of liquid dependent ice nucleation in high-latitude stratiform clouds from surface remote sensors, Geophysical Research Letters, 38, https://doi.org/https://doi.org/10.1029/2010GL046016, 2011.

DeMott, P. J., Prenni, A. J., Liu, X., Kreidenweis, S. M., Petters, M. D., Twohy, C. H., Richardson, M. S., Eidhammer, T., and Rogers, D. C.: Predicting global atmospheric ice nuclei distributions and their impacts on climate, Proceedings of the National Academy of Sciences, 107, 11 217–11 222, https://doi.org/10.1073/pnas.0910818107, 2010.

DeMott, P. J., Hill, T. C. J., McCluskey, C. S., Prather, K. A., Collins, D. B., Sullivan, R. C., Ruppel, M. J., Mason, R. H., Irish, V. E., Lee, T., Hwang, C. Y., Rhee, T. S., Snider, J. R., McMeeking, G. R., Dhaniyala, S., Lewis, E. R., Wentzell, J. J. B., Abbatt, J., Lee, C., Sultana, C. M., Ault, A. P., Axson, J. L., Martinez, M. D., Venero, I., Santos-Figueroa, G., Stokes, M. D., Deane, G. B., Mayol-Bracero, O. L., Grassian, V. H., Bertram, T. H., Bertram, A. K., Moffett, B. F., and Franc, G. D.: Sea spray aerosol as a unique source of ice nucleating particles, Proceedings of the National Academy of Sciences, 113, 5797–5803, https://doi.org/10.1073/pnas.1514034112, 2016.

Diehl, K., Matthias-Maser, S., Jaenicke, R., and Mitra, S.: The ice nucleating ability of pollen:: Part II. Laboratory studies in immersion and contact freezing modes, Atmospheric Research, 61, 125–133, https://doi.org/https://doi.org/10.1016/S0169-8095(01)00132-6, 2002.

Ebell, K., Maturilli, M., and O'Connor, E.: Classification data from Ny-Ålesund on 12 November 2019, https://hdl.handle.net/21.12132/1.9f70b333642f41ab, 2022.

Field, P. R., Lawson, R. P., Brown, P. R. A., Lloyd, G., Westbrook, C., Moisseev, D., Miltenberger, A., Nenes, A., Blyth, A., Choularton, T., Connolly, P., Buehl, J., Crosier, J., Cui, Z., Dearden, C., DeMott, P., Flossmann, A., Heymsfield, A., Huang, Y., Kalesse, H., Kanji, Z. A., Korolev, A., Kirchgaessner, A., Lasher-Trapp, S., Leisner, T., McFarquhar, G., Phillips, V., Stith, J., and Sullivan, S.: Secondary Ice Production: Current State of the Science and Recommendations for the Future, Meteorological Monographs, 58, 7.1 – 7.20, https://doi.org/https://doi.org/10.1175/AMSMONOGRAPHS-D-16-0014.1, 2017.

Fu, S., Deng, X., Shupe, M. D., and Xue, H.: A modelling study of the continuous ice formation in an autumnal Arctic mixed-phase cloud case, Atmospheric Research, 228, 77–85, https://doi.org/https://doi.org/10.1016/j.atmosres.2019.05.021, 2019.

Georgakaki, P., Sotiropoulou, G., Vignon, E., Billault-Roux, A.-C., Berne, A., and Nenes, A.: Secondary ice production processes in wintertime alpine mixed-phase clouds, Atmospheric Chemistry and Physics, 22, 1965–1988, https://doi.org/10.5194/acp-22-1965-2022, 2022.

Gierens, R., Kneifel, S., Shupe, M. D., Ebell, K., Maturilli, M., and Löhnert, U.: Low-level mixed-phase clouds in a complex Arctic environment, Atmospheric Chemistry and Physics, 20, 3459–3481, https://doi.org/10.5194/acp-20-3459-2020, 2020.

Grell, G. A. and Freitas, S. R.: A scale and aerosol aware stochastic convective parameterization for weather and air quality modeling, Atmospheric Chemistry and Physics, 14, 5233–5250, 2014.

Hallett, J. and Mossop, S.: Production of secondary ice particles during the riming process, Nature, 249, 26–28, 1974.

Hartmann, M., Adachi, K., Eppers, O., Haas, C., Herber, A., Holzinger, R., Hünerbein, A., Jäkel, E., Jentzsch, C., van Pinxteren, M., Wex, H., Willmes, S., and Stratmann, F.: Wintertime Airborne Measurements of Ice Nucleating Particles in the High Arctic: A Hint to a Marine, Biogenic Source for Ice Nucleating Particles, Geophysical Research Letters, 47, e2020GL087 770, https://doi.org/https://doi.org/10.1029/2020GL087770, e2020GL087770 10.1029/2020GL087770, 2020.

Hellmuth, F. and Hofer, S.: Weathermaps from MEPS latest runs, https://github.com/franzihe/Weathermap, 2019.

Hersbach, H., Bell, B., Berrisford, P., Biavati, G., Horányi, A., Muñoz Sabater, J., Nicolas, J., Peubey, C., Radu, R., Rozum, I., Schepers, D., Simmons, A., Soci, C., Dee, D., and Thépaut, J.-N.: ERA5 hourly data on pressure levels from 1979 to present, Copernicus Climate Change Service (C3S) Climate Data Store (CDS) (Accessed on 19-MAR-2021), https://doi.org/10.24381/cds.bd0915c6, 2018a.

Hersbach, H., Bell, B., Berrisford, P., Biavati, G., Horányi, A., Muñoz Sabater, J., Nicolas, J., Peubey, C., Radu, R., Rozum, I., Schepers, D., Simmons, A., Soci, C., Dee, D., and Thépaut, J.-N.: ERA5 hourly data on single levels from 1979 to present, Copernicus Climate Change Service (C3S) Climate Data Store (CDS). (Accessed on 21-APR-2021), https://doi.org/10.24381/cds.adbb2d47, 2018b.

Heymsfield, A. J., Schmitt, C., Bansemer, A., and Twohy, C. H.: Improved Representation of Ice Particle Masses Based on Observations in Natural Clouds, Journal of the Atmospheric Sciences, 67, 3303 – 3318, https://doi.org/https://doi.org/10.1175/2010JAS3507.1, 2010.

Hong, S.-Y., Noh, Y., and Dudhia, J.: A new vertical diffusion package with an explicit treatment of entrainment processes, Monthly weather review, 134, 2318–2341, 2006.

Jackson, R. C., McFarquhar, G. M., Korolev, A. V., Earle, M. E., Liu, P. S. K., Lawson, R. P., Brooks, S., Wolde, M., Laskin, A., and Freer, M.: The dependence of ice microphysics on aerosol concentration in arctic mixed-phase stratus clouds during ISDAC and M-PACE, Journal of Geophysical Research: Atmospheres, 117, https://doi.org/https://doi.org/10.1029/2012JD017668, 2012.

Järvinen, E., McCluskey, C. S., Waitz, F., Schnaiter, M., Bansemer, A., Bardeen, C. G., Gettelman, A., Heymsfield, A., Stith, J. L., Wu, W., D'Alessandro, J. J., McFarquhar, G. M., Diao, M., Finlon, J. A., Hill, T. C. J., Levin, E. J. T., Moore, K. A., and DeMott, P. J.: Evidence for Secondary Ice Production in Southern Ocean Maritime Boundary Layer Clouds, Journal of Geophysical Research: Atmospheres, 127, e2021JD036 411, https://doi.org/https://doi.org/10.1029/2021JD036411, 2022.

Kanji, Z. A., Ladino, L. A., Wex, H., Boose, Y., Burkert-Kohn, M., Cziczo, D. J., and Krämer, M.: Overview of Ice Nucleating Particles, Meteorological Monographs, 58, 1.1 – 1.33, https://doi.org/https://doi.org/10.1175/AMSMONOGRAPHS-D-16-0006.1, 2017.

Karalis, M., Sotiropoulou, G., Abel, S. J., Bossioli, E., Georgakaki, P., Methymaki, G., Nenes, A., and Tombrou, M.: Effects of secondary ice processes on a stratocumulus to cumulus transition during a cold-air outbreak, Atmospheric Research, 277, 106 302, 2022.

Kärcher, B. and Marcolli, C.: Aerosol–cloud interactions: the representation of heterogeneous ice activation in cloud models, Atmospheric Chemistry and Physics, 21, 15 213–15 220, https://doi.org/10.5194/acp-21-15213-2021, 2021.

Keinert, A., Spannagel, D., Leisner, T., and Kiselev, A.: Secondary Ice Production upon Freezing of Freely Falling Drizzle Droplets, Journal of the Atmospheric Sciences, 77, 2959 – 2967, https://doi.org/https://doi.org/10.1175/JAS-D-20-0081.1, 2020.

Knight, C. A.: Ice Growth from the Vapor at -5°C, Journal of the Atmospheric Sciences, 69, 2031 – 2040, https://doi.org/10.1175/JAS-D-11-0287.1, 2012.

Kochendorfer, J., Nitu, R., Wolff, M., Mekis, E., Rasmussen, R., Baker, B., Earle, M. E., Reverdin, A., Wong, K., Smith, C. D., Yang, D., Roulet, Y.-A., Buisan, S., Laine, T., Lee, G., Aceituno, J. L. C., Alastrué, J., Isaksen, K., Meyers, T., Brækkan, R., Landolt, S., Jachcik, A.,

and Poikonen, A.: Analysis of single-Alter-shielded and unshielded measurements of mixed and solid precipitation from WMO-SPICE, Hydrology and Earth System Sciences, 21, 3525–3542, https://doi.org/10.5194/hess-21-3525-2017, 2017.

Koike, M., Ukita, J., Ström, J., Tunved, P., Shiobara, M., Vitale, V., Lupi, A., Baumgardner, D., Ritter, C., Hermansen, O., Yamada, K., and Pedersen, C. A.: Year-Round In Situ Measurements of Arctic Low-Level Clouds: Microphysical Properties and Their Relationships With Aerosols, Journal of Geophysical Research: Atmospheres, 124, 1798–1822, https://doi.org/https://doi.org/10.1029/2018JD029802, 2019.

Korolev, A. and Leisner, T.: Review of experimental studies of secondary ice production, Atmospheric Chemistry and Physics, 20, 11 767–11 797, https://doi.org/10.5194/acp-20-11767-2020, 2020.

Korolev, A., Heckman, I., Wolde, M., Ackerman, A. S., Fridlind, A. M., Ladino, L. A., Lawson, R. P., Milbrandt, J., and Williams, E.: A new look at the environmental conditions favorable to secondary ice production, Atmospheric Chemistry and Physics, 20, 1391–1429, https://doi.org/10.5194/acp-20-1391-2020, 2020.

Lacher, L., Lohmann, U., Boose, Y., Zipori, A., Herrmann, E., Bukowiecki, N., Steinbacher, M., and Kanji, Z. A.: The Horizontal Ice Nucleation Chamber (HINC): INP measurements at conditions relevant for mixed-phase clouds at the High Altitude Research Station Jungfraujoch, Atmospheric Chemistry and Physics, 17, 15 199–15 224, https://doi.org/10.5194/acp-17-15199-2017, 2017.

Ladino, L. A., Korolev, A., Heckman, I., Wolde, M., Fridlind, A. M., and Ackerman, A. S.: On the role of ice-nucleating aerosol in the formation of ice particles in tropical mesoscale convective systems, Geophysical Research Letters, 44, 1574–1582, https://doi.org/https://doi.org/10.1002/2016GL072455, 2017.

Ladino Moreno, L. A., Stetzer, O., and Lohmann, U.: Contact freezing: a review of experimental studies, Atmospheric Chemistry and Physics, 13, 9745–9769, https://doi.org/10.5194/acp-13-9745-2013, 2013.

Lauber, A.: In-situ observations of ice multiplication in clouds using a holographic imager and a deep learning algorithm for the classification of cloud particles, Ph.D. thesis, ETH Zürich, https://doi.org/10.3929/ethz-b-000474830, 2020.

Lauber, A., Kiselev, A., Pander, T., Handmann, P., and Leisner, T.: Secondary Ice Formation during Freezing of Levitated Droplets, Journal of the Atmospheric Sciences, 75, 2815 – 2826, https://doi.org/https://doi.org/10.1175/JAS-D-18-0052.1, 2018.

Lauber, A., Henneberger, J., Mignani, C., Ramelli, F., Pasquier, J. T., Wieder, J., Hervo, M., and Lohmann, U.: Continuous secondary-ice production initiated by updrafts through the melting layer in mountainous regions, Atmospheric Chemistry and Physics, 21, 3855–3870, https://doi.org/10.5194/acp-21-3855-2021, 2021.

Lawson, R. P., Woods, S., and Morrison, H.: The Microphysics of Ice and Precipitation Development in Tropical Cumulus Clouds, Journal of the Atmospheric Sciences, 72, 2429 – 2445, https://doi.org/https://doi.org/10.1175/JAS-D-14-0274.1, 2015.

Li, G., Wieder, J., Pasquier, J. T., Henneberger, J., and Kanji, Z. A.: Predicting atmospheric background number concentration of ice-nucleating particles in the Arctic, Atmospheric Chemistry and Physics, 22, 14 441–14 454, https://doi.org/10.5194/acp-22-14441-2022, 2022.

Luo, Y., Xu, K.-M., Morrison, H., and McFarquhar, G.: Arctic Mixed-Phase Clouds Simulated by a Cloud-Resolving Model: Comparison with ARM Observations and Sensitivity to Microphysics Parameterizations, Journal of the Atmospheric Sciences, 65, 1285 – 1303, https://doi.org/https://doi.org/10.1175/2007JAS2467.1, 2008.

Mahrt, F., Marcolli, C., David, R. O., Grönquist, P., Barthazy Meier, E. J., Lohmann, U., and Kanji, Z. A.: Ice nucleation abilities of soot particles determined with the Horizontal Ice Nucleation Chamber, Atmospheric Chemistry and Physics, 18, 13 363–13 392, https://doi.org/10.5194/acp-18-13363-2018, 2018.

Marcolli, C.: Deposition nucleation viewed as homogeneous or immersion freezing in pores and cavities, Atmospheric Chemistry and Physics, 14, 2071–2104, https://doi.org/10.5194/acp-14-2071-2014, 2014.

Marcolli, C., Nagare, B., Welti, A., and Lohmann, U.: Ice nucleation efficiency of AgI: review and new insights, Atmospheric Chemistry and Physics, 16, 8915–8937, https://doi.org/10.5194/acp-16-8915-2016, 2016.

Mason, R. H., Si, M., Li, J., Chou, C., Dickie, R., Toom-Sauntry, D., Pöhlker, C., Yakobi-Hancock, J. D., Ladino, L. A., Jones, K., Leaitch, W. R., Schiller, C. L., Abbatt, J. P. D., Huffman, J. A., and Bertram, A. K.: Ice nucleating particles at a coastal marine boundary layer site: correlations with aerosol type and meteorological conditions, Atmospheric Chemistry and Physics, 15, 12 547–12 566, https://doi.org/10.5194/acp-15-12547-2015, 2015.

Maturilli, M.: Basic and other measurements of radiation at station Ny-Ålesund (2019-11), PANGAEA, https://doi.org/10.1594/PANGAEA.909940, in: Maturilli, M (2020): Basic and other measurements of radiation at station Ny-Ålesund (2006-05 et seq). Alfred Wegener Institute - Research Unit Potsdam, PANGAEA, https://doi.org/10.1594/PANGAEA.914927, 2019.

Maturilli, M.: High resolution radiosonde measurements from station Ny-Ålesund (2019-11), PANGAEA, https://doi.org/10.1594/PANGAEA.911039, in: Maturilli, M (2020): High resolution radiosonde measurements from station Ny-Ålesund (2017-04 et seq). Alfred Wegener Institute - Research Unit Potsdam, PANGAEA, https://doi.org/10.1594/PANGAEA.914973, 2020.

Mauritsen, T., Sedlar, J., Tjernström, M., Leck, C., Martin, M., Shupe, M., Sjogren, S., Sierau, B., Persson, P. O. G., Brooks, I. M., and Swietlicki, E.: An Arctic CCN-limited cloud-aerosol regime, Atmospheric Chemistry and Physics, 11, 165–173, https://doi.org/10.5194/acp-11-165-2011, 2011.

McCluskey, C. S., Ovadnevaite, J., Rinaldi, M., Atkinson, J., Belosi, F., Ceburnis, D., Marullo, S., Hill, T. C. J., Lohmann, U., Kanji, Z. A., O'Dowd, C., Kreidenweis, S. M., and DeMott, P. J.: Marine and Terrestrial Organic Ice-Nucleating Particles in Pristine Marine to Continentally Influenced Northeast Atlantic Air Masses, Journal of Geophysical Research: Atmospheres, 123, 6196–6212, https://doi.org/https://doi.org/10.1029/2017JD028033, 2018.

Meyers, M. P., DeMott, P. J., and Cotton, W. R.: New primary ice-nucleation parameterizations in an explicit cloud model, Journal of Applied Meteorology and Climatology, 31, 708–721, 1992.

Milbrandt, J. and Yau, M.: A multimoment bulk microphysics parameterization. Part II: A proposed three-moment closure and scheme description, Journal of Atmospheric Sciences, 62, 3065–3081, https://doi.org/10.1175/JAS3535.1, 2005.

Moore, R. H., Karydis, V. A., Capps, S. L., Lathem, T. L., and Nenes, A.: Droplet number uncertainties associated with CCN: an assessment using observations and a global model adjoint, Atmospheric Chemistry and Physics, 13, 4235–4251, https://doi.org/10.5194/acp-13-4235-2013, 2013.

Morrison, H., Curry, J., and Khvorostyanov, V.: A new double-moment microphysics parameterization for application in cloud and climate models. Part I: Description, Journal of the atmospheric sciences, 62, 1665–1677, 2005a.

Morrison, H., Shupe, M. D., Pinto, J. O., and Curry, J. A.: Possible roles of ice nucleation mode and ice nuclei depletion in the extended lifetime of Arctic mixed-phase clouds, Geophysical Research Letters, 32, https://doi.org/https://doi.org/10.1029/2005GL023614, 2005b.

Morrison, H., Thompson, G., and Tatarskii, V.: Impact of cloud microphysics on the development of trailing stratiform precipitation in a simulated squall line: Comparison of one-and two-moment schemes, Monthly weather review, 137, 991–1007, 2009.

Morrison, H., De Boer, G., Feingold, G., Harrington, J., Shupe, M. D., and Sulia, K.: Resilience of persistent Arctic mixed-phase clouds, Nature Geoscience, 5, 11–17, 2012.

Mossop, S. C.: The influence of drop size distribution on the production of secondary ice particles during graupel growth, Quarterly Journal of the Royal Meteorological Society, 104, 323–330, https://doi.org/https://doi.org/10.1002/qj.49710444007, 1978.

Motos, G., Freitas, G., Georgakaki, P., Wieder, J., Li, G., Aas, W., Lunder, C., Krejci, R., Pasquier, J. T., Henneberger, J., David, R. O., Ritter, C., Mohr, C., Zieger, P., and Nenes, A.: Aerosol and dynamical contributions to cloud droplet formation in Arctic low-level clouds, Atmospheric Chemistry and Physics, 23, 13 941–13 956, https://doi.org/10.5194/acp-23-13941-2023, 2023.

Nagare, B., Marcolli, C., Welti, A., Stetzer, O., and Lohmann, U.: Comparing contact and immersion freezing from continuous flow diffusion chambers, Atmospheric Chemistry and Physics, 16, 8899–8914, https://doi.org/10.5194/acp-16-8899-2016, 2016.

Nitu, R., Roulet, Y.-A., Wolff, M., Earle, M., Reverdin, A., Smith, C., Kochendorfer, J., Morin, S., Rasmussen, R., Wong, K., Alastrué, J., Arnold, L., Baker, B., Buisán, S., Collado, J., Colli, M., Collins, B., Gaydos, A., Hannula, H.-R., Hoover, J., Joe, P., Kontu, A., Laine, T., Lanza, L., Lanzinger, E., Lee, G., Lejeune, Y., Leppänen, L., Mekis, E., Panel, J.-M., Poikonen, A., Ryu, S., Sabatini, F., Theriault, J., Yang, D., Genthon, C., van den Heuvel, F., Hirasawa, N., Konishi, H., Motoyoshi, H., Nakai, S., Nishimura, K., Senese, A., and Yamashita, K.: WMO Solid Precipitation Intercomparison Experiment (SPICE) (2012 - 2015), Tech. Rep. Instruments and Observing Methods (IOM) Report No. 131, World Meteorological Organization, Geneva, Switzerland, https://library.wmo.int/idurl/4/56317, 2018.

Norgren, M. S., de Boer, G., and Shupe, M. D.: Observed aerosol suppression of cloud ice in low-level Arctic mixed-phase clouds, Atmospheric Chemistry and Physics, 18, 13 345–13 361, https://doi.org/10.5194/acp-18-13345-2018, 2018.

Pasquier, J. T., David, R. O., Freitas, G., Gierens, R., Gramlich, Y., Haslett, S., Li, G., Schäfer, B., Siegel, K., Wieder, J., Adachi, K., Belosi, F., Carlsen, T., Decesari, S., Ebell, K., Gilardoni, S., Gysel-Beer, M., Henneberger, J., Inoue, J., Kanji, Z. A., Koike, M., Kondo, Y., Krejci, R., Lohmann, U., Maturilli, M., Mazzolla, M., Modini, R., Mohr, C., Motos, G., Nenes, A., Nicosia, A., Ohata, S., Paglione, M., Park, S., Pileci, R. E., Ramelli, F., Rinaldi, M., Ritter, C., Sato, K., Storelvmo, T., Tobo, Y., Traversi, R., Viola, A., and Zieger, P.: The Ny-Ålesund Aerosol Cloud Experiment (NASCENT): Overview and First Results, Bulletin of the American Meteorological Society, 103, E2533 – E2558, https://doi.org/https://doi.org/10.1175/BAMS-D-21-0034.1, 2022a.

Pasquier, J. T., Henneberger, J., Ramelli, F., Lauber, A., David, R. O., Wieder, J., Carlsen, T., Gierens, R., Maturilli, M., and Lohmann, U.: Conditions favorable for secondary ice production in Arctic mixed-phase clouds, Atmospheric Chemistry and Physics, 22, 15 579–15 601, 2022b.

Pasquier, J. T., Henneberger, J., Ramelli, F., Wieder, J., Gierens, R., Ebell, K., Li, G., David, R. O., and Carlsen, T.: Data from the NASCENT campaign used in the publications: "Conditions favorable for secondary ice production in Arctic mixed-phase clouds" and "Understanding the history of two complex ice crystal habits deduced from a holographic imager", https://doi.org/10.5281/zenodo.7402285, 2022c.

Phillips, V. T. J., Yano, J.-I., Formenton, M., Ilotoviz, E., Kanawade, V., Kudzotsa, I., Sun, J., Bansemer, A., Detwiler, A. G., Khain, A., and Tessendorf, S. A.: Ice Multiplication by Breakup in Ice–Ice Collisions. Part II: Numerical Simulations, Journal of the Atmospheric Sciences, 74, 2789 – 2811, https://doi.org/https://doi.org/10.1175/JAS-D-16-0223.1, 2017.

Phillips, V. T. J., Patade, S., Gutierrez, J., and Bansemer, A.: Secondary Ice Production by Fragmentation of Freezing Drops: Formulation and Theory, Journal of the Atmospheric Sciences, 75, 3031 – 3070, https://doi.org/https://doi.org/10.1175/JAS-D-17-0190.1, 2018.

Prenni, A. J., Harrington, J. Y., Tjernström, M., DeMott, P. J., Avramov, A., Long, C. N., Kreidenweis, S. M., Olsson, P. Q., and Verlinde, J.: Can Ice-Nucleating Aerosols Affect Arctic Seasonal Climate?, Bulletin of the American Meteorological Society, 88, 541 – 550, https://doi.org/https://doi.org/10.1175/BAMS-88-4-541, 2007.

Ramelli, F., Beck, A., Henneberger, J., and Lohmann, U.: Using a holographic imager on a tethered balloon system for microphysical observations of boundary layer clouds, Atmospheric Measurement Techniques, 13, 925–939, https://doi.org/10.5194/amt-13-925-2020, 2020.

Schemann, V. and Ebell, K.: Simulation of mixed-phase clouds with the ICON large-eddy model in the complex Arctic environment around Ny-Ålesund, Atmospheric Chemistry and Physics, 20, 475–485, https://doi.org/10.5194/acp-20-475-2020, 2020.

Serreze, M. C. and Barry, R. G.: Processes and impacts of Arctic amplification: A research synthesis, Global and Planetary Change, 77, 85 – 96, https://doi.org/https://doi.org/10.1016/j.gloplacha.2011.03.004, 2011.

Shupe, M. D.: Clouds at Arctic Atmospheric Observatories. Part II: Thermodynamic Phase Characteristics, Journal of Applied Meteorology and Climatology, 50, 645 – 661, https://doi.org/https://doi.org/10.1175/2010JAMC2468.1, 2011.

Shupe, M. D., Matrosov, S. Y., and Uttal, T.: Arctic Mixed-Phase Cloud Properties Derived from Surface-Based Sensors at SHEBA, Journal of the Atmospheric Sciences, 63, 697 – 711, https://doi.org/https://doi.org/10.1175/JAS3659.1, 2006.

Sinclair, V. A., Moisseev, D., and von Lerber, A.: How dual-polarization radar observations can be used to verify model representation of secondary ice, Journal of Geophysical Research: Atmospheres, 121, 10,954–10,970, https://doi.org/https://doi.org/10.1002/2016JD025381, 2016.

Skamarock, W. C., Klemp, J. B., Dudhia, J., Gill, D. O., Liu, Z., Berner, J., Wang, W., Powers, J. G., Duda, M. G., Barker, D. M., et al.: A description of the advanced research WRF model version 4, National Center for Atmospheric Research: Boulder, CO, USA, p. 145, http://dx.doi.org/10.5065/1dfh-6p97, 2019.

Solomon, A., Morrison, H., Persson, O., Shupe, M. D., and Bao, J.-W.: Investigation of Microphysical Parameterizations of Snow and Ice in Arctic Clouds during M-PACE through Model–Observation Comparisons, Monthly Weather Review, 137, 3110 – 3128, https://doi.org/https://doi.org/10.1175/2009MWR2688.1, 2009.

Solomon, A., de Boer, G., Creamean, J. M., McComiskey, A., Shupe, M. D., Maahn, M., and Cox, C.: The relative impact of cloud condensation nuclei and ice nucleating particle concentrations on phase partitioning in Arctic mixed-phase stratocumulus clouds, Atmospheric Chemistry and Physics, 18, 17 047–17 059, https://doi.org/10.5194/acp-18-17047-2018, 2018.

Sotiropoulou, G., Sullivan, S., Savre, J., Lloyd, G., Lachlan-Cope, T., Ekman, A. M. L., and Nenes, A.: The impact of secondary ice production on Arctic stratocumulus, Atmospheric Chemistry and Physics, 20, 1301–1316, https://doi.org/10.5194/acp-20-1301-2020, 2020.

Sotiropoulou, G., Vignon, E., Young, G., Morrison, H., O'Shea, S. J., Lachlan-Cope, T., Berne, A., and Nenes, A.: Secondary ice production in summer clouds over the Antarctic coast: an underappreciated process in atmospheric models, Atmospheric Chemistry and Physics, 21, 755–771, https://doi.org/10.5194/acp-21-755-2021, 2021.

Sotiropoulou, G., Lewinschal, A., Georgakaki, P., Phillips, V., Patade, S., Ekman, A. M. L., and Nenes, A.: Sensitivity of Arctic clouds to ice microphysical processes in the NorESM2 climate model, https://doi.org/10.1002/essoar.10512081.1, 2022.

Sze, K. C. H., Wex, H., Hartmann, M., Skov, H., Massling, A., Villanueva, D., and Stratmann, F.: Ice-nucleating particles in northern Greenland: annual cycles, biological contribution and parameterizations, Atmospheric Chemistry and Physics, 23, 4741–4761, https://doi.org/10.5194/acp-23-4741-2023, 2023.

Tobo, Y., Uetake, J., Matsui, H., Moteki, N., Uji, Y., Iwamoto, Y., Miura, K., and Misumi, R.: Seasonal Trends of Atmospheric Ice Nucleating Particles Over Tokyo, Journal of Geophysical Research: Atmospheres, 125, e2020JD033 658, https://doi.org/https://doi.org/10.1029/2020JD033658, e2020JD033658 2020JD033658-T, 2020.

Touloupas, G., Lauber, A., Henneberger, J., Beck, A., and Lucchi, A.: A convolutional neural network for classifying cloud particles recorded by imaging probes, Atmospheric Measurement Techniques, 13, 2219–2239, https://doi.org/10.5194/amt-13-2219-2020, 2020.

Vali, G., DeMott, P. J., Möhler, O., and Whale, T. F.: Technical Note: A proposal for ice nucleation terminology, Atmospheric Chemistry and Physics, 15, 10 263–10 270, https://doi.org/10.5194/acp-15-10263-2015, 2015.

Verlinde, J., Harrington, J. Y., McFarquhar, G. M., Yannuzzi, V. T., Avramov, A., Greenberg, S., Johnson, N., Zhang, G., Poellot, M. R., Mather, J. H., Turner, D. D., Eloranta, E. W., Zak, B. D., Prenni, A. J., Daniel, J. S., Kok, G. L., Tobin, D. C., Holz, R., Sassen, K., Spangenberg, D., Minnis, P., Tooman, T. P., Ivey, M. D., Richardson, S. J., Bahrmann, C. P., Shupe, M., DeMott, P. J., Heymsfield,

A. J., and Schofield, R.: The Mixed-Phase Arctic Cloud Experiment, Bulletin of the American Meteorological Society, 88, 205 – 222, https://doi.org/https://doi.org/10.1175/BAMS-88-2-205, 2007.

Wendisch, M., Brückner, M., Burrows, J., Crewell, S., Dethloff, K., Ebell, K., Lüpkes, C., Macke, A., Notholt, J., Quaas, J., et al.: Understanding causes and effects of rapid warming in the Arctic, Eos, 98, https://doi.org/10.1029/2017EO064803, 2017.

Wendisch, M., Macke, A., Ehrlich, A., Lüpkes, C., Mech, M., Chechin, D., Dethloff, K., Velasco, C. B., Bozem, H., Brückner, M., Clemen, H.-C., Crewell, S., Donth, T., Dupuy, R., Ebell, K., Egerer, U., Engelmann, R., Engler, C., Eppers, O., Gehrmann, M., Gong, X., Gottschalk, M., Gourbeyre, C., Griesche, H., Hartmann, J., Hartmann, M., Heinold, B., Herber, A., Herrmann, H., Heygster, G., Hoor, P., Jafariserajehlou, S., Jäkel, E., Järvinen, E., Jourdan, O., Kästner, U., Kecorius, S., Knudsen, E. M., Köllner, F., Kretzschmar, J., Lelli, L., Leroy, D., Maturilli, M., Mei, L., Mertes, S., Mioche, G., Neuber, R., Nicolaus, M., Nomokonova, T., Notholt, J., Palm, M., van Pinxteren, M., Quaas, J., Richter, P., Ruiz-Donoso, E., Schäfer, M., Schmieder, K., Schnaiter, M., Schneider, J., Schwarzenböck, A., Seifert, P., Shupe, M. D., Siebert, H., Spreen, G., Stapf, J., Stratmann, F., Vogl, T., Welti, A., Wex, H., Wiedensohler, A., Zanatta, M., and Zeppenfeld, S.: The Arctic Cloud Puzzle: Using ACLOUD/PASCAL Multiplatform Observations to Unravel the Role of Clouds and Aerosol Particles in Arctic Amplification, Bulletin of the American Meteorological Society, 100, 841 – 871, https://doi.org/10.1175/BAMS-D-18-0072.1, 2019.

Westbrook, C. D. and Illingworth, A. J.: Evidence that ice forms primarily in supercooled liquid clouds at temperatures > -27°C, Geophysical Research Letters, 38, https://doi.org/https://doi.org/10.1029/2011GL048021, 2011.

Wieder, J., Ihn, N., Mignani, C., Haarig, M., Bühl, J., Seifert, P., Engelmann, R., Ramelli, F., Kanji, Z. A., Lohmann, U., and Henneberger, J.: Retrieving ice-nucleating particle concentration and ice multiplication factors using active remote sensing validated by in situ observations, Atmospheric Chemistry and Physics, 22, 9767–9797, https://doi.org/10.5194/acp-22-9767-2022, 2022a.

Wieder, J., Mignani, C., Schär, M., Roth, L., Sprenger, M., Henneberger, J., Lohmann, U., Brunner, C., and Kanji, Z. A.: Unveiling atmospheric transport and mixing mechanisms of ice-nucleating particles over the Alps, Atmospheric Chemistry and Physics, 22, 3111–3130, https://doi.org/10.5194/acp-22-3111-2022, 2022b.

Wolff, M. A., Isaksen, K., Petersen-Øverleir, A., Ødemark, K., Reitan, T., and Brækkan, R.: Derivation of a new continuous adjustment function for correcting wind-induced loss of solid precipitation: results of a Norwegian field study, Hydrology and Earth System Sciences, 19, 951–967, https://doi.org/10.5194/hess-19-951-2015, 2015.

Yang, F., Cantrell, W. H., Kostinski, A. B., Shaw, R. A., and Vogelmann, A. M.: Is Contact Nucleation Caused by Pressure Perturbation?, Atmosphere, 11, https://doi.org/10.3390/atmos11010001, 2020.

Young, G., Connolly, P. J., Jones, H. M., and Choularton, T. W.: Microphysical sensitivity of coupled springtime Arctic stratocumulus to modelled primary ice over the ice pack, marginal ice, and ocean, Atmospheric Chemistry and Physics, 17, 4209–4227, https://doi.org/10.5194/acp-17-4209-2017, 2017.

Young, G., Lachlan-Cope, T., O'Shea, S. J., Dearden, C., Listowski, C., Bower, K. N., Choularton, T. W., and Gallagher, M. W.: Radiative Effects of Secondary Ice Enhancement in Coastal Antarctic Clouds, Geophysical Research Letters, 46, 2312–2321, https://doi.org/https://doi.org/10.1029/2018GL080551, 2019.

Young, K. C.: The role of contact nucleation in ice phase initiation in clouds, Journal of Atmospheric Sciences, 31, 768–776, 1974.

Zhao, X., Liu, X., Phillips, V. T. J., and Patade, S.: Impacts of secondary ice production on Arctic mixed-phase clouds based on ARM observations and CAM6 single-column model simulations, Atmospheric Chemistry and Physics, 21, 5685–5703, https://doi.org/10.5194/acp-21-5685-2021, 2021.

# Paper IV

# Simulations of the response of an Arctic mixed-phase cloud to aerosol perturbations and warming